SELF-ASSEMBLED NANOGELS OF HYDROPHOBIZED METHYLCELLULOSE

SELF-ASSEMBLED NANOGELS OF HYDROPHOBIZED METHYLCELLULOSE

By MARION JAMARD, B.Eng., M.Eng

A Thesis Submitted to the School of Graduate Studies in Partial Fulfillment of the Requirements for the Degree Doctor of Philosophy in the School of Biomedical Engineering

DOCTOR OF PHILOSOPHY (2016) McMaster University
School of Biomedical Engineering Hamilton, Ontario

TITLE: SELF-ASSEMBLED NANOGELS OF HYDROPHOBIZED METHYLCELLULOSE

AUTHOR: Marion Jamard, B.Eng, M.Eng (Grenoble Institute of Technology)

SUPERVISOR: Dr. Heather Sheardown

NUMBER OF PAGES: xviii , 190

ABSTRACT

Topical administration is the most common method to deliver ocular therapeutics. However, the eye is highly resistant to foreign substances and its clearance mechanisms effectively remove drug, significantly limiting the efficiency of common topical formulations. In the search for improved ocular bioavailability, particle based delivery systems have arisen as a promising strategy to overcome these limitations while retaining the patient friendly aspects of topical formulations. Nanoparticles can be formed via the self-assembly of amphiphilic molecules into nano-sized aggregates consisting of hydrophilic networks crosslinked with hydrophobic domains and referred to as "nanogels". The work presented in this thesis focuses on the design, synthesis and optimization of novel nanogels ultimately intended to improve the efficiency of the delivery of therapeutics to the eye. Methylcellulose, a hydrophilic, non-toxic and biodegradable natural biomaterial, has been extensively investigated for biomedical applications, including ocular applications, and was therefore the polymer of choice for the work. We first describe the synthesis of nanogels via self-assembly of methylcellulose (MC) hydrophobized with side chains of poly(N-tert-butylacrylamide) (MC-g-PNtBAm), and demonstrate that their properties can be tuned by adjusting the degree of hydrophobic grafting (Chapter 2). The results show the formation of stable monodispersed spherical particles of ~140 nm, presenting good cytocompatibility with human corneal epithelium cells. The impact of the methylcellulose molecular weight on the nanogel properties is investigated and the results demonstrate that the polysaccharide backbone length provides another lever to tailor the performances of the nano-aggregates as drug delivery systems (Chapter 3). These materials show the ability to encapsulate dexamethasone with an efficiency superior to 95% and release their payload for over 30 days. Phenylboronic acid (PBA) functionalization is introduced on the surface of the nanogels to improve their mucoadhesiveness and thereby prolong their residence time on the surface of the eye (Chapter 4). Dexamethasone release from the grafted particles is maintained over 12 days, with the results indicating that the additional PBA layer reduce the initial burst. In terms of

mucoadhesion, zeta-potential measurements suggest interaction of some nanogel formulations with mucin. Finally, the surface of the nanogels is covered with chains of poly(ethylene glycol) (PEG) and the effect of PEGylation on the pharmacokinetics and mucoadhesive properties is studied (Chapter 5). PEG functionalization is found to significantly slow the release of dexamethasone phosphate from 1 day to over 8 days, and zeta-potential results also suggest coverage-dependant mucoadhesive properties. These materials show promise for the delivery of drugs to the anterior segment of the eye.

ACKNOWLEDGEMENTS

I would like to thank my supervisor, Dr Heather Sheardown, for her mentorship over the past four years. Despite my rough start, she remained supportive and encouraging when, feeling disheartened, I came to her in challenging times. Heather believed in me when I did not, and her faith helped me to keep going. This year I have had the chance to go abroad work on different projects in other institutions. This would not have been possible without Heather's remarkable support to take advantage of any opportunity to learn and gain different experiences. I also want to mention her particular concern for her students, as well as her care for and understanding of life beside academia, and for that as well, I am extremely grateful.

I would like to thank my committee members, Dr Todd Hoare and Dr Kim Jones for their comments and suggestions on my research. I express my sincere gratitude to Dr Hoare for his time and guidance which were key in the watershed of my Ph.D.

My thanks go out to Lina, the cornerstone of the lab, on whom I could always count. She patiently taught and advised me, always with a kind word to encourage me. I would like to express my gratitude to Stefan, Amanda and Graeme who have been instrumental my progress as a researcher, succeeding one another teaching me and inspiring me each in their own way (Stefan's rule of seven quickly became the basis of my work planning), and helped me to get through tricky times. I am also very grateful to my coworkers Nicole Mangiacotte and Jianfe Zhang. Without their help, I would not have been able to work around the tricky timing of this last year. I really enjoyed working by the side of all these lab companions.

Many thanks to all the members of the Sheardown group, a cheerful team I had great pleasure working with, with a special mention for the Particle Party! My deep appreciation goes out to Megan Dodd, Dr Emily Cranston, Scott Campbell, Scott Fitzpatrick for their kindness and patience answering my questions and sharing their experience. Finally, although I met them for a short period at the very end of my Ph.D., I must express my sincere gratitude to Dr Ilva Rupenthal and Dr Valeria Bosio for letting me join their group, it has been an honor to work for those truly inspiring women.

Behind the curtains of the academic scene, there were as well many important people who contributed in a different way to the completion of my Ph.D.

I would like to thank all my friends. I have been so lucky to be surrounded by such a group of amazing people. They were my distraction from the frustrations of research, my resource for positive energy, my Canadian family while so far from home. Among them, Kendall and Gaby, who I met four years ago, when I just started my Ph.D., have been there all along. I also want to mention Pucca, ma moitié. After 10 years of friendship; how we ended up reunited on the other side of the Atlantic Ocean still puzzles me. You guys supported me in so many ways I can't express; I cannot imagine what it would have been like without you. I hope you know how much your unfailing friendship means to me.

Finally, I thank my family. An amazingly one, unique in so many ways. Words are missing to express how lucky and grateful I am for having such incredible parents and brother. The exceptional complicity we share carried me all along. Through your curiosity, your open mind, your values, your young heart, your adventurous and kind of harebrained sides, you taught me what the priorities in life are. Even though you raised me that way, even though you might have seen it coming as I have been talking about living abroad since I was a kid, I am aware that my choices were not the easiest as they led me far away. However, not only do you accept them, but you also understand them. For this as for everything I have undertaken in my life, you were behind me and encouraged me. It is fortified by your love, your unconditional support, and everything you gave and taught me, that I persevere every day towards my aspirations. You are my strength, the pillar of my life.

Pour terminer, je remercie ma famille. Merveilleusement unique sur bien des côtés. Des mots ne suffiront pas à exprimer mon immense reconnaissance. J'ai des parents et un frère formidables. La complicité exceptionnelle que nous partageons m'a portée tout au long. A travers votre curiosité, votre jeunesse et ouverture d'esprit, vos valeurs, votre côté aventurier et un peu farfelu, vous m'avez appris quelles sont les priorités dans la vie. Et même si vous m'avez élevée de cette manière, même si vous l'avez sans doute vu venir puisque je parle de vivre à l'étranger depuis petite, j'ai conscience que mes choix ne sont pas toujours des plus faciles puisqu'ils m'ont emmenée loin de vous. Et pourtant, non seulement les acceptez-vous, mais vous les comprenez aussi. Pour ça comme pour tout ce que j'ai entrepris dans ma vie, vous étiez à mes côtés, vous m'avez encouragée. Et c'est forte de votre amour, de votre soutien inconditionnel et de tout ce que vous m'avez apporté et appris, que tous les jours je persévère dans mes aspirations. Vous êtes ma force, le pilier de ma vie.

A ma famille

TABLE OF CONTENTS

Chapter 1: Literature Review *1*
Abstract *2*
1.1 Introduction *3*
1.1.1 Nanogels *3*
1.1.2 Self-assembly *3*
1.1.3 Polysaccharides *4*
1.1.4 Transition *7*
1.2 Nanostructuration of the nanogels *7*
1.2.1 Self- assembly mechanism *7*
1.2.1.1 Introduction 7
1.2.1.2 Critical aggregation concentration 8
1.2.1.3 Size 9
1.2.1.4 Structure 10
1.2.1.5 Parameters 13
1.2.2 Tuning of the nanogel characteristics and properties *13*
1.2.2.1 Impact of the polysaccharide structure 13
1.2.2.2 Impact of the degree of hydrophobization 14
1.2.2.2.1 Impact of the nature of the hydrophobic moiety 15
1.2.2.2.2 Impact of the degree of substitution 16
1.2.2.2.2.1 Size 17
1.2.2.2.2.2 CAC 17
1.2.2.2.2.3 Dissociation 18
1.2.2.2.2.4 Drug loading and release 18
1.2.2.2.3 Impact of hydrophobic chain length 19
1.2.2.2.3.1 Polymer surfactant 20
1.2.2.2.3.2 Comb-like copolymer 21
1.2.2.3 Impact of the polysaccharide molecular weight 22
1.2.2.4 Impact of other parameters 23
1.2.3 Summary *24*
1.3 Application to drug delivery *25*
1.3.1 Introduction *25*
1.3.2 Dextran *25*

1.3.2.1 Introduction 25
1.3.2.2 Dextran modified with polycaprolactone 25
1.3.2.3 Dextran modified with poly(D,L-lactide) 27
1.3.2.4 Dextran modified with cholesterol 27
1.3.2.5 Protein release from Dex-g-PLLA and Dex-Chol 28
1.3.2.6 Dextran functionalized with poorly water-soluble drugs (ibuprofen, naproxen) 28
1.3.3 Chitosan 29
1.3.3.1 Introduction 29
1.3.3.2 Chitosan derivative with phosphorylcholine and deoxycholic acid moieties 30
1.3.3.3 Poly(p-dioxanone) end-modified chitosan 30
1.3.3.4 Biotinylated N-palmitoyl chitosan 31
1.3.3.5 Chitosan functionalized with N -acetyl cysteine and vitamin E succinate 32
1.3.4 Hyaluronic Acid 32
1.3.4.1 Introduction 32
1.3.4.2 HA grafted with bromohexyl derivative of riboflavin tetrabutyrate 32
1.3.4.3 HA conjugated with hydrophobic poly(L-histidine) (HA-Phis) 33
1.3.4.4 Alkyl chains grafted HA 33
1.3.4.5 Taxol conjugated HA 34
1.3.5 Cellulose and derivatives 34
1.3.5.1 Introduction 34
1.3.5.2 α-tocopherol succinate-conjugated hydroxyethyl cellulose 35
1.3.5.3 Linoleic acid conjugated hydroxyethyl cellulose 36
1.3.5.4 PLA modified cellulose 36
1.4 Conclusions 37
1.5 Thesis scope 37
1.5.1 Ocular drug delivery limitations 37
1.5.2 Particulate systems 39
1.5.3 Cellulose in topical drug formulations 39
1.5.4 Nanogels of hydrophobized methylcellulose for ocular drug delivery 40
1.6 Acknowledgements 42
1.7 Disclosures 42
Bibliography 43
Chapter 2: Nanogels of Methylcellulose Hydrophobized with N-tert-butylacrylamide for Ocular Drug Delivery 58

Abstract 59
2.1 Introduction 61
2.2 Experimental section 64
2.2.1 Materials 64
2.2.2 Preparation of MC-g-PNtBAm nanogels 64
2.2.3 FT-IR analysis 65
2.2.4 NMR analysis 65
2.2.5 Particle size measurements 66
2.2.6 Transmission electon microscopy study 66
2.2.7 Loading of dexamethasone 66
2.2.8 In vitro release of dexamethasone 67
2.2.9 Cell toxicity studies 67
2.3 Results and discussion 69
2.3.1 Synthesis of MC-g-PNtBAm nanogels 69
2.3.2 Effect of monomer, initiator and acid concentrations on the degreee of hydrophobization 70
2.3.3 Size and morphology of the MC-g-PNtBAm nanogels 71
2.3.4 Viability studies 72
2.3.5 Dexamethasone encapsulation 73
2.3.6 In vitro release of dexamethasone 73
2.4 Conclusion 75
2.5 Tables 76
2.6 Figures 77
2.7 Acknowledgements 86
2.8 Disclosures 86
2.9 Supporting information 87
Bibliography 90
Chapter 3: Effect of Methylcellulose Molecular Weight on the Properties of Self-assembling MC-g-PNtBAm Nanogels. 95
Abstract 96
3.1 Introduction 97
3.2 Materials and Methods 98
3.2.1 Materials 98
3.2.2 Synthesis of MC-g-PNtBAm nanogels 99
3.2.3 ^{1}H NMR analysis 99

3.2.4 Particle size measurements *100*
3.2.5 Transmission electron microscopy study *100*
3.2.6 Loading of dexamethasone *100*
3.2.7 In vitro release of dexamethasone *101*
3.3 Results and Discussion *101*
3.3.1 Synthesis *101*
3.3.2 Impact of MC molecular weight on particle size and morphology *102*
3.3.3 Impact of MC molecular weight on Drug release *104*
3.4 Conclusions *106*
3.5 Tables *107*
3.6 Figures *108*
3.7 Acknowledgements *112*
3.8 Disclosures *112*
Bibliography *113*
Chapter 4: Phenylboronic Acid Functionalization of MC-g-PNtBAm Nanogels for Improved Mucoadhesion *115*
Abstract *116*
4.1 Introduction *118*
4.2 Materials and methods *121*
4.2.1 Materials *121*
4.2.2 MC-g-PNtBAm synthesis *121*
4.2.3 PBA functionalization of the MC-g-PNtBAm nanogels *122*
4.2.4 GPC analysis *123*
4.2.5 ATR FT-IR analysis *123*
4.2.6 NMR analysis *123*
4.2.7 XPS analysis *123*
4.2.8 Particle size measurements *124*
4.2.9 Transmission electon microscopy study *124*
4.2.10 Mucoadhesive evaluation by Zeta-potential measurements *124*
4.2.11 Loading of dexamethasone *125*
4.2.12 In vitro release of dexamethasone *126*
4.2.13 Cell toxicity studies *126*
4.3 Results and Discussion *127*
4.3.1 PBA Functionalization *127*

4.3.2 Size and morphology *129*
4.3.3 Cytocompatibility *130*
4.3.4 Drug entrapment and release *130*
4.3.5 Mucoadhesion *133*
4.4 Conclusion *134*
4.5 Tables *136*
4.6 Figures *137*
4.7 Acknowledgements *148*
4.8 Disclosures *148*
Bibliography *149*
Chapter 5: PEG functionalized methylcellulose based nanogels with potential for improved mucus transport *154*
Abstract *155*
5.1 Introduction *156*
5.2 Materials and Methods *159*
5.2.1 Materials *159*
5.2.2 MC-g-PNtBAm synthesis *160*
5.2.3 PEG functionalization of the MC-g-PNtBAm nanogels *160*
5.2.4 ATR FT-IR analysis *161*
5.2.5 NMR analysis *161*
5.2.6 PEG quantification *161*
5.2.7 Particle size measurements *162*
5.2.8 Transmission electon microscopy (TEM) *162*
5.2.9 Zeta-potential measurements *162*
5.2.10 Drug loading *163*
5.2.11 In vitro drug release *164*
5.2.12 Cell toxicity studies *164*
5.3 Results and discussion *165*
5.3.1 Synthesis *165*
5.3.2 PEG quantification *166*
5.3.3 Size and morphology *167*
5.3.4 Cytotoxicity *168*
5.3.5 Drug release *168*
5.3.5.1 Dexamethasone 168

5.3.5.2 Dexamethasone Phosphate 170
5.3.6 Mucoadhesion *172*
5.4 Conclusions *173*
5.5 Tables *174*
5.6 Figures *175*
5.7 Acknowledgements *184*
5.8 Disclosures *184*
Bibliography *185*
Chapter 6: Conclusions *190*

LIST OF FIGURES

Figure 1-1: Schematic representation of the possible structures of the self-assembled nano-aggregates 12
Figure 2-1: Synthesis of MC-g-PNtBAm copolymers. Grafting reaction of NtBAm on MC via cerium ammonium nitrate 77
Figure 2-2: NMR spectra of a) MC, b) MC-g-PNtBAm 78
Figure 2-3: FT-IR spectra of MC and MC-g-PNtBAm 79
Figure 2-4: Degree of hydrophobization when increase in a) nitric acid concentration b) cerium ammonium nitrate concentration c) NtBAm concentration 80
Figure 2-5: Effect of initiation on the degree of hydrophobization 81
Figure 2-6: Morphology of the MC-g-PNtBAm nanogels with different degrees of hydrophobic modification. 82
Figure 2-7: Comparison of a) cell viability in presence of 1.125 mg/mL MC-g-PNtBAm nanogels and b) metabolism in presence of 1.125 mg/mL and 0.225mg/mL MC-g-PNtBAm nanogels. Data expressed as a percentage relative to control comprising cells not exposed to the nanogels.n=6, error bars corresponding to the standard deviation. 83
Figure 2-8: Cells after 48 hour incubation a) control b) with MC-g-PNtBAm_149% 84
Figure 2-9: Release profiles of dexamethasone from MC-g-PNtBAm nanogels with different degrees of hydrophobic grafting.n=3 with the error bars corresponding to the standard deviation. 85
Figure 3-1: Hydrodynamic diameter of MC-g-PNtBAm nanogels varying the MC molecular weights at two different degrees of hydrophobization (DH), measured by particle tracking analysis. 3 measurements with the error bars corresponding to the standard deviation of the mean size. 108
Figure 3-2: Scheme to illustrate the influence of MC molecular on the swelling ability of the nanogel (simplified with a single hydrophobic domain) at both degrees of hydrophobization. At high levels of hydrophobic modification, the tight mesh of the aggregates is unable to swell. Low levels of hydrophobic grafting create aggregates with a looser mesh, in which only longer MC chains can expend to uptake water while maintaining the cohesion of the nanogel. 109
Figure 3-3: TEM pictures showing the morphology of nanogels with a DH of 30% and synthesized using various MC molecular weights: a) 30 kg/mol, b) 85 kg/mol, c) 165 kg/mol, d) 230 kg/mol 40% DH. The scale bars indicate 500 nm. 110
Figure 3-4: Dexamethasone release from MC-g-PNtBAm nanogels at 30% or 50% DH and synthesized using MC of 30 kg/mol or 230 kg/mol. The bars on the curves of MC(30k)-g-PNtBAm_30% and MC(230k)-g-PNtBAm_50% indicate the time point when the free drug in solution is released from the dialysis bag and the entrapped drug is being released.n=3 with the error bars corresponding to standard deviations. 111
Figure 4-1: Structure of 3-aminophenylboronic acid. 137
Figure 4-2: Structure of PBA functionalized MC-g-PNtBAm nanogels in aqueous solutions. 138
Figure 4-3: Scheme for tethering PBA to MC. Step 1: Sodium m-periodate ($NaIO_4$) oxidation via Malaprade-type reaction, which breaks the C2-C3 bond of vicinal hydroxyl groups to form 2,3-dialdehyde structure. Step 2: Reaction of aldehyde groups of oxidized MC structure with primary amine groups of 3-aminophenylboronic acid via Schiff base linkage. 139
Figure 4-4: ^1H NMR spectrum of PBA functionalized MC-g-PNtBAm nanogels 140

Figure 4-5: NMR spectrum of PBA, PBA functionalized MC-g-PNtBAm nanogels, MC-g-PNtBAm nanogels. 141
Figure 4-6: Comparison of a) cell viability and b) metabolism in presence of 0.3 mg/mL MC(165k)-g-PNtBAm_PBA nanogels at two different PBA coverages. Data expressed as a percentage relative to control comprising cells not exposed to the nanogels.n=6 with error bars corresponding to the standard deviation. 145
Figure 4-7: Dexamethasone release from MC(165k)-g-PNtBAm_PBA nanogels with two different PBA grafting coverages compared to not functionalized nanogels. a) Release plotted as a percentage relative to the total quantity of dexamethasone initially incorporated – 100% thus correspondi to the dexamethasone free in solution and encapsulated. The bars on the curves indicate the time point when the free drug in solution is released from the dialysis bag and the entrapped drug is being released. b) Release plotted as a percentage relative to the quantity of dexamethasone encapsulated – 100% corresponds to the amount of dexamethasone encapsulated.n=3 with error bars corresponding to standard deviation. 146
Figure 4-8: Zeta-potential of MC(x)-g-PNtBAm_PBA(y) formulations compared to a control solution of mucin.6 measurements per solution with error bars corresponding to the standard deviation. 147
Figure 5-1: Reaction scheme of PEG grafting onto methylcellulose. Sodium m-periodate (NaIO4) oxidation via Malaprade-type reaction breaking the C2-C3 bond of vicinal hydroxylgroups from the AGU of methycellulose, followed by the reaction of the newly formed aldehyde groups od oxidized MC with primary amine groups of methoxy-poly(ethylene glycol) amine via Schiff base linkage. 175
Figure 5-2: ^{1}H-NMR spectra of (a) methylcellulose, (b) MC-g-PNtBAm, (c) PEG functionalized MC-g-PNtBAm. 176
Figure 5-3: ATR FT-IR spectra of MC-g-PNtBAm_PEG(x) formulations at different PEG grafting densities, compared to unmodified MC-g-PNtBAm. 177
Figure 5-4: Quantification of PEG grafted on thesurface on the nanogel as a function of feed mass by fluorescence. Scale bars = 50 μm. 178
Figure 5-5: (a) TEM pictures, scale bars represent 500nm and (b) size of PEG functionalized MCg-PNtBAm nanogels.3 measurements per solution, error bars corresponding to the standard deviation of the mean size. 179
Figure 5-6: Comparison of human corneal epithelial cell a) viability and b) metabolism in presence of PEG functionalized MC-g-PNtBAm nanogels with 2 different PEG densities. Data expressed as a percentage relative to control comprising cells not exposed to the nanogels.n=6, error bars corresponding to the standard deviation. 180
Figure 5-7: Dexamethasone release from the nanogel formulations. a) Comparison of the release from PEG functionalized nanogels with unmodified nanogels. The bar on the release curve of MC-g-PNtBAm indicates the end of the release of the free drug in solution. The bars on the curve of MC-g-PNtBAm indicate the time point when the free drug in solution is released from the dialysis bag and the entrapped drug is being released. b) Zoom on the release to compare the release from PEG functionalized nanogels at two grafting densities. n=3, error bars corresponding to the standard deviation. 181
Figure 5-8: Dexamethasone phosphate release from MC-g-PNtBAm_PEG nanogels with two different PEG grafting coverages compared to not functionalized nanogels. a) Release plotted as a percentage relative to the total quantity of dex-P initially incorporated – 100% thus correspondi to the dex-P free in solution and encapsulated. The bars on the curves indicate the time point when the free drug in solution is released from the dialysis bag and the entrapped drug is being released. b)

Release plotted as a percentage relative to the quantity of dex-P encapsulated – 100% corresponds to the amount of dexamethasone encapsulated. n=3, error bars corresponding to the standard deviation. 182
Figure 5-9: Zeta-potential of MC-g-PNtBAm nanogels with different degrees of PEG functionalization, compared to a control of mucin solution.6 measurements per solution, error bars corresponding to the standard deviation. 183

LIST OF TABLES

Table 1-1: Structure and features of commonly used polysaccharides 6
Table 2-1: Concentrations of acid, initiator and monomer used to synthesize MC-g-PNtBAm..... 76
Table 2-2: Loading efficiency of dexamethasone into MC-g-PNtBAm nanogels as a function of feed composition and grafting degree 76
Table 3-1: Molecular weight of MC and CAN concentration used for the synthesis of MC-g-PNtBAm formulations 107
Table 3-2: Degree of hydrophobization (DH) for various MC molecular weights and initiator concentrations. 107
Table 3-3: Entrapment efficiencies of dexamethasone 107
Table 4-1: Nomenclature and content of the formulations synthesized. 136
Table 4-2: Molecular weight of methylcellulose after varying reaction times of periodate oxidation, measured by gel permeation chromatography. 136
Table 4-3: Loading efficiency of dexamethasone into MC(165k)-g-PNtBAm_PBA nanogels as a function of PBA coverage 136
Table 5-1: PEG feed mass, concentration and ratio to MC-g-PNtBAm nanogel for each formulation. 174
Table 5-2: Entrapment efficiencies of dexamethasone and dexamethasone phosphate of different nanogel formulations. 174

LIST OF ABBREVIATIONS AND SYMBOLS

AGU	Anhydroglucose units
ATR	Attenuated total reflectance
BSA	Bovine serum albumin
CAC	Critical aggregation concentration
CAN	Cerium ammonium nitrate
CMC	Critical micelle concentration
CHM	Cholesterol-modified mannan
CHP	Cholesterol modified pullulan
DCA	Deoxycholic acid
Dex	Dexamethasone
Dex-b-PLA	Block copolymer of dextran and poly(D,L-lactide)
Dex-Chol	Dextran-cholesterol conjugate
Dex-g-PLLA	Poly(L-lactide)-grafted dextran
Dex-P	Dexamethasone-phosphate
DH	Degree of hydrophobization
DLS	Dynamic light scattering
DMF	Dimethylformamide
DMSO	Dimethyl sulfoxide
DP	Degree of polymerization
DS	Degree of substitution
Dx-g-PCL	Poly(ε-caprolactone)-grafted dextran
EPR	Enhanced permeation and retention
FT-IR	Fourier transform infrared spectroscopy
GPC	Gel permeation chromatography
HA	Hyaluronic acid
HA-Phe	(L-phenylalanine ethyl ester)-modified hyaluronic acid
HCE	Human corneal epithelium
hCECs	Human corneal epithelium cells
HEC	Hydroxyethyl cellulose
^{1}H NMR	Proton nuclear magnetic resonance spectroscopy
HPC	Hydroxypropyl cellulose
HPLC	High performance liquid chromatography
HPMC	Hydroxypropyl methylcellulose
LA	Linoleic acid
MC	Methylcellulose
MC-g-PNtBAm	Poly(N-tert-butylacrylamide) grafted methylcellulose
MW	Molecular weight
NAC	N-acetyl cysteine
N_{agg}	Aggregaion number
NMR	Nuclear magnetic resonance

NtBAm	N-tert-butylacrylamide
PA	Pullulan acetate
PBA	Phenylboronic acid
PBS	Phosphate buffered saline
PC	Phosphorylcholine
PCL	Poly(ε-caprolactone)
PEG	Poly(ethylene glycol)
PEG-NH_2	Methoxy poly(ethylene glycol) amine
PDI	Polydispersity index
PHis	Poly(L-histidine)
PLA	Poly(D,L-lactide)
PLLA	Poly(L-lactide)
PNtBAm	Poly(N-tert-butylacrylamide)
PorTaxol	Porphyrin modified paclitaxel
PPDO	Block copolymer of chitosan and poly(p-dioxanone)
PTD	Protein transduction domain
RGD	Arginine - glycine - aspartic acid
Rho-NCS	Rhodamine B isothiocyanate
SD	Standard deviation
SEM	Scanning electron microscopy
siRNA	Small interfering RNA
TEM	Transmission electron microscopy
TOC	Tocopherol succinate
UV	Ultraviolet
XPS	X-ray photoelectron spectroscopy

DECLARATION OF ACADEMIC ACHIEVEMENT

In accordance with the guidelines for the preparation of a doctoral thesis set forth by the McMaster University School of Graduate Studies, this work has been prepared as a sandwich thesis. The research conducted in Chapter 4 and 5 was performed with the help of several students. The following statements are intended to outline the contributions of each author to the selected works.

Chapter 2: In this manuscript, Marion was responsible for the synthesis and characterization of the materials, and write-up. Dr Hoare suggested the design of the polymer and provided guidance along the project.

Chapter 4: In this manuscript, Marion was responsible for the synthesis, design, write-up and the majority of materials characterization, including NMR, ATR FT-IR, XPR, drug release study, cell culture studies, and TEM imaging. Nicole performed the zeta-potential measurements to assess the mucoadhesive properties of the materials.

Chapter 5: In this manuscript, Marion was responsible for the synthesis, design, write-up and the majority of materials characterization, including NMR, ATR FT-IR, drug release study, cell culture studies, and TEM imaging. Nicole performed the zeta-potential measurements to assess the mucoadhesive properties of the materials. Jason helped Marion with the grafting of rhodamine onto PEG for the quantification of PEG chains on the nanogels.

CHAPTER 1: LITERATURE REVIEW

Nanogels of self-assembled hydrophobized polysaccharides for drug delivery

Authors: Marion Jamard, and Heather Sheardown

Objectives:

The objective of this literature review was to compile studies on self-assemblies of hydrophobized polysaccharides looking for general trends ruling the relationship between the characteristics of the amphiphilic copolymer and the properties of the resulting self-aggregates, as well as their performance as drug delivery systems. By better understanding the connection between the nature of the moieties, the structure of the molecule and its topology, the polysaccharide-based amphiphile can be designed to synthesize drug delivery platforms tailored for specific applications.

ABSTRACT

Nanogels are swollen nanosized hydrogel networks which can be synthesized through spontaneous aggregation of amphiphilic polymers and have demonstrated a series of attractive properties as drug carriers. Polysaccharides, hydrophilic natural polymers, present outstanding virtues such as biocompatibility, biodegradability and a variety of physicochemical properties. They can be readily modified to introduce hydrophobic segments for the synthesis of amphiphlic copolymer able of self-assembly. The variety of polysaccharides, hydrophobes and structures possible allows for the development of nanogels with different characteristics and properties. This review aims at finding general trends controlling the features of the self-aggregates in order to improve the precision of the copolymer design for its application as drug carrier. Recent progress in the synthesis of self-assembled hydrophobized polysaccharides are subsequently described including their application in drug delivery.

Keywords: Polysaccharide, hydrophobization, drug delivery, self-assembly, nanogel, particle, amphiphilic

1.1 INTRODUCTION

1.1.1 Nanogels

Hydrogels are defined as swollen three-dimensional polymer networks able to uptake large amounts of water or physiological fluid while maintaining their internal network structure[1]. There is an increasing interest in hydrogels of micro- and nanoscopic dimensions, referred to as microgels and nanogels[2,3]. Indeed, while having similar properties to their macro-sized counterparts, they can penetrate more easily through different biological membranes and deploy in less accessible areas of the body[2–5]. Many drug molecules suffer from impediments such as low solubility, off-target toxicity, instability or inefficient transfer across biological barriers, limiting their use in vivo. Their encapsulation into nanogels may thus offer a solution for safe and efficient delivery as it imparts the system with prolonged circulation time in biological media such as blood, excellent stability upon dilution, protection from premature degradation, enhanced permeability, improved biodistribution and pharmacokinetics[6–8]. They can also be taken up by cells[9,10], and are therefore potentially ideal candidates for intracellular delivery of cell targeted therapeutic agents such as siRNAs, peptides and various low molecular weight chemotherapeutics. Furthermore, nanogels provide a large surface area for multivalent conjugations, key to optimizing the particles and targeting the appropriate site of action in vivo. Micro- and nanogels are thus versatile carriers for biomedical applications, as discussed in many review articles[2–5].

1.1.2 Self-assembly

Four basic mechanisms can be used to synthesize polymer-based particles: covalent cross-linking, ionotropic cross-linking, polyelectrolyte complexation, and self-assembly[11,12]. The latter provides a bottom–up paradigm that contrasts with conventional top–down microfabrication[13] and is of

growing interest as a new strategy to develop nanoparticles for pharmaceutical or biotechnological application[14–18]. Self-assembly refers to the spontaneous formation of nanosized aggregates via a secondary force such as hydrogen bonding, electrostatic, van der Waals interactions and the hydrophobic effect[14]. This method takes advantage of the natural tendency of specific, local interactions among the molecules triggered by polymer concentration, or environmental parameters such as solvent, pH or temperature[19], while avoiding the use of photoirradiation, organic solvents, cross-linking agents, and/or other reactive molecules which may damage bioactive agents to be incorporated. Since self-assembling is induced by external parameters, the resulting well-organized three-dimensional structure can present sensitivity to a range of different stimuli giving programmed responses that can be controlled temporally and spatially[20–22].

Amphiphilicity is one of the most important factors triggering their self-organization in aqueous solution owing to intra- and/or inter-molecular hydrophobic interactions as amphiphiles are very close to biological macromolecules[23]. The combination of hydrophilic and hydrophobic groups in the same polymer allows for the spontaneous aggregation into different structures such as micelles, liposomes, hydrogels or nanoparticles[24–28] driven by hydrophobic interactions in order to minimize interfacial energy[29,30]. Self-assembled nanoparticles made of amphiphilic copolymers have aroused great interest in biomedical applications[23,31], and many of them are made using poly(ethylene glycol) (PEG) as the hydrophilic segment[32–35]. However, one drawback of these PEG-based block copolymers is the absence of reactive groups at their molecular chains, which limits further modification or ligand coupling[36]. Polysaccharides thus appear as a promising alternative to PEG.

1.1.3 Polysaccharides

Of natural origin (animal, plant, algal, microbial), polysaccharides are the most abundant group of biopolymers. They are polymers of repeating sugar units (monosaccharides) joined by glycosidic

linkages and are non-toxic[37–41]. Owing to their native presence in the body, most polysaccharides are subject to enzymatic degradation[42,43], providing a release mechanism for polysaccharide-based carrier systems. Biocompatible and biodegradable, they therefore have great potential for complying with in vivo requirements[29,44–48]. They also exhibit excellent properties such as stability, low cost (production and purification), hydrophilicity and bioadhesion ability[41,48–50]. Many polysaccharides possess innate bioactivity such as antimicrobial, and anti-inflammatory properties[51,52] and can be used to enhance the therapeutic efficacy of an associated drug. Some are polyelectrolytes and their surface charge can be used for bio-interactions such as cellular uptake or glomerular filtration[53]. The different chemical structures, including degree and steric configuration of substitutions, linkages of monosaccharides and substitutes, and molar mass, create a great diversity of polysaccharides and provide them with various physicochemical and biological properties[29,54–56]. The functional groups along the chain backbone (including hydroxyl, amino, and carboxylic acid groups) enables site generation or covalent bonding to small molecules, oligomers or other polymers to create derivatives with tailored properties[29,47,57,58]. These reasons suggest polysaccharides to be one of the most promising types of materials for the synthesis of micro- and nano- carriers[29,41,59–61]. The structures and properties of the more commonly used polysaccharides are given in Table 1-1.

Table 1-1: Structure and features of commonly used polysaccharides

Polysaccharide	Structure	Source	Charge	Properties
Chitosan	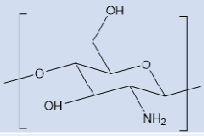	Animal	Cationic	- Biocompatible - Biodegradale - Antibacterial - Mucoadhesive - pH responsive
Dextran	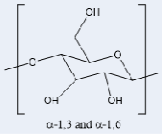	Microbial	Nonionic	- Biocompatible - Biodegradable - hydrophilic
Hyaluronic acid	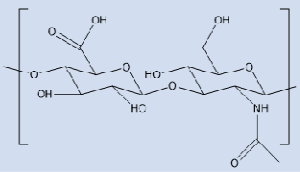	Animal	Anionic	- Biocompatible - Biodegradable - Hydrophilic - Viscoelastic - Mucoadhesive - Bioactive - Retain water
Alginate	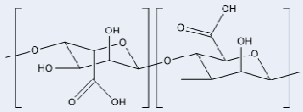	Algal	Anionic	- Biocompatible - Water soluble - Mucoadhesive - Gelling properties
Cellulose	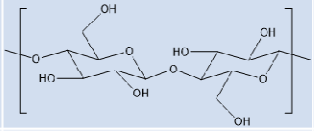	Plant		- Biocompatible - Biodegradable - Water insoluble
Pectins	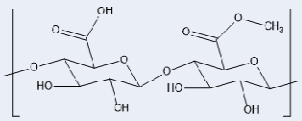	Plant	Anionic	- Biocompatible - Non-toxic - Biodegradable - Gelling properties
Carrageenans	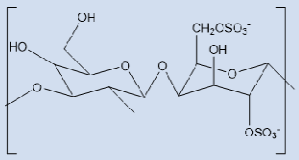	Algal		- Gelling properties - Anti-inflammatory process but also - Anti-tumor - Immunomodulatory - Antiviral - Anticoagulant
Pullulan	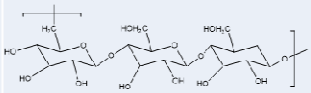	Microbial	Nonionic	- Water soluble - Non-toxic - Immunogenic - Biodegradable
Heparin	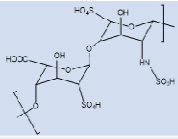	Animal	Anionic	- anti-coagulant - Anti-inflammaroty
Starch	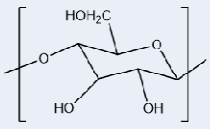	Plant	Nonionic	- non-toxic - Biodegradable

1.1.4 Transition

In 1993, Akiyoshi disclosed that polysaccharides partially modified with hydrophobic moieties could form nanoparticles through a self-assembly process in an aqueous environment[62]. They modified various polysaccharides with palmitoyl/long alkyl chains or cholesterol to form self-aggregates[62–66]. Since then, modification of polysaccharides to synthesize amphiphilic molecules is among the most prominent methods to produce self-assembled nanostructures, as the numerous functionalities along the polysaccharide backbone facilitate attachment of a hydrophobic moiety[29,51,67,68].

The performance of drug carriers relies on key properties: their size, stability, loading capacity, release kinetics, circulation time and biodistribution. The shape and hydrophobic/hydrophilic balance of the amphiphile control the morphology of the self-assemblies morphology which in turn control those propertie[23,65]. More precisely, the factors which impact the nanostructuration of hydrophobized polysaccharides include the nature, size and distribution of the hydrophobic moiety, the nature and size of the polysaccharide, as well as the preparation method and surrounding environment. Thus, controlling the self-assembly to synthesize matrices with distinctive architectures is essential. Self-assembled polysaccharides as drug delivery systems have been reviewed[51,53,62,68,69], but the nanostructuration of hydrophobized polysaccharides in aqueous solutions and the effect of the different parameters which control it has remained virtually unexplored.

1.2 NANOSTRUCTURATION OF THE NANOGELS

1.2.1 Self- assembly mechanism

1.2.1.1 Introduction

Self-assembly is a bottom-up process: during fabrication, molecules spontaneously associate in a disorder-to-order transition through noncovalent interaction with each other, such as van der Waals,

hydrophobic and hydrogen-bonding[70]. It is driven by competing interactions between the incompatibility of moieties and covalent bonding of those moieties within the same molecule. As a result, instead of forming separate homogeneous macroscopic phases, the system can stabilize into microdomain structures.

Hydrophobization of water-soluble polymers drastically changes their solution properties as the polymer conformation is controlled by the association of hydrophobic moieties in aqueous media. The hydrophilic characteristic of polysaccharides is attributed to the polarity of their hydroxyl groups through the formation of hydrogen bonds with water[71,72]. When conjugated with hydrophobic segments, the resulting amphiphilic copolymers self-assemble in response to a shift in the hydrophobic/hydrophilic balance. In this case, the competing interactions are between the solvation of the hydrophilic blocks by water molecules and the exclusion of the hydrophobic blocks from the aqueous medium, thus inducing the self-assembly process in order to minimize the interfacial energy of the system[73,74]. Different approaches have been used to study the interaction and nanostructuration of amphiphilic molecules such as viscosity[75,76], light scattering[62], fluorescent spectroscopy[62], nuclear magnetic resonance[77,78] (NMR) or electron microscopy[79].

1.2.1.2 Critical aggregation concentration

The critical micelle concentration (CMC) is the lowest polymer concentration at which molecules can self-assemble into micelles in aqueous solutions. It is an indicator of micellization ability and micelle stability. Although the self-assemblies might not have a micelle structure, the same concept applies and is called critical aggregation concentration (CAC). Lower CAC values indicate a strong tendency towards formation of stable nanogels. This characteristic is crucial for drug delivery applications as it indicates the nano-aggregate stability when subjected to extensive dilution or "sink conditions" (such

as when circulating in the bloodstream). Therefore, a low CAC is critical to ensuring the morphology of the particle until reaching the target site.

The CAC is often measured using a fluorescence technique using pyrene as a fluorescence probe[77,80–82] to monitor the occurrence, above a given concentration, of aggregates with hydrophobic domains. Upon aggregation of the amphiphilic copolymers, the preferential partitioning of pyrene into the hydrophobic cores of the nanogel occurs, inducing a shift from 335 to 338 nm in the excitation spectra. CAC can also be found by measuring the surface tension of series dilutions of copolymer[83]. Before reaching the CAC, the surface tension decreases strongly with the copolymer concentration as they partition into the air-water interface removing the hydrophobic segments from contact with water and covering the surface. Upon reaching CAC, the addition of further amphiphilic molecules results in aggregation, still in order to decrease the contact area of hydrophobic parts with water, while the surface tension remains relatively constant. The change of slope when plotting the surface tension versus concentrations thus indicates the CAC.

1.2.1.3 Size

The size of the nanogels is a critical factor of drug delivery systems as it largely influences the circulation time and organ distribution of the vehicle[84]. Particles of below 5 μm are able to circulate through small capillaries and particles below 200 nm are less susceptible to clearance through the reticuloendothelial system[84]. Furthermore, particles with a size of less than 200 nm possess the unique feature of selective accumulation in tumor tissue because of their enhanced permeation and retention (EPR) effect[85,86]. Bimodal population distribution is a common problem with block copolymer micelles[87], the large aggregates corresponding to clusters of individual primary micelles due to hydrophobic interactions between the cores of the micelles[87,88]. Unpredictable change in both the

drug's pharmacokinetic parameters and organ biodistribution may result from a broad micelle size distribution.

1.2.1.4 Structure

To assess the structure of aggregates generated from their amphiphilic polysaccharide derivative in aqueous media, Nagahama et al. used NMR, dissolving their copolymer in two different solvent systems: DMSO-d6 and D_2O. As the molecule completely dissolved in DMSO-d6, characteristic peaks of hydrophilic and hydrophobic moieties were observed. In D_2O however, the peaks of the hydrophobic units disappeared, indicating their formation into hydrophobic domains. The peaks of the polysaccharide could still be observed, suggesting the formation of a hydrophilic skeleton[62,77]. However, this method does not give information on the repartition of the hydrophobic domains within the hydrophilic mesh.

A very recent study from Guo et al. on (L-phenylalanine ethyl ester)-modified hyaluronic acid (HA-Phe) reported the formation of vesicles[79]. Their conclusions on the nanostructuration were supported by TEM images showing a clear contrast between the periphery and the central area characteristic of the vesicles[89], and SEM pictures displaying spherical particles with holes on their surface provided evidence to hollow interiors[90]. They suggested that the hydrophobic chains formed a middle layer in the vesicle wall sandwiched by two outer layers of water-associated HA which maintained the stability of the vesicles. The authors hypothesized that the structure was due to stronger hydrophilicity of HA-Phe.

Hydrophobic modification of one end of the polysaccharide creates diblock copolymers with a hydrophilic segment and a hydrophobic segment. They can be described as polymer surfactants and are able to form micelle-like associations with a core-shell structure in aqueous solutions[80,81]. The

association of amphiphilic diblock copolymers made of a hydrophilic head and hydrophobic tail has been extensively studied and the good understanding of the self-assembling mechanism allow to predict the geometry of the resulting aggregates[31,91–94]. In the case of polysaccharides hydrophobically modified along their backbone creating comb-like copolymers, core-shell structures are often assumed without proof of the uniqueness of the hydrophobic domain[95–99]. Unlike end modified polysaccharides, introduction of hydrophobic moieties by chemical modification leads to a relatively regular distribution of the hydrophobic units throughout the copolymer[75]. While the expected feature is that the minority component gathers into domains within a matrix created by the majority component, various morphologies might be formed[23].

The intra-particle distribution of hydrophobic domains has first been investigated by Akiyoshi et al.[63,82] using a fluorescence quenching technique to estimate the number of associating cholesterol moieties in one particle. They showed that the cholesterol moieties associated into noncovalent cross-links forming multiple hydrophobic micro-domains in the highly stable hydrogel network, rather than a single hydrophobic core[62,82,100]. Thus, while other groups suggested rearrangement into a hydrophobic core and a hydrophilic shell[70,101,102], Akiyoshi et al. proposed a polycore model as a plausible structure for their nanoparticle[82]. These physical crosslinks are confined within the hydrophilic network and justify that the nanostructure be referred to as "nanogel"[103]. Since then, other studies have reported the self-assembly of hydrophobized polysaccharides into nanogels with multiple hydrophobic cores[104,105].

The hydrophobic core being single versus multiple hydrophobic domains has been reported to be dependent upon the concentration of the amphiphilic polysaccharide[106], the nature of the hydrophobic group used for polysaccharide modification[107], and the degree of substitution of the hydrophobic group along the polysaccharide backbone[106,107]. The nanostructuration of the

amphiphilic polymers is hard to predict as several of those parameters vary from one study to another (Figure 1-1).

For instance, dextran was hydrophobized with poly(D,L-lactide) (PLA) by grafting a PLA chain at one end[108], or several chains along its backbone[109]. The block polymer, presenting a surfactant-like diblock structure, i.e. with a hydrophilic side/head and a hydrophilic side/tale, was reported to self-assemble into core-shell structured particles. However, the comb-like copolymer of dextran grafted with PLA side chains formed nanogels with a hydrophobic polycore into hydrophilic skeleton structure.

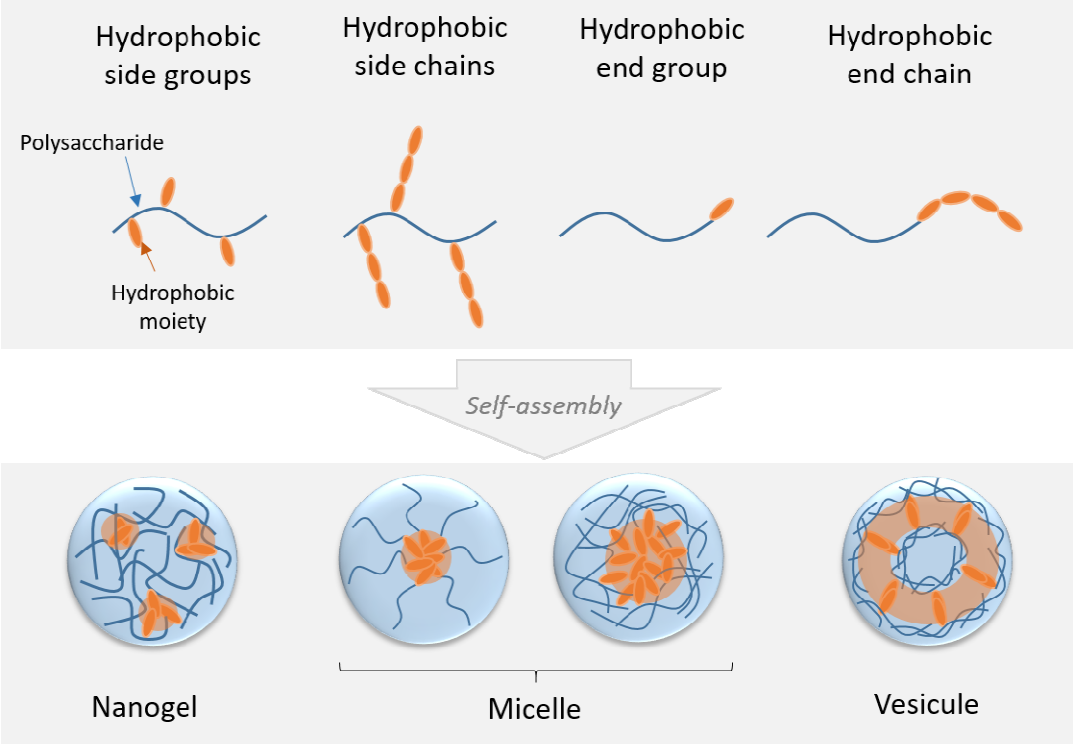

Figure 1-1: Schematic representation of the possible structures of the self-assembled nano-aggregates

1.2.1.5 Parameters

Polysaccharides can be hydrophobized on one end, on both ends, forming block-copolymers, but also by grafting hydrophobic groups or even hydrophobic chains along the backbone, creating a comb-like molecule. The strength of hydrophobic interaction, corresponding to the free energy change, depends on both the number of hydrophobic units and their relative hydrophobicity[75]. However, as seen above with the nanogel structure, the distribution of the hydrophobic groups is also in important factor[74,110,111]. For instance, it has been reported that two copolymers with the same molar quantity of hydrophobic units, one in which they are in blocks and the other in which they are dispersed as discrete units, had very different viscosities[75]. They were higher for the block copolymer as the hydrophobic segments are more likely to form inter- and intra-molecular interactions and aggregates, while single units are more easily solubilized. Thus, the rearrangement of amphiphilic polysaccharides depends on many parameters, such as the nature of the polysaccharide and hydrophobic moiety, their size, the degree of substitution and how they are distributed, the copolymer concentration, as well as the surrounding characteristics of the medium and the preparation technic. All of these parameters make the resulting nanostructure difficult to predict. For each new polysaccharide derivative, the effect of at most a couple of those parameters is usually investigated. Herein the results of studies on self-assembled hydrophobized polysaccharides are combined with the aim of finding general trends and better understanding how all those parameters affect molecular association.

1.2.2 Tuning of the nanogel characteristics and properties

1.2.2.1 Impact of the polysaccharide structure

Copolymer self-assembly is directly connected with the chemical structure[23]. Few studies compare nanogels formed with different types of polysaccharides equally hydrophobized with the same

hydrophobic moiety. Akiyoshi et al. presented a comparative study of cholesterol-modified highly branched mannan (CHM) and cholesterol modified pullulan (CHP) with identical molar mass and level of cholesteryl substitution[64]. While both amphiphilic copolymers formed highly hydrated nanogels in water through the association of the cholesteryl moieties in a similar manner, the structure and level of hydration of the polysaccharide backbone significantly affected the structure of the aggregates and the micro-viscosity of the hydrophobic domains. Compared to CHP, CHM nanogels presented a lower density, a larger hydrodynamic radius, a smaller aggregation number (number of copolymer molecule in one nanogel, N_{agg}) and twice as many cholesteryl moieties per hydrophobic domains. Those differences were attributed to the mobility of the cholesteryl groups predominantly linked to short branches in the case of mannan, whereas they were linked to the main pullulan chain in CHP. The conformational flexibility has been shown by several studies to influence the characteristics of self-assembled structures[29,112].

1.2.2.2 Impact of the degree of hydrophobization

Hydrophobic moieties can be introduced by linking a hydrophobic group, a preformed polymer or by polymerization of a monomer at the end(s) of the polysaccharide chain or along its backbone. The degree of hydrophobization (DH) is defined in this thesis as the extent of hydrophobic modification of the polysaccharide. It increases with the hydrophobicity of the moiety, the degree of substitution (DS) or, in the case of hydrophobic monomers, the degree of polymerization (DP). The hydrophobic domains are postulated to serve as the cargo space for hydrophobic drugs. Thus, in order to exploit the loading space available, it is necessary to understand the impact of the hydrophobic segment characteristics.

1.2.2.2.1 Impact of the nature of the hydrophobic moiety

The structure or hydrophobicity of the hydrophobic group has been shown to influence the size, density and stability of the nanoparticles[65]. Indeed, intra- and intermolecular interactions among the hydrophobic units is the main driving force for self-assembly, so their physiochemical properties are expected to affect the ability to form nanogels. Higher hydrophobic nature of the pendant group expectedly led to more strongly driven assemblies inducing lower CAC values, as shown in a study comparing dextran modified with different bile acids with the same degree of substitution[107].

Nagahama et al. compared poly(L-lactide)-grafted dextran (Dex-g-PLLA) with dextran-cholesterol conjugate (Dex-Chol) with a similar hydrophobic unit content (in terms of weight) [77] to investigate the effect of the nature of the hydrophobic unit. Dex-Chol formed nanogels with significantly larger sizes compared to Dex-g-PLLA nanogels, suggesting that the difference in character between PLLA side-chains and cholesterol side-groups played an important role in the nanogel forming behavior. Dex-Chol showed a significantly higher CAC (thus lower stability) compared to Dex-g(PLLA) with a similar hydrophobic unit content. However, cholesterol is a low molecular weight compound and PLLA is a macromolecule with a relatively longer chain, Dex-Chol therefore possesses a higher DS than Dex-g-PLLA. To explain the lower stability of Dex-Chol, the authors suggested the existence of an interaction other than hydrophobic - entanglement - leading to lower CAC values. However, entanglement occurs once the molecules are self-assembled, while CAC characterizes the concentration at which the amphiphilic molecules start to self-assemble. The length of the PLLA chains and their topology as hydrophobic blocks (compared to the more numerous but discrete cholesteryl groups scattered along the backbone) are harder to solubilize as explained above[75], hence aggregate at lower concentrations explaining the lower CAC values. Dex-Chol nanogels showed a significantly faster dissociation rate than Dex-g-PLLA nanogels with similar hydrophobic content

because of gradual hydrolysis of the numerous ester bonds of PLLA chains inducing gradual erosion, and Dex-g-PLLA assemblies exhibited higher colloidal stability in the presence of destabilizing agent. Higher entrapment efficiencies of lysozyme also revealed a larger mesh size and higher flexibility of the dextran network in Dex-Chol nanogels, characteristics which might also have contributed in their faster dissociation rate.

Therefore, many parameters are to be taken into account when considering the nature of the hydrophobic moiety. Its hydrophobicity but also its size, chemical structure and charge can all influence the assembling process of the amphiphilic derivative.

1.2.2.2.2 Impact of the degree of substitution

The degree of substitution (DS) characterizes the number/frequency of hydrophobic units (groups or chains) along the backbone, hence it does not apply to end-modified polysaccharides. It is the most investigated parameter in the self-assembling mechanism of hydrophobized polysaccharides. It is generally controlled by varying the feed ratio of the hydrophobic moiety[95,96,113,114], polysaccharide concentration[74], and reported as the number of units per polysaccharide chain or per hundred anhydroglucos units[62,96,115].

All studies report that higher DS result in stronger self-assembly interactions[70,95,96], which is expected as higher substitution of the same hydrophobic moiety implies higher hydrophobic content (higher DH). There is thus a stronger tendency to maintain the conformational structure of the nanogel based on hydrophobic interaction. However, the higher DS is not necessarily better as excessive hydrophobicity can lead to precipitation of the copolymer in aqueous media instead of self-assembly[116].

1.2.2.2.2.1 Size

While some studies report that with increasing DS, particles tend to become larger and less uniform[117], and others find no impact at all[109], most studies show that the size of the self-aggregates decreases when increasing the DS[63,74,79,95–97,113,115,116,118,119]. It appears that increasing the content of hydrophobic segment in the copolymer would not lead to expanded volume, but rather results in the shrinkage of the aggregates driven by enhanced hydrophobic interactions. Indeed, higher frequency of hydrophobic units along the polysaccharide would induce stronger assembly into a more condensed mesh[63]. Assuming a homogeneous distribution of the hydrophobic domains in a nanogel, Akiyoshi et al. estimated the average distance between the hydrophobic domains and found indeed that it decreased with increasing the DS[63], results supporting the hypothesis of a more compact matrix.

Conversely, lower hydrophobic modification implies stronger hydophilicity of the polysaccharide derivative which then leads to molecules that self-assemble into looser thus more swollen particles[79,120]. When considering assemblies with a vesicle structure, Zhang found that increasing the modification degree would form smaller vesicles but also result in an increase in their wall thickness[79].

1.2.2.2.2.2 CAC

Higher DS implies higher hydrophobicity of the overall copolymer. Thus, the same way lower CAC values were obtained for moieties with a higher hydrophobicity, the same trend was observed when increasing the DS. All studies thus reported that polysaccharides with higher hydrophobic substitutions presented a lower CAC value[74,77,95,97,107,109,115,116]. The aqueous solubility of the copolymer decreases when increasing the DS[97], as the increase of hydrophobic groups enforces the

hydrophobicity of the polysaccharide derivative facilitating aggregation in aqueous media and leading to smaller CAC values.

When self-assembling particles by adding water to a solution of cinnamic acid modified dextran, Zhang et al. showed that less water was needed to induce aggregation when increasing the DS[113]. While CAC studies showed that fewer copolymers are needed to trigger self-assembly, these results showed the same mechanism in a reverse manner; a higher content of hydrophobic moieties leads to the necessity for a lower water content is to induce the hydrophobic aggregation to balance the reduced solubility.

1.2.2.2.2.3 Dissociation

When comparing the effect of the DS on dextran grafted with PLLA side-chains, Nagahama et al. showed that higher DS led to slower dissociation rate as the higher hydrophobic content induced a stronger cohesion of the assemblies[77]. Other studies have also indicated that more highly-substituted polysaccharides were more stable against hydrolysis[117]. In addition, more PLLA chains also suggests that there are more ester bonds to be hydrolyzed in order to dissociate the nano-aggregates.

1.2.2.2.2.4 Drug loading and release

Generally, higher loading efficiencies were achieved with higher DS[74,95], indicating that more hydrophobic groups in the amphiphilic polymer improves its association in aqueous solution and thus facilitates drug loading. These results could also be due to higher affinity between the more numerous hydrophobic substituents and the hydrophobic drug[87,121]. For example, Wu et al. found that with lower DS of deoxychloric acid on chitosan, the aggregates could not form nanocomplexes with bovine serum albumin because of weaker interaction between the hydrophobic segments and the protein[121]. The increased loading capacity could also be attributed to larger hydrophobic domains. Indeed, there are more hydrophobic units, hence the hydrophobic domains are more numerous or

composed of more hydrophobic moieties, or higher nanogel concentration for equal copolymer concentration (assuming a smaller aggregation number). A study from Akiyoshi et al. showed that the number of hydrophobic domains in a particle increased with increasing DS while the number of hydrophobic moieties in each domain was almost independent[63]. Thus, more hydrophobic segments are available to interact and provide space to entrap drug molecules. While higher DS leads blank nanogels to shrink in aqueous media, the size change in water is due to the decreased swelling of the hydrophilic network. The trend is reversed in the dry state; the hydrophobic domains are therefore larger and can lodge more drug. Further, while the hydrophobic domains should have a high loading capacity and allow for a controlled drug release profile, the compatibility of the drug with the substituents has also been found to be a key determinant for the carrier efficiency[121,122].

It has been reported that higher DS induced slower release of the payload[77]. These results were interpreted as the consequence of the slower dissociation behavior[77], but Nagahama et al. also suggested that higher DS might induce smaller mesh size[77]. Indeed, the self-assemblies might be denser as the hydrophobic segments are more numerous thus closer along the polysaccharide backbone, inducing a more compact polymeric mesh. This could also explain the results of higher hydrophobicity inducing higher interaction with the hydrophobic drug.

1.2.2.2.3 Impact of hydrophobic chain length

The impact of the chain length has been much less studied. Indeed, even though the degree of polymerization (DP) is not always applicable as it concerns polymeric hydrophobic moieties, studies grafting side chains along the polysaccharide backbone generally only investigate the degree of substitution[77,96]. Like DS, increasing the DP – corresponding to the length of the side chains - results in higher hydrophobic content, thus stronger self-assembly interactions[70].

1.2.2.2.3.1 Polymer surfactant

Nichifor et al. reported the synthesis of dextran derivatives with hydrophobic alkyl end groups of different lengths[80]. The copolymer thus presented a surfactant di-block structure resulting in the formation of micelles. They found that CAC decreased with increasing the length of the alkyl chains, which is in concordance with previously described studies for the DS as longer hydrophobic chains mean higher hydrophobicity. Thus longer chains also imply enhanced stability of colloids, which is in accordance with other studies on polymeric micelles[81,87]. The aggregation number was significantly decreased by increasing the alkyl chain length. This could be attributed to steric hindrance of the long chains, and/or less molecules necessary to form and stabilize aggregates due to the higher hydrophobicity. When studying the size, all polymeric surfactants showed a bimodal distribution: the smaller population identified as single micelles and the larger population as clusters of associated micelles. The size and relative percent of the two populations depended on the alkyl end group length. Longer alkyl chains decreased the size of single micelles but enhanced their tendency to aggregate. Those results were attributed to the lower N_{agg}.

Other studies investigating the impact of the hydrophobic chain length reported increased micelle size for longer hydrophobic segments[108,123]. These results could be explained by the presence of larger hydrophobic cores due to the larger hydrophobic segments, and possibly less packed depending on chain flexibility. For polymer surfactants, an increase in the length of the hydrophobic block has been found to change the partition coefficient of the drug between the micelles and the external medium in favor of the core[87], thus increasing drug loading. As with the DS, the longer hydrophobic segment might provide higher interactions with the hydrophobic drug, but also provide a larger space to entrap the drug molecules. A longer hydrophobic segment has also been found to result in slower

drug release, which may be attributed to a stronger hydrophobic interaction between the drug and the hydrophobic core[123].

1.2.2.2.3.2 Comb-like copolymer

Nagahama et al. studied the impact of chain length on a comb-like copolymer of polylactide grafted dextran[109], and in this case, a polycore structure was assumed in this study. The different geometry of the copolymer might be the reason for the variation in the structure of the resulting nanogels, as unlike polymer surfactants, comb-like copolymers can not only show intermolecular but also intramolecular interactions. As for end-modified polysaccharides, they found that longer hydrophobic chains induced lower CAC values, but reported much larger particles. It is noticeable that while increasing the DS was reported to decrease the size of the aggregates, longer chains increased their size for both block and grafted copolymers. As in both cases the hydrophobicity of the copolymer increases with the amount of hydrophobic units, the size change is most likely controlled by their distribution within the copolymer. Higher DS means that the hydrophobic segments are more frequent, hence closer along the polysaccharide backbone, preventing the hydrophobic chain from expanding in water and thus impeding the swelling ability of the nanogel. For block and grafted copolymers, increasing the length of the hydrophobic segment does not reduce the expansion ability of the hydrophilic block or backbone. In all cases the increased amount of hydrophobic units increases the volume of hydrophobic domains as mentioned earlier. So with longer chains, as the swelling remains the same the overall size of the particle increases, while with more numerous chains the decreased swelling prevails inducing smaller particles.

When considering longer hydrophobic side chains for a same DS, both the higher degree of hydrophobization and the distribution can be factors contributing to the observed change. Therefore, it would be interesting to compare comb-like polymers with the same hydrophobic content, but

distributed throughout the polysaccharide among many short chains or fewer long chains in order to investigate the effect of the copolymer structure alone.

The extent of the influence of the length of the side chains also depends on the overall size of the molecule, specifically the size of the hydrophilic polysaccharide segment[80]. Varying DP would have a much stronger impact on a shorter polysaccharide and this impact is reduced by increasing the molar mass of the polymer backbone. The key parameter here might be the ratio of the length of the side chains compared to the length of the backbone.

1.2.2.3 Impact of the polysaccharide molecular weight

The length of the backbone polymer has been reported to affect self-assembly of the nanoparticle[13]. Nichifor et al. studied the effect of the polysaccharide length on their dextran based polymer surfactant[80]. They found that CAC values decreased with decreasing dextran length. Considering that the polysaccharide chain is the hydrophilic part of the copolymer, a shorter chain means an overall more hydrophobic molecule. The derivatives are thus more strongly driven towards self-assembly. As for the length of the hydrophobic block, particles presented a decreasing N_{agg} when increasing MW of dextran. Steric hindrance of the long polysaccharide chains forming the hydrophilic shell might limit the number of molecules forming each aggregate. Those results on CAC and N_{agg} are in accordance with previous reports on block copolymer aggregates[87]. It was also found that longer polysaccharide chains increased the size of the micelles[80,87]. Indeed, the longer hydrophilic block forms thicker shell and provides higher swelling ability. A study of a block copolymer of dextran and PLA reported a reverse effect of the MW of dextran[108] which was attributed to its ability to "fold-down" into a mushroom conformation[124].

Very few studies investigate the impact of the polysaccharide length as the backbone of a comb-like structured copolymer. Zhang et al. compared nanogels of poly(ε-caprolactone) grafted trimethylated chitosan with two different chitosan molecular weights[125]. They found that the CAC of aggregates decreased when increasing the chitosan MW. Those results were explained by the fact that at similar DS, longer chains were grafted with more PCL side chains than the shorter ones, thereby favoring intramolecular hydrophobic interactions and lowering the concentration necessary for aggregation. They also reported that a shorter chitosan backbone resulted in smaller particles, in concordance with a study from Akiyoshi et al. showing that the aggregation number decreased when increasing the polysaccharide MW while the hydrodynamic diameter of the aggregate increased[63].

1.2.2.4 Impact of other parameters

Some studies reported that the formation of the particles strongly depended on preparation parameters such as the method used for self-assembly, the solvent used or the concentration of polymer solution[87,117]. For instance, Hornig et al. compared particles synthesized by dropping acetone into water or adding water into acetone[117]. Small and uniformly sized particles were obtained in the first case while the second method lead to larger particles. In a study from Zhang et al. self-assembly of their cinnamic acid grafted dextran was induced by adding water to a solution of copolymer dissolved in DMF[113]. This method resulted in the formation of bowl-shaped structures with a dimple on the surface. DMF remaining inside the aggregate during the formation process would, upon water addition, move to the thinner wall as a solvent "bubble" under the action of asymmetry force and finally break through, resulting in the formation of the dimple. A very slow rate of water addition did not induce dimple formation. The slow change in water concentration would indeed allow more homogeneous mixing and slower self-assembly, preventing the formation of a DMF bubble entrapped within the aggregates.

The method of particle formation depends on the degree of hydrophobization. For amphiphiles with high solubility, the self-assembly process could be accomplished by direct dissolution with slight stirring[95,126,127], while those with low solubility due to high MW or strong hydrogen bonds require the assistance of sonication[106,118,128]. For derivatives with high hydrophobic modification, dissolution in organic solvents and dialysis against water is necessary to initiate self-assembly[95,129].

Several other groups have reported that the copolymer concentration influenced the particle formation in terms of size and shape of the aggregates[70,107,113,117]. However, once the particles formed, Nichifor et al. compared solutions of different concentrations and only observed a low influence of dilution on aggregate size for their polymer surfactant[80]. The characteristics of the surrounding medium, including pH, temperature and electrolyte concentration, have also been found to strongly influence molecular interactions, thus modifying the size and shape of the structures[70].

1.2.3 Summary

The degree of hydrophobization (through the nature of the hydrophobic moiety, its distribution on the polysaccharide and its length), the nature and molecular weight of the polysaccharide, the preparation technique and the surrounding media, alter the properties of self-assembled nanogels. Comprehending the impact of these different levers on the self-assemblies structures and properties is key to tailoring their size, surface charge, loading efficiency, stability, swelling capacity and degradation for specific drug delivery applications. However, many of the performance related properties are influenced by the same factors, and while some general rules seem to apply, the nature of moieties involved and the chemistry used maintain a large degree of unpredictability. It is therefore difficult to design nanogels which possess all of the ideal characteristics.

1.3 APPLICATION TO DRUG DELIVERY

1.3.1 Introduction

In this part of the review, the most recent studies on self-assemblies made of hydrophobized polysaccharides focusing on their application and performance as drug delivery systems will be discussed. Drugs can be loaded within the nanogels or covalently linked to the polymer chains thus acting, at the same time, as the hydrophobic moiety responsible for the self-assembly. In general terms, the drug release mechanism will depend upon the rate of diffusion of the drug from the carrier, the stability of the aggregate and/or the rate of biodegradation of the copolymer. In case of good stability and slow biodegradation, other factors will control the kinetics, such as material-drug interactions, molecular weight of the copolymer, hydrophobic-hydrophilic balance, localization of the drug within the nanogel, amount loaded and dimensions of the nanogels, among others.

1.3.2 Dextran

1.3.2.1 Introduction

Dextran, mainly obtained from enzymatic processes performed by specific bacterial species[46,130], is a high molecular weight polysaccharide consisting of α-1,6-linked D-glucopyranoses with some degree of 1,3-branching. Highly water soluble, it is biocompatible, biodegradable and resistant to protein adsorption[47]. It also presents a large quantity of hydroxyl groups per monomer unit, available for chemical modification via reactive hydroxyl chemistries[47].

1.3.2.2 Dextran modified with polycaprolactone

Several studies on nano-aggregate preparation from dextran-Poly (ε-caprolactone) copolymers have been reported. Poly(ε-caprolactone) (PCL) is a hydrophobic polyester with excellent biodegradability,

biocompatibility, low immunogenicity, nontoxicity, good mechanical and thermoplastic properties. It has been frequently applied as an implantable biomedical material and sustainable bionanocomposite[131–133], and has been used as the hydrophobic component in micelle-forming materials[134,135].

Liu and coworkers synthesized diblock copolymers of dextran and PCL[36]. They self-assembled into spherical particles with diameters ranging from 20 to 50 nm and a CMC of 0.06 mg/ml. When applied to the release of doxorubicin[123], those nanogels made of dextran-b-poly(ε-caprolactone) diblock copolymers showed a drug loading content of 8.47–10.43% and an encapsulation efficiency of about 40–50%. Larger sizes (90-125 nm) of black particles were reported in this study with a slight increase upon drug loading, while maintaining a narrow distribution. After a 10-hour burst of 40%, doxorubicin was released in a sustained manner up to 70-80% in 96 hours, depending on the PCL length. Doxorubicin was shown to remain pharmacologically active after encapsulation, and the loaded carriers were found to be easily taken up by SH-SY5Y cells. Another group reported the synthesis of disulfide-linked dextran-b-poly(ε-caprolactone) diblock copolymer for the formation of reduction-responsive biodegradable micelles and tested them for triggered release of doxorubicin in vitro and inside cells[136].

More recently, amphiphilic copolymers of poly(ε-caprolactone)-grafted dextran (Dx-g-PCL) were synthesized by ring opening polymerization[137]. The Dx-g-PCL nano-aggregates were prepared by emulsion and solvent evaporation, using poly(ethylene glycol) (PEG) as a stabilizing agent to prevent agglomeration, and resulting in spherical particles of an average size of 86 nm. These showed an entrapment efficiency of Amoxicillin of 78% (w/w) with decreased stability when loaded with the drug. The quick 50 hour release of 85% of the drug was followed by a plateau stage suggesting that

the drug might be located in the micellar shell and was released by a combination of diffusion and eroding mechanisms.

1.3.2.3 Dextran modified with poly(D,L-lactide)

Polylactide (PLA) is a biodegradable and biocompatible polymer that is widely used in the biomedical field[138,139]. A self-assembling block copolymer of dextran and poly(D,L-lactide) (Dex-b-PLA) was developed and reported to form particles with core-shell structures[108]. Their size could be precisely tuned in the 15-70 nm range by altering the molecular weight of the blocks. Using doxorubicin as a model drug, the nanogels could carry up to 21% (w/w) of the drug payload, and provided sustained release for over 6 days. By tuning of the copolymer molecular weight, a long circulation lifetime almost eight times longer than PEG-coated nanoparticles could be achieved.

Dextran was also hydrophobized with PLA by grafting PLA chains onto the polysaccharide backbone[109]. The resulting copolymers were able to spontaneously self-assemble into spherical nanogels with a hydrophobic polycore and hydrophilic skeleton structure. They exhibited hydrodynamic diameters ranging from 16 to 73 nm and CAC varying between 2.1-8.0 mg/L. A DLS study over time revealed that the nanogels dissociated by hydrolysis. Size, stability and degradation could be tuned by varying the size and number of PLA chains.

1.3.2.4 Dextran modified with cholesterol

PLA grafted dextran (dex-g-PLLA) was compared to dextran modified with cholesterol (dex-chol) with varying hydrophobic unit content[77]. Dex-chol self-assembled into nanogels of 125 nm, with a CAC of 12.6×10^{-4} wt%. Their size decreased due to fast dissociation upon collapsing of the cholesterol cores by hydrolysis of the ester bond.

1.3.2.5 Protein release from Dex-g-PLLA and Dex-Chol

The self-aggregates made of Dex-g-PLLA and Dex-Chol were studied for entrapment and release of protein[77]. Entrapment of lysozyme during nanogel formation was shown to be more successful than the soaking method, and the loading efficiency and release kinetics could be controlled with the hydrophobic content. The amount of protein encapsulated increased by increasing the initial amount of protein, showing great potential of the inner space of the nanogels for lysozyme loading. At 3mg/mL protein, Dex-g-PLLA showed 5.1-6.3% loading capacity while Dex-Chol showed approximately 8.2%. The nanogel size increased when loading increased for both copolymers, indicating that the change can be attributed to an increase in physical space and swelling capacity due to the loaded hydrophilic lysozyme. Although slightly faster for Dex-Chol, all nanogels exhibited a sustained release over 1 week without any initial burst release, and conservation of the lysozyme structure.

1.3.2.6 Dextran functionalized with poorly water-soluble drugs (ibuprofen, naproxen)

The hydrophobic moiety can also be the drug itself. Hornig et al. reported the functionalization of dextran with poorly water-soluble drugs (ibuprofen and naproxen)[117]. The resulting amphiphilic molecules self-assembled into nanoparticles in the range of 102-287 nm for the ibuprofen-modified ones, and 177-387 nm for the naproxen-modified ones. The sizes were strongly influenced by the degree of substitution and preparation technique. The particle suspensions remained stable over months solutions with a pH value of between 4 and 11. For the use of those dextran derivatives as potential prodrugs in drug delivery systems, their cleavage under physiological conditions is an essential prerequisite. In a preliminary experiment, dextranase, the enzyme responsible for dextran biodegradation in living organisms[140,141], showed efficient depolymerization of the dextran-drug conjugates.

1.3.3 Chitosan

1.3.3.1 Introduction

Chitosan is a linear heteropolymer consisting of varying amounts of b-(1,4)- linked D-glucosamine and N-acetyl-D-glucosamine. It is obtained by partial deacetylation of chitin, the second most abundant polysaccharide in nature after cellulose[142]. Recognized as biocompatible, chitosan has been demonstrated to be non-toxic in both animal and human models[142,143]. It can be biodegraded by enzymes[144,145], resulting in amino sugars as degradation products which are also non-toxic and completely adsorbed by the human body[146,147]. Unlike chitin which is insoluble in aqueous and many organic solvents, chitosan is soluble in water at low pH by protonation of the free amine groups[147]. Although mainly hydrophilic, the presence of N-acetyl groups induces a slight degree of hydrophobic behavior. Chitosan is the only natural, positively charged polysaccharide[148,149] providing inherent mucoadhesive properties via ionic interaction between its quaternary amino and negative sialic acid groups of mucin[142,146,150,151]. It is also beneficial for cellular uptake and opening of tight junctions[152] through interactions with the negative charges carried by membrane proteins[30,151]. In addition, this cationic nature of chitosan can be manipulated giving pH-responsiveness[13]. Chitosan has well established antibacterial activity[153,154], as it was found to be toxic to several bacteria, fungi and parasites[42]. The backbone is rich in functional groups such as hydroxyl, amino and acetylamino groups, endowing chitosan with versatile chemical properties and allowing chemical modification[155].

This unique combination of properties makes chitosan an extremely useful material in the pharmaceutical and biomedical fields[156] for its application in drug delivery[157,158] and can be tailored to suit to specific use in the form of micro and nanoparticles or hydrogels[159–162]. A recent study reviewed all types of chitosan-based self-assemblies and their application in drug delivery[70]. Chitosan is amphiphilic as the chemical structure of chitosan already includes hydrophobic sites, but its

amphiphilicity is limited as the polysaccharide is unable to self-aggregate in aqueous solution. Besides, only acidic conditions allow solubility of chitosan in water. Thus, chitosan derivatives were prepared to enhance water solubility of the polysaccharide backbone as well as to provide hydrophobic segments to allow self-assembly.

1.3.3.2 Chitosan derivative with phosphorylcholine and deoxycholic acid moieties

A biodegradable amphiphilic chitosan derivative (DCA–PCCs) was synthesized by grafting hydrophilic cell membrane mimic phosphorylcholine (PC) and hydrophobic deoxycholic acid (DCA) moieties along its backbone[121]. A tuned hydrophilic-hydrophobic balance by controlling both DS values DCA allowed the copolymer to self-assemble. Bovine serum albumin (BSA) was used as model protein. BSA loaded nano-complexes had a size of 213 nm with a PDI of 0.195 while the blank nanoparticles had a larger size and size distribution of 285 nm and 0.253 respectively. These results suggest that the interaction between the copolymer and the protein induced smaller aggregates. A biphasic release of BSA following first order exponential decay kinetics was observed with 45% rapidly released at first 12 hours, followed by a slow release up to 72 hours reaching a cumulative release of BSA close to 85%. Both loaded and blank particles showed excellent biocompatibility with cytotoxicity and hemocompatibility assays due to the presence of cell membrane mimic phosphorylcholine

1.3.3.3 Poly(p-dioxanone) end-modified chitosan

An amphiphilic block copolymer of chitosan and poly(p-dioxanone) (PPDO) was synthesized with two different MW of PPDO-macromers[81]. The polymer surfactant could self-assemble into micelles with pH-responsive shells based on chitosan with a CAC in the range of 5-9.10-2 mg/mL. The micelles were 115 nm for the short PPDO copolymer and 77 nm for the long PPDO copolymer. These results are reverse of the previously discussed effect of the length of the hydrophobic block in

polymer surfactant, and were attributed to the fact that the short PPDO chain had poorer crystallization properties resulting in a looser core. Decreasing the pH caused the diameter of the micelles to increase suggesting increased hydrophilicity of the chitosan and swelling of the micelle. Camptothecin was encapsulated into the micelles with a loading of 8.21% and a loading efficiency of 82.05%, and showed much faster release at pH 5.0 than at pH 7.4. The pH-responsive micelles could thus realize differential drug release inside and outside of the cellular environment. Blank particles were found to be nontoxic and the loaded carriers could be effectively internalized by Hela cells and showed potent antitumor cell efficacy.

1.3.3.4 Biotinylated N-palmitoyl chitosan

Chitosan, previously hydrophobized with palmitoyl chloride,[163] was further modified with biotin for active tumor cell targeting[99]. The copolymer self-assembled into positively charged spherical particles with sizes in the range of 300–400 nm and a narrow size distribution. The low content of biotin reduced their diameter compared to assemblies based on N-palmitoyl chitosan reported to be 429 nm, but only induced a slight decrease of the CAC from 0.083 mg/mL to 0.081 mg/mL. The carriers were loaded with docetaxel with an encapsulation efficiency of 79% and a drug loading of 8.92%, improved compared to N-palmitoyl chitosan reported to be 68% and 5.84% respectively. They exhibited a biphasic drug release pattern with an intitial 6-hour burst and a subsequent sustained release phase. A slight pH-dependency was noticed as the release was slower at pH5.5 compared to pH 7.4. The rates were much slower for the biotinylated copolymer, with only 10-20% released in 72 hours compared to 45-60% for the non-biotinylated one. The particles also showed susceptibility to biodegradation and hemocompatibility.

1.3.3.5 Chitosan functionalized with N -acetyl cysteine and vitamin E succinate

Chitosan was modified with N-acetyl cysteine (NAC) as the hydrophilic group and vitamin E succinate as the hydrophobic group[164]. The resulting copolymer was able to self-aggregate into particles with a hydrodynamic diameter in the range of 220-250 nm. The carriers were loaded with paclitaxel, showing significant improvements in pharmacokinetics as the relative bioavailability of the nanoparticle system was 425% compared with a simple paclitaxel solution.

1.3.4 Hyaluronic Acid

1.3.4.1 Introduction

Hyaluronic acid (HA) is a linear, anionic, high molecular weight polysaccharide made up of repeating disaccharide units of D-glucuronic acid and N-acetylglucosamine[43]. It is the only non-sulfated glycosaminoglycan that occurs primarily in vivo as sodium hyaluronate, present in the extracellular matrix. Biocompatible, biodegradable and hydrophilic, it holds remarkable viscoelastic properties and the ability to retain water[165]. Intracellular degradation of HA occurs within a low pH environment, as is the case in the lysosome[165]. It has also shown mucoadhesion through hydrogen bonding[166,167]. HA serving within the extracellular matrix as a direct receptor for cell behavior, is capable of specific recognition to interact with transmembrane glycoprotein CD44, that is over expressed on the surface of different tumor cells[168–170]. HA based nanoparticles hold thus a major advantage over other polysaccharides, which is the ability to combine both passive targeting by utilizing the EPR effect in tumors and active targeting towards the HA receptors overexpressed by the majority of tumors.

1.3.4.2 HA grafted with bromohexyl derivative of riboflavin tetrabutyrate

Di Meo et al. report the synthesis of HA and pullulan grafted with bromohexyl derivative of riboflavin tetrabutyrate[171]. The copolymers presented a different derivatization degree: 30% mol/mol

for HA and only 5% mol/mol for pullulan. The copolymers self-assembled into aggregates with sizes of about 312 and 210 nm for hyaluronan and pullulan respectively. They exhibited long-term stability in water and physiological conditions, and excellent cytocompatibility. Only the HA-based particles were loaded with levofloxacin, a water soluble drug, showing an encapsulation efficiency of 15% w/w, a value higher than was previously obtained with HA-cholesterol derivatives[172,173].

1.3.4.3 HA conjugated with hydrophobic poly(L-histidine) (HA-Phis)

HA was conjugated with hydrophobic poly(L-histidine) (PHis) to prepare a pH-responsive and tumor-targeted copolymer able to self-assemble into a nanocarrier for anti-cancer drugs[118]. Copolymers formed monodispersed spherical aggregates in the range of 150-215 nm with low PDI. Average sizes and zeta potentials could be changed with the DS values. Unlike the tendency reported in most studies, drug loading and encapsulation efficiency of doxorubicin slightly decreased with an increase in the DS. The authors suggested that it could be because the stronger hydrophobicity would result in weak exclusion between the hydrophobic drug and the micellar core region. In vitro drug release studies demonstrated slower doxorubicin release at physiological pH than at lysosomal pH. Studies also showed that the particles were taken up in significant amounts by receptor-mediated endocytosis and doxorubicin was efficiently delivered into cytosol. Therefore, the study suggested that the nanogels could be able to accumulate at the tumor site by the EPR effect, selectively taken up and internalized into the tumor cells via CD44 receptor-mediated endocytosis and transported to lysosomes, where they would release their payload.

1.3.4.4 Alkyl chains grafted HA

HA grafted with alkyl chains self-assembled into nanogels with sizes in the range of 177 to 293 nm, negative surface charge and narrow size distribution[119]. The CAC value was determined to be in the range of 0.1–0.3 mg/mL. Loading amount of budesonide was varied from 5.7 to 9.3%, depending on

the drug to polymer feed ratio. The drug release was divided into three phases based on the release rate. An initial burst of 2 hours corresponding to the budesonide soaked on the nanogel surface, a slower release up to 20 hours corresponding to the diffusion of the drug inside the particles driven by the concentration gradient, and a final plateau phase. The cumulative release in 50 hours was not equal to the total amount of budesonide loaded, attributed to the fact that the particles were still intact at that point and the reduced concentration gradient. The carriers showed an enhanced cellular uptake via CD44 receptor mediated endocytosis and using a cellular model of inflamed intestinal mucosa, the authors demonstrated that the particles may improve the anti-inflammatory efficacy of budesonide.

1.3.4.5 Taxol conjugated HA

Porphyrin modified paclitaxel (PorTaxol) was conjugated with permethyl-β-CD modified HA taking advantage of the strong affinity between porphyrin unit in PorTaxol and the permethyl-β-CD cavity by simply mixing them in aqueous solution[98]. It formed an amphiphilic complex able to self-assemble into nanoparticles made of a hydrophilic HA shell and a hydrophobic PorTaxol core. The spherical assemblies with sizes of around 171 nm were found to be stable. PorTaxol was shown to be released by hyaluronidase-mediated hydrolyzation breaking the HA chains and degrading the complexes. The particles exhibited specific targeting internalization into cancer cells with much lower side effects that regular solution of paclitaxel.

1.3.5 Cellulose and derivatives

1.3.5.1 Introduction

Cellulose is the most abundant polysaccharide in nature. Cellulose fibers constitute the basic structural element of wood and annual plants. It is a linear polymer composed of of (1→4) linked β-

D-glucopyranosyl units. Cellulose has been reported to have outstanding biocompatibillity and biodegradability[174]. Its water insolubility is assigned to inter/intramolecular association, leading to the formation of ordered crystalline regions[175]. The abundant hydroxyl functionalities of cellulose[174] allow chemical modification through various polymerization techniques in order to control elasticity, ion exchangeability, thermal stability and mechanical properties[176–179]. While cellulose is insoluble in water, it has been converted to water-soluble polymer with various chemical modifications. An important class of cellulose derivatives are cellulose ethers, such as methylcellulose (MC), hydroxyethyl cellulose (HEC), hydroxypropyl cellulose (HPC), and hydroxypropyl methylcellulose (HPMC), all of which are commercially available

1.3.5.2 α-tocopherol succinate-conjugated hydroxyethyl cellulose

Tocopherol succinate (TOC), also known as vitamin E succinate, is a lipophilic vitamin[180] which has been recognized as an excellent solvent for many water-insoluble drugs due to its good hydrophobicity[181,182]. TOC has thus been introduced into the backbone of hydroxyethyl cellulose (HEC) as the hydrophobic moiety, and the amphiphilic HEC-TOS conjugates were shown to self-assemble into spherical micelles[95]. They had a size in the range of 24.5-115.1 nm and a CMC of 16-99 μg/ml. By encapsulation, the nanocarriers provided a concentration of paclitaxel about 50 times higher than water, and released their payload over a period of 4 days. Three stages could be identified in the release: an initial burst release of 40.0% in the first 24 hours possibly corresponding to the paclitaxel in the outer shell of the particle, a second slower stage where 40% of the drug was released over the following 3 days, and a final plateau stage where the 20% of drug left remained encapsulated attributed to the low concentration gradient with the outside media or possible interaction of paclitaxel with the conjugates.

1.3.5.3 Linoleic acid conjugated hydroxyethyl cellulose

Linoleic acid (LA) is an essential fatty acid for metabolism in human body which, because of its high hydrophobicity, has been successfully applied to the encapsulation and controlled release of fat-soluble compounds[183]. A series of HEC-g-LA copolymers with different contents of LA were synthesized and showed the ability to self-assemble into monodispersed spherical particles in aqueous solution, stable at room temperature for at least ten days[97]. The sizes and CMC of the aggregates were found to be correlated with the LA content of copolymers, and varied in the range of 20–50 nm and 1.92–21.76 μg/ml, respectively. The carriers were investigated for loading and release of the hydrophobic active component β-carotene. The encapsulation efficiency and loading content changed upon drug concentration in the initial phase and were found to be up to 84.67% (w/w) and 4.23% respectively. β-carotene was gradually released from the nanogels over a period of about 200 hours. A 10 hour initial burst of 20% was followed by a sustained release with a decreasing rate up to 150 hours where it seemed to plateau with 20% of β-carotene remaining the particles.

1.3.5.4 PLA modified cellulose

Many studies report the grafting copolymerization of PLA onto cellulose derivatives[184–187]. A recent study from Guo et al. reports the synthesis of a series of cellulose-graft-PLA copolymers with various structural factors, including grafting ratio, PLA chain length, and final copolymer molecular weight[74]. In this work, self-assembled particles were used as carriers for paclitaxel. Their size varied from 6 to 52 nm and increased when loaded in the range of 97 to 167 nm. The loading capacity was found to increase with DS values of PLA, the highest obtained being a drug loading of 4.97% and encapsulation efficiency of 89.30%. Unfortunately, no release study and cytotoxicity assay were carried out.

1.4 CONCLUSIONS

Polysaccharides partially modified with hydrophobic moieties are able to self-assembled into nanogels in aqueous media. They present a spherical shape and diameters generally below 300 nm with a narrow size distribution and a low CAC. The examples discussed in this review demonstrate that hydrophobized polysaccharide-based nanogels have already offered significant improvements to the field of drug delivery such as increasing drug solubility, controlling its release, protecting it from adverse external environmental factors thus enhancing its efficacy. The large variety of polysaccharides and hydrophobic groups provides infinite possibilities, multiplied by other factors such as distribution of the hydrophobic moiety and other preparation parameters. The effects of different levers on the characteristics and properties of the self-assemblies were reviewed in an effort to gain insight into the role of the polymer structure on intra- and intermolecular interaction, the mechanism of nano-structuration, and the resulting features of the self-aggregates. By providing an overview of general rules on the impact of the hydrophobic/hydrophilic moieties, their size and the copolymer topology, we hope to enable better prediction and tuning of the nanogels to meet the requirements of its application in drug delivery.

1.5 THESIS SCOPE

1.5.1 Ocular drug delivery limitations

The anatomy of the human eye is divided into two regions called the anterior and the posterior segments. The anterior segment composed of the cornea, the conjunctiva, the iris, the ciliary body, the anterior and posterior chambers, the lens, the lachrymal apparatus and the eyelids. The sclera, the choroid, the retina, and the vitreous constitute the posterior segment[188,189]. Eye drops have been globally accepted as a formulation for the management of diseases in the anterior segment of the eye.

Convenient and easy to use, they are still largely preferred over intravitreal or periocular injections and account for 90% of ophthalmic formulations[190,191]. However, topical formulations are associated with some limitations in terms of pharmacological and pharmacokinetic profile, dosing frequency, systemic untoward effects, patient non-compliance, low drug bioavailability, and rapid washout from the ocular surface. Therefore, only 0.1–5% of the topically administered dose is absorbed through the corneal epithelium and roughly 1% reaches the aqueous humor[192–195].

The eye indeed presents numerous barriers to topical drug delivery[196]. The pre-corneal barrier mechanisms include dilution, elimination from the lachrymal fluid either by drainage from the conjunctival sac into the naso-lachrymal duct, conjunctival absorption or clearance by tearing[197–200]. The corneal barrier is mainly the result of the corneal epithelium presenting a pore size in the range of 1-5 nm[201] due to intercellular tight-junctions surrounding epithelial cells, therefore impeding the diffusion of macromolecules as well as hydrophilic molecules via the paracellular route[202]. In addition, the corneal and conjunctival membranes present efflux pumps restricting the entry of substrates into the deeper ocular tissues[203–205]. The sclera also largely influences the pharmacokinetics of drug diffusion[206,207], its highly hydrophilic tissue being a rate-limiting barrier for most lipophilic drugs. The sclera is 10 times more permeable than the cornea and the conjunctiva is 15–25 times more permeable than the sclera[208]. Characteristics of the drug such as hydrophobicity, molecular size, charge, ionization and solubility affect the rate of its penetration in the cornea[209–211].

Thus, because of the structural organization of the eye and its numerous clearance mechanisms, efficient ocular drug delivery remains a major challenge. Ideally, the formulation should specifically and efficiently reach the target tissue to reduce systemic uptake and side effects, provide a sustained and controlled release to maintain therapeutic concentration of the drug for a prolonged period of time, all the while remaining patient friendly.

1.5.2 Particulate systems

Nanocarriers appear as a promising tool to overcome the limitations of conventional delivery systems in ocular drug delivery and the different barriers of the eye[212,213]. Suspended in aqueous solution, they can be administered topically as liquid dosage formulations. Due to their small sizes, they are likely to have high diffusivity across membranes such as the corneal epithelium thereby improving the corneal permeability of drugs via topical administration[192,196,214–216]. Their high surface-area-to-volume ratio may show improved interaction with the outer mucous membrane of the corneal surface, prolonging pre-corneal retention. Slowly cleared and releasing the drug for a longer duration, nanoparticles are expected to enhance the ocular bioavailability and offer sustained therapeutic drug concentration for a longer duration and thereby reduce frequency of administration with improved patient compliance[217,218]. Therefore, nanocarrier-based ocular drug delivery systems have been widely explored for ocular drug delivery as they appear to be a promising strategy to meet its primary requirements of therapeutic efficacy, compliance and safety[196,219,220].

1.5.3 Cellulose in topical drug formulations

Cellulose and its derivatives have been extensively investigated for ophthalmic applications including the synthesis of ophthalmic drug delivery systems. They have been used for artificial tear solutions[221,222]. Early findings suggested that hydroxypropyl methylcellulose provided long coverage and protection for the ocular surface, potentially suitable for patients with severe dry eye[223]. They were also employed as viscosity enhancers in ophthalmic solution and suspension formulations[224–229]. By increasing the viscosity and wettability, cellulose ethers increase the contact time of the drug on the ocular surface and thereby its bioavailability[228,230]. Their film forming ability has been exploited for the synthesis of platforms for the delivery of drugs[231], or drug loaded nanoparticles[232]. Inserts were also developed by film casting and compression moulding[233] such as Lacrysert[234], or as lyophylisate which would hydrate with the tear fluid once deposited in the cul-de-sac[235].

Hydroxypropyl mcethylcellulose has been used with PLGA to make a biodegradable matrix implant, Surodex™ (Allergan, Inc., Irvine, CA), for insertion in the anterior chamber following cataract surgery to control postoperative inflammation[236–239]. Hydroxypropyl methylcellulose and carboxymethyl cellulose were used for the fabrication of a nanowafer, a small transparent circular disc containing arrays of drug loaded nanoreservoirs to be applied on the ocular surface[240]. Transparent cellulose-based hydrogels were also fabricated with a contact lens geometry for use as a corneal bandage immediately following ocular trauma[241]. Some cellulose derivatives such as methylcellulose and hydroxypropyl methylcellulose are temperature responsive. At low concentrations (1–10 wt.%), their aqueous solutions are liquid at low temperature, but gel upon heating. This sol-gel transformation has been exploited to design in situ gelling systems[242]. Ophthalmic in situ gelling vehicles have mainly been developed combining cellulose derivatives with others polymers such as Poloxamer, sodium alginate, polyacrylic acid or Carbopol for scaffold formation in the cul-de-sac of the eye[243–250]. Cellulose derivatives were also added to improve drugs retention or solubility[251,252]. In vivo studies on cellulose or cellulose derivative-based ophthalmic systems demonstrated good in vivo tolerance[236,241,253].

1.5.4 Nanogels of hydrophobized methylcellulose for ocular drug delivery

As a target organ for drug delivery, the eye is physiologically unique. Ocular diseases have been most often treated by topical administration of drug solutions, preferred to systemic routes as they tend to enhance drug distribution to the ocular tissues while minimizing systemic exposure and potential side effects. However, the anterior segment of the eye presents natural barriers such as dosage spill-over, nasolacrimal drainage, blinking, tear film and tear mucin, and low corneal permeability. These clearance mechanisms and biological barriers of the eye allow only 5% or less of the applied dose can reach intraocular tissues[254–257]. All of these factors result in poor drug delivery efficiency of topical formulations. While high drug concentrations and frequent administration are used to achieve

therapeutic efficacy, those strategies have a potential negative impact on therapeutic efficacy and disease control. Patient noncompliance also remains a significant issue with this strategy[258–260]. Improving the bioavailability of drugs to obtain an optimal drug concentration at the target site for a prolonged period of time is therefore one of the biggest challenges in ocular drug delivery.

We hypothesize the widespread acceptability of topical formulations make them a logical target for improving the release kinetics of drugs in the treatment of diseases of the eye, and in particular diseases of the anterior segment. Particulate systems thus appear as a promising approach as suspended in liquid formulations, they can be delivered topically. They have shown the ability to encapsulate bioactive compounds, thereby improving their stability, and to sustain the release of their payload, thus avoiding drug concentration fluctuations. The enhanced ability of particles to cross biological membranes, potentially improved by surface functionalization, is also an attractive feature to overcome the effective clearance mechanisms of the eye, allowing the drug to reach the tissues to be treated. Self-assembly is an attractive method of particle synthesis as it avoids the use of reactive compounds which may damage the bioactive payload. Amphiphilic polymers have demonstrated the ability to spontaneously aggregate in aqueous media into stable suspensions of nano-sized particles composed of a hydrophilic mesh physically crosslinked by hydrophobic domains called "nanogels"[103].

In the current work, self-assembled nanogels of hydrophobized polysaccharides were developed as a potential drug delivery platform to treat diseases in a localized and efficient manner, thereby addressing the limitations of current topical formulations. Biocompatible and biodegradable, polysaccharides appear as an ideal biomaterial choice for the design of nanoparticles. The variety of chemical structures provides them with a great range of physicochemical and biological properties which can be readily tuned by conjugation of different molecules to their numerous functional groups. When modified with hydrophobic moieties, the resulting amphiphilic polysaccharide can self-assemble in aqueous media and spontaneously form highly stable nanogels without harsh synthesis

conditions[261]. Those nano-aggregates can be loaded with therapeutics offering protection against premature degradation as well as enhanced solubility, increasing permeation through longer residence times on the eye and improving pharmacokinetics. The properties of these nanogel carriers can be tailored by the choice of polysaccharide and hydrophobic moiety, and further adjusted with the size and distribution of each segment, in order to match the pharmacokinetic requirements of the therapeutic to be delivered. Furthermore, their surface can be functionalized to target the precorneal tissue for prolonged residence time on the ocular surface allowing enhanced corneal penetration. Therefore, nanogels of self-assembled hydrophobized polysaccharides have tremendous potential to overcome some of the current obstacles of ocular drug delivery and improve the bioavailability of the therapeutics, while remaining patient friendly.

1.6 ACKNOWLEDGEMENTS

Funding support from NSERC and the CREATE Biointerface Training Program is gratefully acknowledged.

1.7 DISCLOSURES

The authors state no conflict of interest.

BIBLIOGRAPHY

1. Kalshetti, P. P., Rajendra, V. B., Dixit, D. N. & Parekh, P. P. HYDROGELS AS A DRUG DELIVERY SYSTEM AND APPLICATIONS : A REVIEW. **4,** (2012).
2. Nayak, S. & Lyon, L. A. Soft nanotechnology with soft nanoparticles. *Angew. Chem. Int. Ed. Engl.* **44,** 7686–708 (2005).
3. Oh, J. K., Drumright, R., Siegwart, D. J. & Matyjaszewski, K. The development of microgels/nanogels for drug delivery applications. *Prog. Polym. Sci.* **33,** 448–477 (2008).
4. Peppas, N. A., Hilt, J. Z., Khademhosseini, A. & Langer, R. Hydrogels in biology and medicine: From molecular principles to bionanotechnology. *Adv. Mater.* **18,** 1345–1360 (2006).
5. Gupta, P., Vermani, K. & Garg, S. Hydrogels: From controlled release to pH-responsive drug delivery. *Drug Discov. Today* **7,** 569–579 (2002).
6. Tao, Y., Liu, R., Chen, M., Yang, C. & Liu, X. Cross-linked micelles of graftlike block copolymer bearing biodegradable ε-caprolactone branches: A novel delivery carrier for paclitaxel. *J. Mater. Chem.* **22,** 373–380 (2012).
7. Li, Y.-Y. *et al.* Dual-vectors of anti-cancer drugs and genes based on pH-sensitive micelles self-assembled from hybrid polypeptide copolymers. *J. Mater. Chem.* **21,** 3100–3106 (2011).
8. Peer, D. *et al.* Nanocarriers as an emerging platform for cancer therapy. *Nat. Nanotechnol.* **2,** 751–760 (2007).
9. Sugahara, S. ichi, Kajiki, M., Kuriyama, H. & Kobayashi, T. ru. Complete regression of xenografted human carcinomas by a paclitaxel-carboxymethyl dextran conjugate (AZ10992). *J. Control. Release* **117,** 40–50 (2007).
10. Vinogradov, S. V., Bronich, T. K. & Kabanov, A. V. Nanosized cationic hydrogels for drug delivery: Preparation, properties and interactions with cells. *Adv. Drug Deliv. Rev.* **54,** 135–147 (2002).
11. Liechty, W. B., Kryscio, D. R., Slaughter, B. V. & Peppas, N. a. Polymers for Drug Delivery Systems. *Annu. Rev. Chem. Biomol. Eng.* **1,** 149–173 (2010).
12. Peng, C., Zhao, Q. & Gao, C. Sustained delivery of doxorubicin by porous CaCO3 and chitosan/alginate multilayers-coated CaCO3 microparticles. *Colloids Surfaces A Physicochem. Eng. Asp.* **353,** 132–139 (2010).
13. Payne, G. F. Biopolymer-based materials: the nanoscale components and their hierarchical assembly. *Curr. Opin. Chem. Biol.* **11,** 214–219 (2007).
14. Cui, W., Li, J. & Decher, G. Self-Assembled Smart Nanocarriers for Targeted Drug Delivery. *Adv. Mater.* **28,** 1302–1311 (2016).
15. Lecommandoux, S. & Garanger, É. Precision polymers with biological activity: Design towards self-assembly and bioactivity. *Comptes Rendus Chim.* **19,** 143–147 (2016).
16. Tahara, Y. & Akiyoshi, K. Current advances in self-assembled nanogel delivery systems for immunotherapy. *Adv. Drug Deliv. Rev.* **95,** 65–76 (2015).
17. Sasaki, Y. & Akiyoshi, K. Self-assembled Nanogel Engineering for Advanced Biomedical Technology. *Chem. Lett.* **41,** 202–208 (2012).
18. Palao-Suay, R., Gómez-Mascaraque, L. G., Aguilar, M. R., Vázquez-Lasa, B. & Román, J. S.

Self-Assembling Polymer Systems for Advanced Treatment of Cancer and Inflammation. *Prog. Polym. Sci.* **53,** 207–248 (2015).

19. Yu, S., Hu, J., Pan, X., Yao, P. & Jiang, M. Stable and pH-sensitive nanogels prepared by self-assembly of chitosan and ovalbumin. *Langmuir* **22,** 2754–2759 (2006).
20. Hirakura, T., Nomura, Y., Aoyama, Y. & Akiyoshi, K. Photoresponsive nanogels formed by the self-assembly of spiropyrane-bearing pullulan that act as artificial molecular chaperones. *Biomacromolecules* **5,** 1804–1809 (2004).
21. Morimoto, N., Qiu, X. P., Winnik, F. M. & Akiyoshi, K. Dual stimuli-responsive nanogels by self-assembly of polysaccharides lightly grafted with thiol-terminated poly(N-isopropylacrylamide) chains. *Macromolecules* **41,** 5985–5987 (2008).
22. Morimoto, N., Obeid, R., Yamane, S., Winnik, F. M. & Akiyoshi, K. Composite nanomaterials by self-assembly and controlled crystallization of poly(2-isopropyl-2-oxazoline)-grafted polysaccharides. *Soft Matter* **5,** 1597 (2009).
23. Khalatur, P. G. & Khokhlov, A. R. Self-organization of amphiphilic polymers. *Polimery/Polymers* **59,** 74–79 (2014).
24. Arot??ar??na, M., Heise, B., Ishaya, S. & Laschewsky, A. Switching the inside and the outside of aggregates of water-soluble block copolymers with double thermoresponsivity. *J. Am. Chem. Soc.* **124,** 3787–3793 (2002).
25. Weaver, J. V. M. *et al.* Preparation of shell cross-linked micelles by polyelectrolyte complexation. *Angew. Chemie - Int. Ed.* **43,** 1389–1392 (2004).
26. Gaucher, G. *et al.* Block copolymer micelles: preparation, characterization and application in drug delivery. *J. Control. release* **109,** 169–188 (2005).
27. Wei, H., Zhuo, R. X. & Zhang, X. Z. Design and development of polymeric micelles with cleavable links for intracellular drug delivery. *Prog. Polym. Sci.* **38,** 503–535 (2013).
28. Diaz, I. L. & Perez, L. D. Synthesis and micellization properties of triblock copolymers PDMAEMA-b-PCL-b-PDMAEMA and their applications in the fabrication of amphotericin B-loaded nanocontainers. *Colloid Polym. Sci.* **293,** 913–923 (2015).
29. Liu, Z., Jiao, Y., Wang, Y., Zhou, C. & Zhang, Z. Polysaccharides-based nanoparticles as drug delivery systems. *Adv. Drug Deliv. Rev.* **60,** 1650–62 (2008).
30. Park, J. H., Saravanakumar, G., Kim, K. & Kwon, I. C. Targeted delivery of low molecular drugs using chitosan and its derivatives. *Adv. Drug Deliv. Rev.* **62,** 28–41 (2010).
31. Blanazs, A., Armes, S. P. & Ryan, A. J. Self-assembled block copolymer aggregates: From micelles to vesicles and their biological applications. *Macromol. Rapid Commun.* **30,** 267–277 (2009).
32. Alli, A., Hazer, B., Menceloğlu, Y. & Süzer, Ş. Synthesis, characterization and surface properties of amphiphilic polystyrene-b-polypropylene glycol block copolymers. *Eur. Polym. J.* **42,** 740–750 (2006).
33. Chen, C., Yu, C. H., Cheng, Y. C., Yu, P. H. F. & Cheung, M. K. Biodegradable nanoparticles of amphiphilic triblock copolymers based on poly(3-hydroxybutyrate) and poly(ethylene glycol) as drug carriers. *Biomaterials* **27,** 4804–4814 (2006).
34. He, G., Ma, L. L., Pan, J. & Venkatraman, S. ABA and BAB type triblock copolymers of PEG and PLA: A comparative study of drug release properties and 'stealth' particle characteristics. *Int. J. Pharm.* **334,** 48–55 (2007).

35. Yang, J., Yan, J., Zhou, Z. & Amsden, B. G. Dithiol-PEG-PDLLA micelles: Preparation and evaluation as potential topical ocular delivery vehicle. *Biomacromolecules* **15,** 1346–1354 (2014).

36. Liu, J. Y. & Zhang, L. M. Preparation of a polysaccharide-polyester diblock copolymer and its micellar characteristics. *Carbohydr. Polym.* **69,** 196–201 (2007).

37. Shukla, R. K. & Tiwari, A. Carbohydrate polymers: Applications and recent advances in delivering drugs to the colon. *Carbohydr. Polym.* **88,** 399–416 (2012).

38. Dang, J. M. & Leong, K. W. Natural polymers for gene delivery and tissue engineering. *Adv. Drug Deliv. Rev.* **58,** 487–499 (2006).

39. Ratner, B. D. & Bryant, S. J. B IOMATERIALS : Where We Have Been and Where We Are Going. *Rev. Lit. Arts Am.* 41–75 (2004). doi:10.1146/annurev.bioeng.6.040803.140027

40. Chen, J., Jo, S. & Park, K. Polysaccharide hydrogels for protein drug delivery. *Carbohydr. Polym.* **28,** 69–76 (1995).

41. Mizrahy, S. & Peer, D. Polysaccharides as building blocks for nanotherapeutics. *Chem. Soc. Rev.* **41,** 2623–40 (2012).

42. Kean, T. & Thanou, M. Biodegradation, biodistribution and toxicity of chitosan. *Adv. Drug Deliv. Rev.* **62,** 3–11 (2010).

43. Toole, B. P. Hyaluronan: from extracellular glue to pericellular cue. *Nat. Rev. Cancer* **4,** 528–39 (2004).

44. Beneke, C. E., Viljoen, A. M. & Hamman, J. H. Polymeric plant-derived excipients in drug delivery. *Molecules* **14,** 2602–2620 (2009).

45. Malafaya, P. B., Silva, G. A. & Reis, R. L. Natural-origin polymers as carriers and scaffolds for biomolecules and cell delivery in tissue engineering applications. *Adv. Drug Deliv. Rev.* **59,** 207–233 (2007).

46. Sinha, V. R. & Kumria, R. Polysaccharides in colon-specific drug delivery. *Int. J. Pharm.* **224,** 19–38 (2001).

47. Baldwin, A. D. & Kiick, K. L. Polysaccharide-modified synthetic polymeric biomaterials. *Biopolymers* **94,** 128–140 (2010).

48. Avachat, A. M., Dash, R. R. & Shrotriya, S. N. Recent Investigations of Plant Based Natural Gums , Mucilages and Resins in Novel Drug Delivery Systems. *Indian J. Pharm. Education Res.* **45,** 86–99 (2011).

49. Sung, H. W., Sonaje, K., Liao, Z. X., Hsu, L. W. & Chuang, E. Y. PH-responsive nanoparticles shelled with chitosan for oral delivery of insulin: From mechanism to therapeutic applications. *Acc. Chem. Res.* **45,** 619–629 (2012).

50. Seeberger, P. H. & Werz, D. B. Synthesis and medical applications of oligosaccharides. *Nature* **446,** 1046–1051 (2007).

51. Zhang, N., Wardwell, P. R. & Bader, R. A. Polysaccharide-based micelles for drug delivery. *Pharmaceutics* **5,** 329–352 (2013).

52. Liao, Y.-H., Jones, S. a, Forbes, B., Martin, G. P. & Brown, M. B. Hyaluronan: pharmaceutical characterization and drug delivery. *Drug Deliv.* **12,** 327–342 (2005).

53. Myrick, J. M., Vendra, V. K. & Krishnan, S. Self-assembled polysaccharide nanostructures for controlled-release applications. *Nanotechnol. Rev.* **3,** 319–346 (2014).

54. Coviello, T., Matricardi, P., Marianecci, C. & Alhaique, F. Polysaccharide hydrogels for modified release formulations. *J. Control. Release* **119,** 5–24 (2007).

55. Ngo, D. H. & Kim, S. K. Sulfated polysaccharides as bioactive agents from marine algae. *Int. J. Biol. Macromol.* **62,** 70–75 (2013).

56. Saravanakumar, G., Jo, D.-G. & H. Park, J. Polysaccharide-Based Nanoparticles: A Versatile Platform for Drug Delivery and Biomedical Imaging. *Curr. Med. Chem.* **19,** 3212–3229 (2012).

57. Yang, J. S., Xie, Y. J. & He, W. Research progress on chemical modification of alginate: A review. *Carbohydr. Polym.* **84,** 33–39 (2011).

58. Seliktar, D. Designing Cell-Compatible Hydrogels for Biomedical Applications. *Science (80-.).* **336,** 1124–1128 (2012).

59. Bosio, V. E. *et al.* Synthesis and characterization of CaCO3–biopolymer hybrid nanoporous microparticles for controlled release of doxorubicin. *Jounal Nanoparticles Res.* **132,** 4833794 (2013).

60. R. Khathuriya, T. Nayyar, S. Sabharwal, U. K. J. and R. T. RECENT APPROACHES AND PHARMACEUTICAL APPLICATIONS OF NATURAL POLYSACCHARIDES: A REVIEW. **4,** 2312–2321 (2015).

61. Karewicz. Modified Polysaccharides as Versatile Materials in Controlled Delivery of Antidegenerative Agents. *Curr. Pharm. Des.* **18,** 2518–2535 (2012).

62. Akiyoshi, K., Deguchi, S., Moriguchi, N., Yamaguchi, S. & Sunamoto, J. Self-aggregates of hydrophobized polysaccharides in water. Formation and characteristics of nanoparticles. *Macromolecules* **26,** 3062–3068 (1993).

63. Akiyoshi, K., Deguchi, S., Tajima, H., Nishikawa, T. & Sunamoto, J. Microscopic Structure and Thermoresponsiveness of a Hydrogel Nanoparticle by Self-Assembly of a Hydrophobized Polysaccharide. *Macromolecules* **9297,** 857–861 (1997).

64. Akiyama, E. *et al.* Self-assembled nanogels of cholesteryl-modified polysaccharides: Effect of the polysaccharide structure on their association characteristics in the dilute and semidilute regimes. *Biomacromolecules* **8,** 2366–2373 (2007).

65. Akiyoshi, K. & Sunamoto, J. Supramolecular assembly of hydrophobized polysaccharides. *Supramol. Sci.* **3,** 157–163 (1996).

66. Takahashi, H., Sawada, S. I. & Akiyoshi, K. Amphiphilic polysaccharide nanoballs: A new building block for nanogel biomedical engineering and artificial chaperones. *ACS Nano* **5,** 337–345 (2011).

67. Meng, X. & Edgar, K. J. 'Click' reactions in polysaccharide modification. *Prog. Polym. Sci.* **53,** ASAP (2015).

68. Alhaique, F., Matricardi, P., Di Meo, C., Coviello, T. & Montanari, E. Polysaccharide-based self-assembling nanohydrogels: An overview on 25-years research on pullulan. *J. Drug Deliv. Sci. Technol.* **30,** 300–309 (2015).

69. Hassani, L. N., Hendra, F. & Bouchemal, K. Auto-associative amphiphilic polysaccharides as drug delivery systems. *Drug Discov. Today* **17,** 608–614 (2012).

70. Yang, Y. *et al.* Advances in self-assembled chitosan nanomaterials for drug delivery. *Biotechnol. Adv.* **32,** 1301–1316 (2014).

71. Utracki, L. A. & Lyngaae-Jørgensen, J. Dynamic melt flow of nanocomposites based on poly-

ε-caprolactam. *Rheol. Acta* **41,** 394–407 (2002).

72. Hernández-Marín, N. Y., Lobato-Calleros, C. & Vernon-Carter, E. J. Stability and rheology of water-in-oil-in-water multiple emulsions made with protein-polysaccharide soluble complexes. *J. Food Eng.* **119,** 181–187 (2013).

73. Aranaz, I., Harris, R. & Heras, A. Chitosan Amphiphilic Derivatives. Chemistry and Applications. *Curr. Org. Chem.* **14,** 308–330 (2010).

74. Guo, Y., Wang, X., Shu, X., Shen, Z. & Sun, R. C. Self-assembly and paclitaxel loading capacity of cellulose-graft- poly(lactide) nanomicelles. *J. Agric. Food Chem.* **60,** 3900–3908 (2012).

75. Biggs, S., Selb, J. & Candau, F. Effect of Surfactant on the Solution Properties of Hydrophobically Modified Polyacrylamide. *Am. Chem. Soc.* **8,** 838–847 (1992).

76. Puerta-Gomez, A. F. & Castell-Perez, M. E. Studies on self-assembly interactions of proteins and octenyl succinic anhydrate (OSA)-modified depolymerized waxy rice starch using rheological principles. *J. Appl. Polym. Sci.* **133,** 1–11 (2016).

77. Nagahama, K., Ouchi, T. & Ohya, Y. Biodegradable nanogels prepared by self-assembly of poly(L-lactide)-grafted dextran: Entrapment and release of proteins. *Macromol. Biosci.* **8,** 1044–1052 (2008).

78. Konuma, T., Sakurai, K. & Goto, Y. Promiscuous Binding of Ligands by ??-Lactoglobulin Involves Hydrophobic Interactions and Plasticity. *J. Mol. Biol.* **368,** 209–218 (2007).

79. Zhang, C. *et al.* Polymer vesicles prepared from the (l-phenylalanine ethyl ester)-modified hyaluronic acid. *Mater. Lett.* **164,** 15–18 (2016).

80. Nichifor, M., Mocanu, G. & Stanciu, M. C. Micelle-like association of polysaccharides with hydrophobic end groups. *Carbohydr. Polym.* **110,** 209–18 (2014).

81. Tang, D.-L., Song, F., Chen, C., Wang, X.-L. & Wang, Y.-Z. A pH-responsive chitosan-b-poly(p-dioxanone) nanocarrier: formation and efficient antitumor drug delivery. *Nanotechnology* **24,** 145101 (2013).

82. Akiyoshi, K., DEGUCHI, S., TAJIMA, H., Nishikawa, T. & Sunamoto, J. Self-assembly of hydrophobized polysaccharide. *Proc. Japan Acad. Ser. B Phys. Biol. Sci.* **71,** 15–19 (1995).

83. Lee, J. M., Cho, J. E., Kim, J. H., Cho, H. K. & Cheong, I. W. Poly(styrene/hydroxypropyl methylcellulose phthalate) latex particles prepared by resin-fortified emulsion polymerization. *Colloids Surfaces A Physicochem. Eng. Asp.* **307,** 35–44 (2007).

84. Li, Q., Liu, W., Dai, J. & Zhang, C. Synthesis of Polysaccharide-Block-Polypeptide Copolymer for Potential Co-Delivery of Drug and Plasmid DNA. *Macromol. Biosci.* 756–764 (2015). doi:10.1002/mabi.201400454

85. Matsumura, Y. & Maeda, H. A new concept for macromolecular therapeutics in cnacer chemotherapy: mechanism of tumoritropic accumulatio of proteins and the antitumor agents Smancs. *Cancer Res.* **46,** 6387– 6392 (1986).

86. Li, Y. *et al.* Synthesis and characterization of an amphiphilic graft polymer and its potential as a pH-sensitive drug carrier. *Polymer (Guildf).* **52,** 3304–3310 (2011).

87. Allen, C., Maysinger, D. & Eisenberg, A. Nano-engineering block copolymer aggregates for drug delivery. *Colloids Surfaces B Biointerfaces* **16,** 3–27 (1999).

88. Gammas, S. *et al.* Thermo-responsive polymer nanoparticles with a core-shell micelle structure

as site-specific drug carriers. *J. Control. Release* **48,** 157–164 (1997).

89. Dong, J. *et al.* Stabilized vesicles consisting of small amphiphiles for stepwise photorelease via UV light. *Langmuir* **28,** 1733–1737 (2012).

90. Sun, T. *et al.* Self-assembled vesicles prepared from amphiphilic cyclodextrins as drug carriers. *Langmuir* **28,** 8625–8636 (2012).

91. Letchford, K. & Burt, H. A review of the formation and classification of amphiphilic block copolymer nanoparticulate structures: micelles, nanospheres, nanocapsules and polymersomes. *Eur. J. Pharm. Biopharm.* **65,** 259–269 (2007).

92. Torchilin, V. P. Structure and design of polymeric surfactant-based drug delivery systems. *J. Control. Release* **73,** 137–172 (2001).

93. Bates, F. S. & Fredrickson, G. H. Block Copolymer Thermodynamics - Theory and Experiment. *Annu. Rev. Phys. Chem.* **41,** 525–557 (1990).

94. Halperin, A. Polymeric vs. Monomeric Amphiphiles: Design Parameters. *J. Macromol. Sci. Part C Polym. Rev.* **46,** 173–214 (2006).

95. Yanzhu Guo; Li Zhang; Haiming Li; Ying Han; Jinghui Zhou; Xiaohui Wang. Self-assembly and paclitaxel loading capacity of α-tocopherol succinate-conjugated hydroxyethyl cellulose nanomicelle. *Colloid Polym Sci* **294,** 135–143 (2016).

96. Guo, Y., Wang, X., Shen, Z., Shu, X. & Sun, R. Preparation of cellulose-graft-poly(ε-caprolactone) nanomicelles by homogeneous ROP in ionic liquid. *Carbohydr. Polym.* **92,** 77–83 (2013).

97. Yang, Y., Guo, Y., Sun, R. & Wang, X. Self-assembly and β-carotene loading capacity of hydroxyethyl cellulose-graft-linoleic acid nanomicelles. *Carbohydrate Polymers* **145,** 56–63 (2016).

98. Yang, Y., Zhang, Y.-M., Chen, Y., Chen, J.-T. & Liu, Y. Polysaccharide-based Noncovalent Assembly for Targeted Delivery of Taxol. *Sci. Rep.* **6,** 19212 (2016).

99. Balan, V., Redinciuc, V., Tudorachi, N. & Verestiuc, L. Biotinylated N-palmitoyl chitosan for design of drug loaded self-assembled nanocarriers. *Eur. Polym. J.* **81,** 284–294 (2016).

100. Akiyoshi, K., Sasaki, Y. & Sunamoto, J. Molecular chaperone-like activity of hydrogel nanoparticles of hydrophobized pullulan: Thermal stabilization with refolding of carbonic anhydrase B. *Bioconjug. Chem.* **10,** 321–324 (1999).

101. Thurmond, K. B., Kowalewski, T. & Wooley, K. L. Water-soluble Knedel-like structures: The preparation of shell-cross-linked small particles. *J. Am. Chem. Soc.* **118,** 7239–7240 (1996).

102. Thurmond, K. B., Remsen, E. E., Kowalewski, T. & Wooley, K. L. Packaging of DNA by shell crosslinked nanoparticles. *Nucleic Acids Res.* **27,** 2966–2971 (1999).

103. Kabanov, A. V. & Vinogradov, S. V. Nanogels as pharmaceutical carriers: Finite networks of infinite capabilities. *Angew. Chemie - Int. Ed.* **48,** 5418–5429 (2009).

104. Choi, K. Y. K. *et al.* Self-assembled hyaluronic acid nanoparticles as a potential drug carrier for cancer therapy: synthesis, characterization, and in vivo biodistribution. *J. Mater. Chem.* **19,** 4102 (2009).

105. Choi, K. Y. *et al.* Preparation and characterization of hyaluronic acid-based hydrogel nanoparticles. *J. Phys. Chem. Solids* **69,** 1591–1595 (2008).

106. Lee, K. Y., Jo, W. H., Kwon, I. C., Kim, Y. & Jeong, S. Y. Structural Determination and Interior Polarity of Self-Aggregates Prepared from Deoxycholic Acid-Modified Chitosan in

Water. *Macromolecules* **31,** 378–383 (1998).

107. Nichifor, M., Lopes, A., Carpov, A. & Melo, E. Aggregation in Water of Dextran Hydrophobically Modified with Bile Acids. *Macromolecules* **32,** 7078–7085 (1999).

108. Verma, M. S., Liu, S., Chen, Y. Y., Meerasa, A. & Gu, F. X. Size-tunable nanoparticles composed of dextran-b-poly(D,L-lactide) for drug delivery applications. *Nano Res.* **5,** 49–61 (2012).

109. Nagahama, K., Mori, Y., Ohya, Y. & Ouchi, T. Biodegradable nanogel formation of polylactide-grafted dextran copolymer in dilute aqueous solution and enhancement of its stability by stereocomplexation. *Biomacromolecules* **8,** 2135–2141 (2007).

110. Qiu, L. Y. & Bae, Y. H. Polymer architecture and drug delivery. *Pharm. Res.* **23,** 1–30 (2006).

111. Borisov, O. V. & Zhulina, E. B. Amphiphilic graft copolymer in a selective solvent: Intramolecular structures and conformational transitions. *Macromolecules* **38,** 2506–2514 (2005).

112. Glagolev, M. K., Vasilevskaya, V. V. & Khokhlov, A. R. Effect of Induced Self-Organization in Mixtures of Amphiphilic Macromolecules with Different Stiffness. *Macromolecules* **48,** 3767–3774 (2015).

113. Zhang, C., Yang, S., Zhu, Y., Zhang, R. & Liu, X. Formation of bowl-shaped nanoparticles by self-assembly of cinnamic acid-modified dextran. *Carbohydr. Polym.* **133,** 637–643 (2015).

114. Ferramosca, A. *et al.* Conjugated linoleic acid and hepatic lipogenesis in mouse: role of the mitochondrial citrate carrier. *J. Lipid Res.* **47,** 1994–2003 (2006).

115. Zhu, Y. *et al.* Self-assembly and emulsification of dopamine-modified hyaluronan. *Carbohydr. Polym.* **123,** 72–79 (2015).

116. Choi, K. Y. *et al.* Self-assembled hyaluronic acid nanoparticles for active tumor targeting. *Biomaterials* **31,** 106–114 (2010).

117. Hornig, S., Bunjes, H. & Heinze, T. Preparation and characterization of nanoparticles based on dextran-drug conjugates. *J. Colloid Interface Sci.* **338,** 56–62 (2009).

118. Qiu, L. *et al.* Self-assembled pH-responsive hyaluronic acid-g-poly(l-histidine) copolymer micelles for targeted intracellular delivery of doxorubicin. *Acta Biomater.* **10,** 2024–2035 (2014).

119. Vafaei, S. Y. *et al.* Self assembled hyaluronic acid nanoparticles as a potential carrier for targeting the inflamed intestinal mucosa. *Carbohydr. Polym.* **144,** 371–381 (2016).

120. Zhang, G., Liu, L., Zhao, Y., Ning, F. & Jiang, M. Self-Assembly of Carboxylated Poly (styrene- b -ethylene- co -butylene- b -styrene) Triblock Copolymer Chains in Water via a Microphase Inversion. *Macromolecules* **33,** 6340–6343 (2000).

121. Wu, M. *et al.* Self-assemblied nanocomplexes based on biomimetic amphiphilic chitosan derivatives for protein delivery. *Carbohydr. Polym.* **121,** 115–121 (2015).

122. Akiyoshi, K. *et al.* Self-assembled hydrogel nanoparticle of cholesterol-bearing pullulan as a carrier of protein drugs: Complexation and stabilization of insulin. *J. Control. Release* **54,** 313–320 (1998).

123. Li, B., Wang, Q., Wang, X., Wang, C. & Jiang, X. Preparation, drug release and cellular uptake of doxorubicin-loaded dextran-b-poly(?-caprolactone) nanoparticles. *Carbohydr. Polym.* **93,** 430–437 (2013).

124. Zahr, A. S., Davis, C. A. & Pishko, M. V. Macrophage uptake of core-shell nanoparticles surface modified with poly(ethylene glycol). *Langmuir* **22,** 8178–8185 (2006).

125. Zhang, H., Cai, G., Tang, G., Wang, L. & Jiang, H. Synthesis, self-assembly, and cytotoxicity of well-defined trimethylated chitosan-O-poly(e-caprolactone): Effect of chitosan molecular weight. *J. Biomed. Mater. Res. - Part B Appl. Biomater.* **98 B,** 290–299 (2011).

126. Liu, J., Li, J., Ma, Y., Chen, F. & Zhao, G. Synthesis, characterization, and aqueous self-assembly of octenylsuccinate oat ??-glucan. *J. Agric. Food Chem.* **61,** 12683–12691 (2013).

127. Termsarasab, U. *et al.* Chitosan oligosaccharide-arachidic acid-based nanoparticles for anti-cancer drug delivery. *Int. J. Pharm.* **441,** 373–380 (2013).

128. Li, D., Wang, X., Guo, Y., Huang, H. & Sun, R. Preparation of Long-Chain Fatty Acyl-Grafted Chitosan in an Ionic Liquid and Their Self-Assembled Micelles in Water. *J. Macromol. Sci. Part B* **51,** 2483–2492 (2012).

129. Zhang, C., Qineng, P. & Zhang, H. Self-assembly and characterization of paclitaxel-loaded N-octyl-O-sulfate chitosan micellar system. *Colloids Surfaces B Biointerfaces* **39,** 69–75 (2004).

130. Shamala, T. R. & Prasad, M. S. Preliminary studies on the production of high and low viscosity dextran by Leuconostoc spp. *Process Biochem.* **30,** 237–241 (1995).

131. Habibi, Y. *et al.* Bionanocomposites based on poly(ε-caprolactone)-grafted cellulose nanocrystals by ring-opening polymerization. *J. Mater. Chem.* **18,** 5002 (2008).

132. Labet, M. & Thielemans, W. Improving the reproducibility of chemical reactions on the surface of cellulose nanocrystals: ROP of ??-caprolactone as a case study. *Cellulose* **18,** 607–617 (2011).

133. Paquet, O., Krouit, M., Bras, J., Thielemans, W. & Belgacem, M. N. Surface modification of cellulose by PCL grafts. *Acta Mater.* **58,** 792–801 (2010).

134. Cai, S., Vijayan, K., Cheng, D., Lima, E. M. & Discher, D. E. Micelles of different morphologies - Advantages of worm-like filomicelles of PEO-PCL in paclitaxel delivery. *Pharm. Res.* **24,** 2099–2109 (2007).

135. Li, X. *et al.* Preparation, Characterization, and Self-assembly Behavior of a Novel MPEG/PCL- *g* -Chitosan Copolymer. *Soft Mater.* **8,** 320–337 (2010).

136. Sun, H. *et al.* Shell-sheddable micelles based on dextran-SS-poly(??-caprolactone) diblock copolymer for efficient intracellular release of doxorubicin. *Biomacromolecules* **11,** 848–854 (2010).

137. Saldías, C., Velásquez, L., Quezada, C. & Leiva, A. Physicochemical assessment of Dextran-g-Poly (ε-caprolactone) micellar nanoaggregates as drug nanocarriers. *Carbohydr. Polym.* **117,** 458–467 (2015).

138. Oh, J. K. Polylactide (PLA)-based amphiphilic block copolymers: synthesis, self-assembly, and biomedical applications. *Soft Matter* **7,** 5096–5108 (2011).

139. Hoffman, A. S. Hydrogels for biomedical applications. *Adv. Drug Deliv. Rev.* **64,** 18–23 (2012).

140. Mehvar, R. Dextrans for targeted and sustained delivery of therapeutic and imaging agents. *J. Control. Release* **69,** 1–25 (2000).

141. Vercauteren, R., Bruneel, D., Schacht, E. & Duncan, R. Effect of the Chemical Modification of Dextran on the Degradation by Dextranase. *J. Bioact. Compat. Polym.* **5,** 4–15 (1990).

142. Janes, K. A., Calvo, P. & Alonso, M. J. Polysaccharide colloidal particles as delivery systems for macromolecules. *Adv. Drug Deliv. Rev.* **47,** 83–97 (2001).

143. KANAUCHI, O., DEUCHl, K., IMASATO, Y. & KOBAYASHI, E. Increasing Effect of a

Chitosan and Ascorbic Acid Mixture on Fecal Dietary Fat Excretion Osamu. *Biotech. Biochem.* **58,** 1617–1620 (1994).

144. Grenha, A., Al-Qadi, S., Seijo, B. & Remuñán-López, C. The potential of chitosan for pulmonary drug delivery. *J. Drug Deliv. Sci. Technol.* **20,** 33–43 (2010).

145. Park, J. H., Cho, Y. W., Chung, H., Kwon, I. C. & Jeong, S. Y. Synthesis and characterization of sugar-bearing chitosan derivatives: Aqueous solubility and biodegradability. *Biomacromolecules* **4,** 1087–1091 (2003).

146. Dash, M., Chiellini, F., Ottenbrite, R. M. & Chiellini, E. Chitosan - A versatile semi-synthetic polymer in biomedical applications. *Prog. Polym. Sci.* **36,** 981–1014 (2011).

147. Agnihotri, S. A., Mallikarjuna, N. N. & Aminabhavi, T. M. Recent advances on chitosan-based micro- and nanoparticles in drug delivery. *J. Control. Release* **100,** 5–28 (2004).

148. Hu, L., Sun, Y. & Wu, Y. Advances in chitosan-based drug delivery vehicles. *Nanoscale* **5,** 3103–11 (2013).

149. Ravi Kumar, M. N. . A review of chitin and chitosan applications. *React. Funct. Polym.* **46,** 1–27 (2000).

150. Bernkop-Schnürch, A., Hornof, M. & Guggi, D. Thiolated chitosans. *Eur. J. Pharm. Biopharm.* **57,** 9–17 (2004).

151. Sogias, I. a., Williams, A. C. & Khutoryanskiy, V. V. Why is chitosan mucoadhesive? *Biomacromolecules* **9,** 1837–1842 (2008).

152. Illum, L., Jabbal-Gill, I., Hinchcliffe, M., Fisher, A. N. & Davis, S. S. Chitosan as a novel nasal delivery system for vaccines. *Adv. Drug Deliv. Rev.* **51,** 81–96 (2001).

153. Rabea, E. I., Badawy, M. E. T., Stevens, C. V., Smagghe, G. & Steurbaut, W. Chitosan as antimicrobial agent: Applications and mode of action. *Biomacromolecules* **4,** 1457–1465 (2003).

154. Raafat, D., Von Bargen, K., Haas, A. & Sahl, H. G. Insights into the mode of action of chitosan as an antibacterial compound. *Appl. Environ. Microbiol.* **74,** 3764–3773 (2008).

155. Chopra, S. *et al.* Advances and potential applications of chitosan derivatives as mucoadhesive biomaterials in modern drug delivery. *J. Pharm. Pharmacol.* **58,** 1021–32 (2006).

156. Rodrigues, S., Dionísio, M., López, C. R. & Grenha, A. Biocompatibility of Chitosan Carriers with Application in Drug Delivery. *J. Funct. Biomater.* **3,** 615–641 (2012).

157. Bernkop-Schnürch, A. & Dünnhaupt, S. Chitosan-based drug delivery systems. *Eur. J. Pharm. Biopharm.* **81,** 463–9 (2012).

158. Buschmann, M. D. *et al.* Chitosans for delivery of nucleic acids. *Adv. Drug Deliv. Rev.* **65,** 1234–1270 (2013).

159. Vauthier, C., Zandanel, C. & Ramon, A. L. Chitosan-based nanoparticles for in vivo delivery of interfering agents including siRNA. *Curr. Opin. Colloid Interface Sci.* **18,** 406–418 (2013).

160. Chaturvedi, K., Ganguly, K., Nadagouda, M. N. & Aminabhavi, T. M. Polymeric hydrogels for oral insulin delivery. *J. Control. Release* **165,** 129–138 (2013).

161. Duceppe, N. & Tabrizian, M. Advances in using chitosan-based nanoparticles for *in vitro* and *in vivo* drug and gene delivery. *Expert Opin. Drug Deliv.* **7,** 1191–1207 (2010).

162. Bhattarai, N., Gunn, J. & Zhang, M. Chitosan-based hydrogels for controlled, localized drug delivery. *Adv. Drug Deliv. Rev.* **62,** 83–99 (2010).

163. Balan, V. *et al.* Doxorubicin-loaded magnetic nanocapsules based on N-palmitoyl chitosan and magnetite: Synthesis and characterization. *Chem. Eng. J.* **279,** 188–197 (2015).

164. Lian, H. *et al.* Enhanced oral delivery of paclitaxel using acetylcysteine functionalized chitosan-vitamin E succinate nanomicelles based on a mucus bioadhesion and penetration mechanism. *Mol. Pharm.* **10,** 3447–3458 (2013).

165. Kogan, G., ??olt??s, L., Stern, R. & Gemeiner, P. Hyaluronic acid: A natural biopolymer with a broad range of biomedical and industrial applications. *Biotechnol. Lett.* **29,** 17–25 (2007).

166. Toole, B. P. Hyaluronan-CD44 interactions in cancer: Paradoxes and possibilities. *Clin. Cancer Res.* **15,** 7462–7468 (2009).

167. Oh, E. J. *et al.* Target specific and long-acting delivery of protein, peptide, and nucleotide therapeutics using hyaluronic acid derivatives. *J. Control. Release* **141,** 2–12 (2010).

168. Plattt, V. M. & Szoka, F. C. Anticancer therapeutics: Targeting macromolecules and nanocarriers to hyaluronan or CD44, a hyaluronan receptor. *Mol. Pharm.* **5,** 474–486 (2008).

169. Zöller, M. CD44: physiological expression of distinct isoforms as evidence for organ-specific metastasis formation. *J. Mol. Med. (Berl).* **73,** 425–38 (1995).

170. Molecules, A. & Cancer, I. N. Adhesion molecules in cancer biology. **44,** 115–126 (2000).

171. Di Meo, C. *et al.* Highly versatile nanohydrogel platform based on riboflavin-polysaccharide derivatives useful in the development of intrinsically fluorescent and cytocompatible drug carriers. *Carbohydr. Polym.* **115,** 502–509 (2015).

172. Montanari, E. *et al.* Chasing bacteria within the cells using levofloxacin-loaded hyaluronic acid nanohydrogels. *Eur. J. Pharm. Biopharm.* **87,** 518–523 (2014).

173. Montanari, E. *et al.* One-step formation and sterilization of gellan and hyaluronan nanohydrogels using autoclave. *J. Mater. Sci. Mater. Med.* **26,** 1–6 (2015).

174. Roy, D., Semsarilar, M., Guthrie, J. T. & Perrier, S. Cellulose modification by polymer grafting: a review. *Chem. Soc. Rev.* **38,** 2046–64 (2009).

175. Credou, J. & Berthelot, T. Cellulose: from biocompatible to bioactive material. 4767–4788 (2014). doi:10.1039/c4tb00431k

176. Jang, J., Ha, J. & Kim, S. Fabrication of polyaniline nanoparticles using microemulsion polymerization. *Macromol. Res.* **15,** 154–159 (2007).

177. Han, S. *et al.* Electrolyte effect on the particle characteristics prepared by soap-free emulsion polymerization. *Macromolecular Research* **15,** 403–411 (2007).

178. Barani, H. & Bahrami, S. H. Investigation on Polyacrylonitrile/Cellulose Acetate Blends. *Macromol. Res.* **15,** 605–609 (2007).

179. Myung, S. J., Kim, H.-S., Kim, Y., Chen, P. & Jin, H.-J. Fluorescent silk fibroin nanoparticles prepared using a reverse microemulsion. *Macromol. Res.* **16,** 604–608 (2008).

180. Birringer, M., EyTina, J. H., Salvatore, B. a & Neuzil, J. Vitamin E analogues as inducers of apoptosis: structure-function relation. *Br. J. Cancer* **88,** 1948–1955 (2003).

181. Tao, Y., Han, J. & Dou, H. Paclitaxel-loaded tocopheryl succinate-conjugated chitosan oligosaccharide nanoparticles for synergistic chemotherapy. *J. Mater. Chem.* **22,** 8930 (2012).

182. Tao, Y., Han, J., Wang, X. & Dou, H. Nano-formulation of paclitaxel by vitamin E succinate functionalized pluronic micelles for enhanced encapsulation, stability and cytotoxicity. *Colloids*

Surfaces B Biointerfaces **102,** 604–610 (2013).

183. Gerhard Jahreis, J. K. F. T. F. S. C. von L. Conjugated linoleic acids: Physiological effects in animal and man with special regard to body composition. *Eur. J. Lipid Sci. Technol.* **102,** 695–703 (2000).

184. Teramoto, Y. & Nishio, Y. Cellulose diacetate-graft-poly(lactic acid)s: Synthesis of wide-ranging compositions and their thermal and mechanical properties. *Polymer (Guildf).* **44,** 2701–2709 (2003).

185. Yuan, W., Yuan, J., Zhang, F. & Xie, X. Syntheses, characterization, and in vitro degradation of ethyl cellulose-graft-poly (ε-caprolactone)-block-poly (l-lactide) copolymers by sequential ring-opening polymerization. *Biomacromolecules* **8,** 1101–1108 (2007).

186. Chen, D. & Sun, B. New tissue engineering material copolymers of derivatives of cellulose and lactide: Their synthesis and characterization. *Mater. Sci. Eng. C* **11,** 57–60 (2000).

187. Dong, H. *et al.* The synthesis of biodegradable graft copolymer cellulose-graft-poly(l-lactide) and the study of its controlled drug release. *Colloids Surfaces B Biointerfaces* **66,** 26–33 (2008).

188. Presland, A. & Price, J. Ocular anatomy and physiology relevant to anaesthesia. *Anaesth. Intensive Care Med.* **15,** 20–25 (2014).

189. Wichmann, W. & Müller-Forell, W. Anatomy of the visual system. *Eur. J. Radiol.* **49,** 8–30 (2004).

190. Sharma, U. K., Verma, A., Prajapati, S. K. & Pandey, H. OCULAR DRUG DELIVERY : ASSORTED OBSTRUCTIONS AND CONTEMPORARY PROGRESSES. *Int. J. Res. Dev. Pharm. Life Sci.* **2,** 464–473 (2013).

191. Urtti, A. Challenges and obstacles of ocular pharmacokinetics and drug delivery. *Adv. Drug Deliv. Rev.* **58,** 1131–1135 (2006).

192. Bucolo, C., Drago, F. & Salomone, S. Ocular drug delivery: A clue from nanotechnology. *Front. Pharmacol.* **3,** 1–3 (2012).

193. Urtti, a. *et al.* Controlled drug delivery devices for experimental ocular studies with timolol 2. Ocular and systemic absorption in rabbits. *Int. J. Pharm.* **61,** 241–249 (1990).

194. Hughes, P. M., Olejnik, O., Chang-Lin, J. E. & Wilson, C. G. Topical and systemic drug delivery to the posterior segments. *Adv. Drug Deliv. Rev.* **57,** 2010–2032 (2005).

195. Sieg, J. W. & Robinson, J. R. Vehicle effects on ocular drug bioavailability II: Evaluation of pilocarpine. *J Pharm Sci* **66,** 1222–1228 (1977).

196. Wadhwa, S., Paliwal, R., Paliwal, S. R. & Vyas, S. P. Nanocarriers in Ocular Drug Delivery: An Update Review. *Curr. Pharm. Des.* **15,** 2724–2750 (2009).

197. Lee, V. H. & Robinsonx, J. R. Mechanistic and Quantitative Evaluation of Precorneal Pilocarpine Disposition in Albino Rabbits. **68,** (1979).

198. Dartt, D. A., Hodges, R. R. & Zoukhri, D. Tears and Their Secretion. *Adv. Organ Biol.* **10,** 21–82 (2005).

199. Urtti, A., Salminen, L. & Miinalainen, O. Systemic absorption of ocular pilocarpine is modified by polymer matrices. *Int. J. Pharm.* **23,** 147–161 (1985).

200. Urtti, A. & Salminen, L. Minimizing systemic absorption of topically administered ophthalmic drugs. *Surv. Ophthalmol.* **37,** 435–456 (1993).

201. Prausnitz, M. R. & Noonan, J. S. Permeability of cornea, sclera, and conjunctiva: A literature analysis for drug delivery to the eye. *J. Pharm. Sci.* **87,** 1479–1488 (1998).

202. Crosson, C. E. Transport processes across the rabbit corneal epithelium: a review. **4,** 323–331 (1985).

203. Komarova, Y. & Malik, A. B. *Regulation of endothelial permeability via paracellular and transcellular transport pathways. Annual review of physiology* **72,** (2010).

204. Saha, P., Yang, J. J. & Lee, V. H. L. Existence of a p-glycoprotein drug efflux pump in cultured rabbit conjunctival epithelial cells. *Investig. Ophthalmol. Vis. Sci.* **39,** 1221–1226 (1998).

205. Mannermaa, E., Vellonen, K. S. & Urtti, A. Drug transport in corneal epithelium and blood-retina barrier: Emerging role of transporters in ocular pharmacokinetics. *Adv. Drug Deliv. Rev.* **58,** 1136–1163 (2006).

206. Myles, M. E., Neumann, D. M. & Hill, J. M. Recent progress in ocular drug delivery for posterior segment disease: Emphasis on transscleral iontophoresis. *Adv. Drug Deliv. Rev.* **57,** 2063–2079 (2005).

207. Lach, J. L., Huang, H.-S. & Schoenwald, R. D. Corneal Penetration Behavior of β-Blocking Agents II: Assessment of Barrier Contributions. *J. Pharm. Sci.* **72,** 1272–1279 (1983).

208. Hämäläinen, K. M., Kananen, K., Auriola, S., Kontturi, K. & Urtti, A. Characterization of paracellular and aqueous penetration routes in cornea, conjunctiva, and sclera. *Investig. Ophthalmol. Vis. Sci.* **38,** 627–634 (1997).

209. Sahay, G., Alakhova, D. Y. & Kabanov, A. V. Endocytosis of nanomedicines. *J. Control. Release* **145,** 182–195 (2010).

210. Polli, G. P. Physicochemical Determinants of Drug Diffusion across the Conjunctiva, Sclera, and Cornea. *J. Pharm. Sci.* **14,** 959–803 (1967).

211. Harrison, J. C., Karcioglu, Z. a & Johnson, M. K. Lipophilicity influence on conjunctival drug penetration in the pigmented rabbit: a comparison with corneal penetration. *Curr. Eye Res.* **2,** 705–710 (1983).

212. Sultana, Y., Jain, R., Aqil, M. & Ali, A. Review of ocular drug delivery. *Curr. Drug Deliv.* **3,** 207–217 (2006).

213. Vandervoort, J. & Ludwig, A. Ocular drug delivery: nanomedicine applications. *Nanomedicine (Lond).* **2,** 11–21 (2007).

214. Nagarwal, R. C., Kant, S., Singh, P. N., Maiti, P. & Pandit, J. K. Polymeric nanoparticulate system: a potential approach for ocular drug delivery. *J. Control. Release* **136,** 2–13 (2009).

215. Yaw-Chong Tong, Shwu-Fen Chang, Chia-Yang Liu, Winston W.-Y. Kao, Chong Heng Huang, J. L. Eye drop delivery of nano-polymericmicelle formulated genes with cornea-specific promoters. *J. Gene Med.* **10,** 610–618 (2008).

216. Zarbin, M. A., Montemagno, C., Leary, J. F. & Ritch, R. Nanomedicine in ophthalmology: The new frontier. *Am. J. Ophthalmol.* **150,** 144–162 (2010).

217. Kayser, O., Lemke, a & Hernández-Trejo, N. The impact of nanobiotechnology on the development of new drug delivery systems. *Curr. Pharm. Biotechnol.* **6,** 3–5 (2005).

218. Xu, Q., Kambhampati, S. P. & Kannan, R. M. Nanotechnology approaches for ocular drug delivery. *Middle East Afr. J. Ophthalmol.* **20,** 26–37 (2013).

219. Mehra, N. K., Cai, D., Kuo, L., Hein, T. & Palakurthi, S. Safety and toxicity of nanomaterials

for ocular drug delivery applications. *Nanotoxicology* **5390,** 1–22 (2016).

220. Liu, S., Jones, L. & Gu, F. X. Nanomaterials for ocular drug delivery. *Macromol. Biosci.* **12,** 608–20 (2012).

221. Calonge, M. The Treatment of Dry Eye. *Surv. Ophthalmol.* **45,** S227–S239 (2001).

222. LIN, C.-P. & BOEHNKE, M. Influences of Methylcellulose on Corneal Epithelial Wound Healing. *J. Ocul. Pharmacol. Ther.* **15,** 59–63 (1999).

223. Toda, I., Shinozaki, N., Ph, D. & Tsubota, K. Hydroxypropyl Methylcellulose for the Treatment of Severe Dry Eye Associated with Sjogren ' s Syndrome. **15,** (1996).

224. Attar, M., Schiffman, R., Borbridge, L., Farnes, Q. & Welty, D. Ocular pharmacokinetics of 0.45% ketorolac tromethamine. *Clin. Ophthalmol.* **4,** 1403–1408 (2010).

225. Shastri, D., Patel, L. & Parikh, R. Studies on In situ Hydrogel: A Smart Way for Safe and Sustained Ocular Drug Delivery. *J. Young Pharm.* **2,** 116–20 (2010).

226. Centre, M., Greaves, J. L. & Wilson, C. G. Treatment of diseases of the eye with mucoadhesive delivery systems. *Adv. Drug Deliv. Rev.* **11,** 349–383 (1993).

227. El-Kamel, a H. In vitro and in vivo evaluation of Pluronic F127-based ocular delivery system for timolol maleate. *Int. J. Pharm.* **241,** 47–55 (2002).

228. Muellert, B. W. H. & Deardorff, D. L. Ophthalmic Vehicles : The Effect of Methylcellulose & the Penetration of Homatropine Hydrdbrornide Through the Cornea. 334–341

229. Meseguer, G., Buri, P., Plazonnet, B., Rozier, A. & Gurny, R. Gamma scintigraphic comparison of eyedrops containing pilocarpine in healthy volunteers. *J. Ocul. Pharmacol. Ther.* **12,** 481–8 (1996).

230. Chrai, S. S. Ocular Evaluation of Methylcellulose Vehicle in Albino Rabbits. 0–5

231. Khutoryanskaya, O. V *et al.* Hydrogen-Bonded Complexes and Blends of Poly(acrylic acid) and Methylcellulose: Nanoparticles and Mucoadhesive Films for Ocular Delivery of Riboflavin. *Macromol. Biosci.* **14,** 1–10 (2013).

232. El-Sousi, S. *et al.* Hydroxypropylmethylcellulose films for the ophthalmic delivery of diclofenac sodium. *J. Pharm. Pharmacol.* **65,** 193–200 (2013).

233. KARATAS, A. & BAYKARA, T. Studies of indomethacin inserts prepared using water-soluble polymers. I. Effect of the preparation method and polymers on drug release. *STP pharma Sci.* **10,** 187–193

234. Cordonnier, M. The treatment of dry eye with Lacrisert. *Bull. Soc. Belge Ophtalmol* **212,** 65–69 (1984).

235. Lux, A., Maier, S., Dinslage, S., Süverkrüp, R. & Diestelhorst, M. A comparative bioavailability study of three conventional eye drops versus a single lyophilisate. *Br. J. Ophthalmol.* **87,** 436–40 (2003).

236. Chang, D. F., Garcia, I. H., Hunkeler, J. D. & Minas, T. Phase II Results of an Intraocular Steroid Delivery System for Cataract Surgery. 1172–1177

237. Tan, D. T., Chee, S. P., Lim, L. & Lim, a S. Randomized clinical trial of a new dexamethasone delivery system (Surodex) for treatment of post-cataract surgery inflammation. *Ophthalmology* **106,** 223–231 (1999).

238. Tan, D. T. H., Chee, S., Lim, L., Theng, J. & Ede, M. Van. Randomized Clinical Trial of

Surodex Steroid Anterior versus Posterior Placement of Two Surodex in. **6420,** 2172–2181 (2001).

239. Seah, S. K. L. *et al.* Use of surodex in phacotrabeculectomy surgery. *Am. J. Ophthalmol.* **139,** 927–928 (2005).

240. Yuan, X. *et al.* Ocular Drug Delivery Nanowafer with Enhanced Therapeutic Efficacy. 1749–1758 (2015).

241. Patchan, M. W. *et al.* Evaluation of the biocompatibility of regenerated cellulose hydrogels with high strength and transparency for ocular applications. *J. Biomater. Appl.* **30,** 1049–1059 (2016).

242. Nanjawade, B. K., Manvi, F. V & Manjappa, a S. In situ-forming hydrogels for sustained ophthalmic drug delivery. *J. Control. Release* **122,** 119–34 (2007).

243. Wagh, V., Inamdar, B. & Samanta, M. Polymers used in ocular dosage form and drug delivery systems. *Asian J. Pharm.* **2,** 12 (2008).

244. Srividya, B., Cardoza, R. M. & Amin, P. D. Sustained ophthalmic delivery of ofloxacin from a pH triggered in situ gelling system. *J. Control. Release* **73,** 205–11 (2001).

245. Sultana, Y., Aqil, M., Ali, A. & Zafar, S. Evaluation of carbopol-methyl cellulose based sustained-release ocular delivery system for pefloxacin mesylate using rabbit eye model. *Pharm. Dev. Technol.* **11,** 313–9 (2006).

246. Dewan, M. *et al.* Effect of methyl cellulose on gelation behavior and drug release from poloxamer based ophthalmic formulations. *Int. J. Biol. Macromol.* **72,** 706–710 (2015).

247. Morsi, N., Ghorab, D., Refai, H. & Teba, H. Ketoroloac tromethamine loaded nanodispersion incorporated into thermosensitive in situ gel for prolonged ocular delivery. *Int. J. Pharm.* **506,** 57–67 (2016).

248. Khan, N., Aqil, M., Imam, S. S. & Ali, A. Development and evaluation of a novel in situ gel of sparfloxacin for sustained ocular drug delivery: in vitro and ex vivo characterization. *Pharm. Dev. Technol.* **7450,** 1–8 (2014).

249. Nagaich, U., Jain, N., Kumar, D. & Gulati, N. Controlled ocular drug delivery of ofloxacin using temperature modulated in situ gelling system. *J. Sci. Soc.* **40,** 90 (2013).

250. Singh, V. *et al.* Stimuli-sensitive hydrogels: a novel ophthalmic drug delivery system. *Indian J. Ophthalmol.* **58,** 477–81 (2010).

251. Ito, Y., Nagai, N. & Shimomura, Y. Reduction in Intraocular Pressure by the Instillation of Eye Drops Containing Disulfiram Included with 2-Hydroxypropyl-beta-cyclodextrin in Rabbit. *Biol. Pharm. Bull.* **33,** 1574–8 (2010).

252. Desai, S. D. & Blanchard, J. Evaluation of Pluronic F127-based sustained-release ocular delivery systems for pilocarpine using the albino rabbit eye model. *J. Pharm. Sci.* **87,** 1190–1195 (1998).

253. Andrés-Guerrero, V. *et al.* The use of mucoadhesive polymers to enhance the hypotensive effect of a melatonin analogue, 5-MCA-NAT, in rabbit eyes. *Invest. Ophthalmol. Vis. Sci.* **52,** 1507–15 (2011).

254. Patel, P. B., Shastri, D. H., Shelat, P. K. & Shukla, A. K. Ophthalmic drug delivery system: Challenges and approaches. *Syst. Rev. Pharm.* **1,** 113–120 (2010).

255. Cholkar, K., Patel, S. P., Vadlapudi, A. D. & Mitra, A. K. Novel Strategies for Anterior

Segment Ocular Drug Delivery. *J. Ocul. Pharmacol. Ther.* **29,** 106–123 (2013).

256. Singh, V., Ahmad, R. & Heming, T. The Challenges of Ophthalmic Drug Delivery: A Review. *Int. J. Drug Discov.* **3,** 56–51 (2011).

257. Molokhia, S. A., Thomas, S. C., Garff, K. J., Mandell, K. J. & Wirostko, B. M. Anterior Eye Segment Drug Delivery Systems : Current Treatments and Future Challenges. **29,** 92–105 (2013).

258. Ingersoll, K. S. & Cohen, J. The impact of medication regimen factors on adherence to chronic treatment: A review of literature. *J. Behav. Med.* **31,** 213–224 (2008).

259. Patel, S. C. & Spaeth, G. L. Compliance in Patients Prescribed Eyedrops for Glaucoma. *Ophthalmic Surgery, Lasers Imaging Retin.* **26,** 233–236 (1995).

260. Olthoff, C. M. G., Schouten, J. S. A. G., Van De Borne, B. W. & Webers, C. A. B. Noncompliance with ocular hypotensive treatment in patients with glaucoma or ocular hypertension: An evidence-based review. *Ophthalmology* **112,** 953–961 (2005).

261. Yang, J., Han, S., Zheng, H., Dong, H. & Liu, J. Preparation and application of micro/nanoparticles based on natural polysaccharides. *Carbohydr. Polym.* **123,** 53–66 (2015).

CHAPTER 2: NANOGELS OF METHYLCELLULOSE HYDROPHOBIZED WITH N-TERT-BUTYLACRYLAMIDE FOR OCULAR DRUG DELIVERY

Authors: Marion Jamard, Todd Hoare and Heather Sheardown

Objectives: Design of self-assembled nanogels based of methylcellulose grafted with poly(N-tert-butylacrylamide) side chains for topical delivery of pharmaceuticals to the anterior segment of the eye.

Main Scientific contributions:

- Hydrophobically modified methylcellulose by grafting poly(N-tert-butylacrylamide) side chains onto the polysaccharide backbone.
- Produced a copolymer capable of self-assembly into a stable suspension of spherical monodispersed nanogels in aqueous media.
- Demonstrated the ability of the nanogels to encapsulate a hydrophobic model drug and sustain its release.
- Showed tunability of the properties of the self-aggregates varying the degree of hydrophobization of methylcellulose.
- Demonstranted in vitro cytocompatibility of the nanogels after 48-hour incubation with human corneal epithelium cells.

Publication information:
Submitted January 2016 to the special Ocular Drug Delivery issue of Drug Delivery and Translational Research.

Author contributions:
Marion was responsible for the synthesis and characterization of the materials, and paper write-up. The design of the polymer was suggested by Dr Hoare who also provided guidance along the project.

ABSTRACT

While eye drops account for the majority of ophthalmic formulations for drug delivery, their efficiency is limited by rapid pre-corneal loss. In this study, we investigate nanogel suspensions in order to improve the topical ocular therapy by reducing dosage and frequency of administration. We synthesized self-assembling nanogels of 140 nm by grafting side chains of poly(N-tert-butylacrylamide) on methylcellulose via cerium ammonium nitrate. Successful grafting of PNtBAm onto methylcellulose was confirmed by both NMR and ATR FT-IR. Synthesized molecules (MC-g-PNtBAm) self-assembled in water driven by hydrophobic interaction of the grafted side chains creating colloid solutions. Materials were synthesized changing feed ratios of acid, initiator and monomer in order to control the degree of hydrophobic modification. The nanogels were tested for different degrees of grafting. Viability studies performed with human corneal epithelial (hCE) cells testified to the biocompatibility of poly(N-tert-butylacrylamide) grafted methylcellulose nanogels. Dexamethasone was entrapped with an efficiency superior to 95% and its release presented minimal burst phase. Diffusion of drug from the nanogels was found to be delayed by increasing the degree of grafting. The release profile of the entrapped compound from the MC-g-PNtBAm nanogels can thus be tuned by simply adjusting the degree of hydrophobic modification. MC-g-PNtBAm nanogels present promising properties for ocular drug delivery.

Keywords: Methylcellulose, polysaccharide, hydrophobization, self-assembly, nanogels, ophthalmic, drug delivery/release

2.1 INTRODUCTION

Topical administration is the most common delivery method employed to treat diseases of the anterior segment of the eye. Due to their convenience, eye drops account for approximately 90% of commercially available ophthalmic formulations[1,2]. However, the eye is characterized by its high resistance to foreign substances[3]. Rapid drainage through the naso-lacrimal duct, constant dilution by the turnover of tears and low drug permeability across the corneal epithelium[4,5] significantly limit the efficiency of common topical formulations. Only 1% to 5% of the drug reaches the intraocular tissues[6,7]; the remainder of the drug dosage undergoes spillage or nonproductive systemic uptake the latter of which may result in serious adverse effects[8,9]. Multiple daily administrations are then often necessary to achieve therapeutic efficacy, resulting in a higher potential for side effects and lower patient compliance. Thus, there is a need to improve ocular bioavailability and extend drug effect in targeted tissues. The drug delivery system should allow for prolonged contact time with the precorneal tissue to enhance corneal penetration, while remaining patient-friendly.

There is a growing interest in the development of particulate topical formulations[3,6,10–15] to overcome the limitations associated with topical administration methods. Indeed, nanoparticle carriers have been shown to improve drug stability in water and prolong drug activity through the controlled release of encapsulated compounds[3,4,10,15,16]. Hydrophilic nanogels are easily dispersed in aqueous media forming free-flowing opalescent solutions[17–21], and can thus be administered in liquid dosage forms for parenteral or mucosal administration. Able to encapsulate bioactive compounds and release their payload in a controlled fashion[20,22], such formulations could improve topical ocular therapy by reducing

dosage and frequency of administration. Furthermore, previous studies demonstrated that the drug penetration capability across the cornea could be significantly improved when the particle size of nanoparticles is decreased[23–25].

However, a few limitations remain in the currently developed nanoparticle formulations. The synthesis of those nanogels often involves harsh conditions, including the use of organic solvents and high temperatures which can be detrimental to the encapsulated compound[26,27]. Furthermore, an additional step is needed in most cases to induce nanogel formation. When entrapped in particulate systems, the payload is sometimes released within a day with a significant burst phase[14,15,28,29].

As natural biomaterials, polysaccharides are highly stable, non-toxic, hydrophilic and biodegradable. Numerous studies have been conducted on polysaccharides and their derivatives for potential application as nanoparticle drug delivery systems[29–31]. The modification of polysaccharides with hydrophobic moieties has been shown to result in the formation of nanogels in an aqueous environment through a self-assembly process driven by hydrophobic interaction. The resulting stable monodispersed hydrogel nanoparticles have been used to encapsulate and release various bioactive compounds[32–35]. By formation of hydrophobic domains within the nanoparticles in aqueous solution, the hydrophobic moieties are expected to efficiently encapsulate hydrophobic compounds, thus enhancing their water solubility[23–25,36,37].

The aim of the present work was to hydrophobically modify methylcellulose (MC) in order to form nanogels for use as a drug carrier for improving ophthalmic drug availability. MC is a

water-soluble cellulose derivative with a heterogeneous structure consisting of regions substituted with methoxy groups called hydrophobic zones and less substituted regions called hydrophilic zones[38]. This natural biopolymer has been extensively investigated for biomedical applications, including ocular applications due to its biocompatibility and degradablility[39–41] and was thus chosen as the base polysaccharide for the nanogels. N-substituted acrylamides are temperature-sensitive monomers, which can produce thermosensitive polymeric structure and have been repeatedly used for the synthesis of biomaterials[42–45], especially for hydrophobization[42–48]. N-tert butylacrilamide (NtBAm) was thus selected as the hydrophobic moiety.

Nanogels were synthesized by grafting hydrophobic branches of poly(N-tert-butylacrylamide) (PNtBAm) onto methylcellulose, using cerium ammonium nitrate (Figure 2-1). Often used on polysaccharides[49–51], grafting via cerium ammonium nitrate (CAN) results in high grafting efficiency[52–57] with minimal undesirable side-reactions[58–60], and has the advantage of being carried out in water at room temperature. Cellulose and its derivatives have previously been grafted using CAN with poly-N-isopropylacrylamide[61], polyacrylonitrile[62–64], methylmethacrylate[64] and polyacrylic acid[65]. The nanogels prepared with PNtBAm grafted MC (MC-g-PNtBAm) were synthesized with varying feed ratios of monomer, initiator and acid in order to examine the impact of those factors on the amount of NtBAM grafted, and how the degree of hydrophobic modification would influence the nanogel properties. MC-g-PNtBAm nanogels were then characterized including morphological structure, size, biocompatibility with HCE cells, and loaded with dexamethasone to evaluate their potential for delivery of drugs.

2.2 EXPERIMENTAL SECTION

2.2.1 Materials

Methylcellulose (MC) Metholose SM-15 was purchased from Shin-Etsu (Totowa, NJ, USA). N-tert-butylacrylamide (NtBAm), Cerium ammonium nitrate (CAN) and dimethyl sulfoxide-d6 (DMSO-d6) were purchased from Sigma-Aldrich, and Dexamethasone from Sigma Life Science (D1756) (St Louis, MO, USA). Phosphate buffered saline (PBS) 10 times concentrate was obtained from BioShop (McMaster University – Ontario, Canada). Nitric acid 70% was bought from EMD Chemical Inc. Vybrant MTT cell proliferation assay kit and LIVE/DEAD viability/cytotoxicity kit were purchased from Molecular Probes by Life Technologies (Eugene, Oregon, USA) and cell growth media – Keratinocyte-SFM came from Gibco by Life Technologies (Grand Island, NY, USA). Human corneal epithelial cells[66] (hCECs) were the kind gift of Dr. May Griffith.

2.2.2 Preparation of MC-g-PNtBAm nanogels

In a round bottom flask, 0.25g of MC was dissolved in 50mL of water (0.5% w/v). NtBAm at different ratios, was incorporated into the solution, and when dissolved, nitric acid (at 70%) was added. The mixture was purged with nitrogen for 30 minutes. Finally, CAN dissolved in 1 mL of purified water prepared in a Millipore Milli-Q system, was syringed into the solution to start the polymerization. The reaction was left stirring at room temperature for 24 hours, followed by extensive dialysis (Pre-wetted RC tubing 3.5kDa, Spectrum Laboratories) to remove any unreacted compound.

Various amounts of NtBAm, nitric acid and CAN were used to synthesise the nanogels as shown in Table 2-1.

2.2.3 FT-IR analysis

FT-IR spectra of freeze dried samples were measured (Bruker Vertex 70 Bench and HTS plate reader) as KBr discs in the range of 400 to 4000 cm^{-1}.

2.2.4 NMR analysis

Freeze dried materials (Labconco 7752020) were dissolved in DMSO-d6 and analyzed by nuclear magnetic resonance (NMR, Bruker AVANCE 600 MHz NMR spectrometer). Nanogel nomenclature was based on the degree of hydrophobization, calculated as the average number of NtBAm monomer for 100 anhydroglucose units (AGU) of the MC following the equation below. For example, MC-g-PNtBAm_50% denotes a nanogel with 50 NtBAm units for 100 AGU.

$$DH = \frac{\frac{A_{NtBAm}}{9}}{A_{MC}} * 100$$

A_{NtBAm}: Area under the peak corresponding to the tert-butyl group = 9 hydrogens (1.26 ppm) for each NtBAm monomer.

A_{MC}: Area under the peak corresponding to the hydrogen in C2 position (2.81 ppm) = 1 hydrogen for each AGU.

2.2.5 Particle size measurements

Particle mean size was measured by single nanoparticle tracking (Malvern NanoSight LM10).

2.2.6 Transmission electon microscopy study

After diluting the sample 10-fold or 40-fold with purified water, 5 μL of the suspension was spread on 200 mesh Formvar coated cooper grids without staining and allowed to dry under ambient atmospheric conditions. The morphology of nanogel samples was viewed and photographed using transmission electron microscopy (TEM, JEOL 1200EX TEMSCAN) with 80kv electron beam.

2.2.7 Loading of dexamethasone

To load dexamethasone into the nanogels, MC-g-PNtBAm synthesis was performed in a 0.01% w/v aqueous solution of dexamethasone. The nanogel suspension was then ultracentrifuged (Sorvall WX90) at 50,000 rpm at 23°C for 30 min. The amount of drug in the supernatant was measured by high performance liquid chromatography (HPLC, Waters 2707 Autosampler, 1525 Binary HPLC Pump, 2489 UV/Visible detector, Waters Atlantis dC18, 5 μm column) using 1mL/min isocratic flow rate of 40:60 (v/v) acetonitrile:water, a 10μL sample injection volume and a 254 nm detection wavelength. Sample concentrations were determined based on a standard calibration curve of dexamethasone in 40:60 (v/v) acetonitrile:water.

The loading efficiency of dexamethasone into the nanogel particles was calculated using the following equation:

$$Loading\ efficiency\ (\%) = 100 * \frac{Initial\ amount\ of\ drug - Amount\ of\ drug\ in\ supernatant}{Initial\ amount\ of\ drug}$$

2.2.8 In vitro release of dexamethasone

The in vitro release of dexamethasone from the nanogels was evaluated in phosphate buffered saline (PBS). A dialysis membrane (molecular weight cutoff 3500 Da, Spectra/Por, Spectrum laboratories) was first soaked in the dissolution medium and tied at one end. The dispersion of drug-loaded particles in PBS was placed into this bag and its other end was tied. The bag was immersed into 5 mL of PBS maintained at 32 ± 1 °C by a shaking water bath. Released dexamethasone was sampled at selected time intervals by removing the release medium and replacing it with fresh pre-warmed PBS. Concentrations of dexamethasone in the releasate were determined by HPLC (using the same method as described for loading). The release profile of dexamethasone was compared with a control sample in which dexamethasone was dissolved directly in PBS and placed on the dialysis membrane. All measurements were performed in triplicate and plotted as mean ± SD.

2.2.9 Cell toxicity studies

The determination of cell viability is a common assay to evaluate the in vitro cytotoxicity of biomaterials. In the present study, cell viability was assessed by the MTT assay and Calcein AM – Ethidium homodimer-1 staining assay.

MC-g-PNtBAm samples were sterilized by the 1% of penicillin-streptomycin and UV irradiation (254 nm) overnight. Human corneal epithelium cells (hCECs) were seeded onto 96-well plates at a density of 5,000 cells/well and cultured in 100µL of keratinocyte serum free medium for 24 hours in a CO_2 incubator. The spent medium was replaced with nanogel formulations and diluted with culture medium to give a methylcellulose concentration of 0.225 and 1.125 mg/ml. After 48 hours of incubation at 37°C, the nanogel containing media was replaced with 100µL of PBS and 10µL of MTT stock (5 mg/ml) or 100µL of calcein AM-ethidium homodimer-1 working solution (2µM calcein AM, 4µM ethicium homodimer-1).

For the calcein AM – Ethidium homodimer-1 assay, the cells were incubated for 45 minutes at room temperature. For the MTT assay, the cells were incubated for 4 hours. Then, the supernatant was replaced by 50µL of DMSO and incubated at 37°C for 10 minutes. The resultant solutions were measured in a microplate reader (Tecan Infinite 200 Pro) at 540 nm (MTT assay) or 530 and 645 nm (Calcein and Ethidium) in a microplate reader (Tecan Infinite 200 Pro).

Cell viability was expressed as percentage of absorbance relative to control comprising cells not exposed to the nanogels. Experiments were performed on 4 different nanogels at two concentrations with six replicate wells for each sample and control per assay.

2.3 RESULTS AND DISCUSSION

2.3.1 Synthesis of MC-g-PNtBAm nanogels

Grafting of PNtBAm side chains from a MC backbone in an aqueous solution produced nanogels through a self-assembly mechanism driven by hydrophobic interactions. At the first stage of the synthesis process, radicals are formed along the MC backbone from which chain polymerization of NtBAm occurs. When the hydrophobic modification reaches a critical degree, the PNtBAm chains gather to form hydrophobic domains, thus driving self-assembly of the MC-g-PNtBAm molecules into nanogels. Based on Akiyoshi et al., it was proposed that the self-assembled particle was as a nanosized hydrogel, in which the polysaccharide chains are cross-linked noncovalently by associating hydrophobic moieties forming a polycore model [67]. As no macroscopic precipitation takes place in this process, it is suggested that the PNtBAm chains are mostly contained in the bulk of the nanogels while the periphery of the nanoparticles is mostly methylcellulose, which stabilizes the colloid.

Successful grafting of PNtBAm onto methylcellulose was confirmed by both NMR and FTIR. The NMR spectra showed the peak for the butyl groups at 1.26ppm (Figure 2-2). FTIR analysis revealed the appearance of a peak at 1651cm^{-1} assigned to the characteristic absorption of the carbonyl groups of the ring opening of the MC backbone. An absorbance band at 1510cm^{-1} is attributed to the secondary amine bending and peaks at 1390/1361/1224cm^{-1} are associated with the butyl groups of PNtBAm (Figure 2-3).

2.3.2 Effect of monomer, initiator and acid concentrations on the degreee of hydrophobization

Different materials were synthesized by changing acid, initiator and monomer concentrations, with the aim of looking into the impact of those factors on the degree of hydrophobic modification and the corresponding properties of the nanogels.

The amount of hydrophobic modification varying acid and initiator concentrations was compared with a constant concentration of NtBAM at its maximum solubility in solution (9 g/L). With increased acid concentration, hydrophobic grafting increased. However, the impact is limited at low initiator concentration as shown in Figure 2-4-a. Similarly, increasing the initiator concentration increases the grafting percentage, but does not have an impact at low acid concentration (Figure 2-4-b). Supplementary data support these trends at different values of monomer, initiator and acid concentrations (Figures A1, A2 and A3).

The role of nitric acid in the grafting mechanism is to prevent hydration of the ceric(IV) ions[61]. Thus, in the presence of insufficient concentrations of nitric acid, ceric(IV) ions are hydrated and are hence inactive for generating active sites on the MC for grafting of PNtBAm. Thus, increasing the feed concentration of initiator to 9.12×10^{-3} mol/L does not increase initiation unless there is additional acid available to minimize hydration. An excess of nitric acid compared to initiator did not have an impact on the grafting reaction (Figure 2-4-a).

The trends observed when increasing NtBAm concentration in solution with high initiator concentration (Figure 2-4-c) suggest that the concentration of initiator requires a matching

concentration of nitric acid to allow for all of the CAN to be active. Indeed, in the presence of high acid concentration, grafting increased consistently by increasing the amount of monomer, while it plateaued with a lower acid concentration. In accordance with previous studies[61,62], it was also shown that with sufficient active ceric(IV) ions to initiate, increasing monomer concentration increased the grafting degree. These observations clearly indicate that sufficient nitric acid has to be available in the mixture to maintain the oxidation potential of ceric(IV), otherwise the efficiency of ceric(IV) ions is changed significantly.

Based on the trends, it appears that initiation is key to grafting efficiency. Indeed, at high acid and monomer concentrations, increasing the amount of CAN increases the amount of NtBAm grafted on MC (Figure 2-4-b). Higher initiation implies that more growing chains are visible on which the monomers can graft before the hydrophobic modification reaches a sufficiently high degree to trigger self-assembly of the MC-g-PtBAm molecules into nanoparticles. Then, graft polymerization stops as the grafted chains are gathered into the hydrophobic domains where they are no longer accessible to the remaining monomers in the aqueous phase (Figure 2-5).

2.3.3 Size and morphology of the MC-g-PNtBAm nanogels

The effect of the degree of hydrophobization (DH) on the nanogel morphology was studied using Nanosight and TEM. Irrespective of the DH, Nanosight revealed that all materials were unimodal and monodispersed self-aggregates, as reported for other self-assembled particles made of hydrophobized polysaccharides[67]. In the swollen state, the nanogels are 143 nm ± 22 nm, with no significant impact of the DH on their average size. Longer grafted

chains have been reported to lead to larger particles[68] and higher hydrophobicity can reduce swelling in water leading to smaller particles[33,67]. We postulate that the absence of impact of grafting on the nanogel size is likely due to a trade-off between these two effects. An optimum size range is required to enhance the bioavailability of the drug at ocular surface or disease site. Smaller particles (100 nm) were shown to exhibit the highest uptake compared to larger particles (800 nm and 1000 nm) and particles of 100 nm were able to penetrate the corneal barrier[69]. The MC-g-PNtBAm nanogels, at 140 nm, thus seem to be in the suitable range for ocular drug delivery.

The nanogels were observed under TEM for different grafting percentages, and appeared monodispersed with a spherical morphology (Figure 2-6). When suspended in water, their size was smaller than in swollen state and increased from 10 nm to about 100 nm with increasing DH. Indeed, the degree of hydrophobic modification would be expected to impact the water content of the nanoparticles. A high DH implies more hydrophobic domains which decrease the swelling capacity. Therefore, when dried for TEM observation, the nanogel size was reduced accordingly. For example, the self-aggregate MC-g-PNtBAm_149% is composed of 37% (by volume) polysaccharide and 63% (by volume) water. Hence, the self-aggregate is regarded as a nanosize hydrogel. Its density increases with the DH, the MC chain behaving as an expanded flexible coil[67,70].

2.3.4 Viability studies

A preliminary biocompatibility test of the nanogels was carried out using human corneal epithelial cells. The nanogels were tested for different degrees of grafting at concentrations

of 2.5 mg and 0.5 mg per mL of media for 48 hours. After incubating for 48 hours, the relative cell viability was higher than 90% for all of the nanogels, indicating that their presence did not negatively impact cell viability (Figure 2-7-a). Percentages above 100% are due the fact that the data is expressed relative to the control. The MTT assay verified that there was no negative effect on the metabolism (Figure 2-7-b). The cells continue to proliferate in the presence of the material at a similar rate. Figure 2-8 shows the morphology of the cells incubated in presence of MC-g-PNtBAm_149% compared to the control cells.

2.3.5 Dexamethasone encapsulation

Four materials were chosen to perform a drug encapsulation and release study. The nanogels were loaded with dexamethasone during their synthesis: NtBAm grafting was performed in an aqueous solution of dexamethasone, and the drug was entrapped during the self-assembly of MC-g-PNtBAm. It could be seen from Table 2-2 that all materials showed an encapsulation efficiency superior to 95%. As the binding constants have been reported to become larger with increase in the hydrophobicity of the probes[33], this high complexation of dexamethasone with the nanogel is believed to be mainly driven by hydrophobic interaction[71]. The drug would thus mostly be entrapped within the hydrophobic domains formed by the PNtBAm chain self-aggregates.

2.3.6 In vitro release of dexamethasone

With simple eye drops, it is not possible to maintain therapeutic concentration on the ocular surface for a prolonged time, and frequent dosing often leads to compliance failures as well as an increased risk of side effects. A sustained drug release system has the potential to

improve patient compliance through a reduction in the frequency of administration. Release from the nanogels was evaluated using the model ophthalmic drug dexamethasone. Dexamethasone, loaded into MC-g-PNtBAm nanogels, was released at 32 ± 1 °C in PBS to mimic the front of the eye conditions. The release profiles of dexamethasone-loaded nanogels with different degrees of grafting were compared with that of a control sample of dexamethasone dissolved directly in PBS, in order to ensure that the release profile was not an artefact of the method.

The cumulative release of dexamethasone from the different samples was plotted as a function of time is shown in Figure 2-9. The nanogels showed release profiles that were characterized by a very slight initial burst followed by a sustained-release phase. The first release region presumably corresponds to drugs soaked into the hydrophilic MC part of the nanogels, or drugs encapsulated near the surface[72,73] whereby a quick release should be expected to occur. As a result, less swollen particles with higher DH, show a smaller burst. The nanogels exhibited the burst-release during the initial 48 hours, releasing from 2.5% to 20% of the drug.

The second stage is remarkably slower, remaining relatively steady until the release assay is fully carried out. Only up to 28% of the dexamethasone was released in the time frame of the study, but the study was terminated as the nangels are expected to be cleared from the surface of the eye by 30 days. This sustained-release phase most likely corresponds to the diffusional release of the drugs from the hydrophobic PNtBAm domains of the nanogels[74]. It was found that different release profiles could be obtained depending on the degree of grafting. The more NtBAm was grafted, the slower the drug was released.

The release appeared to reach a plateau at the final phase (after 7-20 days depending on the material), with an accumulative release which did not equal the total amount of dexamethasone loaded into the nanogels. This stage has been observed in previous release studies from aggregates of hydrophobized polysaccharides[27,75–78], and was attributed to the the high affinity of the dexamethasone for the hydrophobic PNtBAm domains.

A higher degree of grafting presumably leads to more hydrophobic domains within the nanogels. The affinity of the dexamethasone for the PNtBAM domains within the nanogel resulted in a delay of the diffusion and release of dexamethasone in solution. The rate of the release can thus be tuned by the degree of hydrophobic modification depending on the application and dosage needed.

2.4 CONCLUSION

Novel MC-g-PNtBAm nanogels were successfully prepared using cerium ammonium nitrate. The mild reaction conditions (no organic solvent, room temperature) are suitable for encapsulation of biological compounds. The ability of these materials to self-assemble prevents the need for an extra step. Grafting degree could be controlled on tuning the nitric acid, CAN and NtBAm feed ratios, forming spherical particles of 140 nm diameter in water. Viability studies performed with HCE cells demonstrated in vitro biocompatibility. As well the synthesized nanogels showed efficient entrapment of dexamethasone. The drug presented no significant burst phase and was released slowly over several weeks, with a release rate that was tunable with the degree of grafting. Those properties suggest that the MC-g-PNtBAm nanogels may have possible application as ocular drug carriers.

2.5 TABLES

Table 2-1: Concentrations of acid, initiator and monomer used to synthesize MC-g-PNtBAm

		Nitric acid	CAN	NtBAm
1		75 mL	50 mg	50 mg
	Concentration	2.52×10^{-2} mol/L	1.82×10^{-3} mol/L	7.86×10^{-3} mol/L
2		150 mL	150 mg	250 mg
	Concentration	5.04×10^{-2} mol/L	5.48×10^{-3} mol/L	3.94×10^{-2} mol/L
3		300 mL	250 mg	450 mg
	Concentration	1.01×10^{-1} mol/L	9.12×10^{-3} mol/L	7.08×10^{-2} mol/L

Table 2-2: Loading efficiency of dexamethasone into MC-g-PNtBAm nanogels as a function of feed composition and grafting degree

Feed composition	Entrapment (%)
MC-g-PNtBAm_30%	96.13 ± 0.07
MC-g-PNtBAm_33%	99.84 ± 0.01
MC-g-PNtBAm_54%	98.56 + 0.06
MC-g-PNtBAm_149%	98.84 ± 0.03

2.6 FIGURES

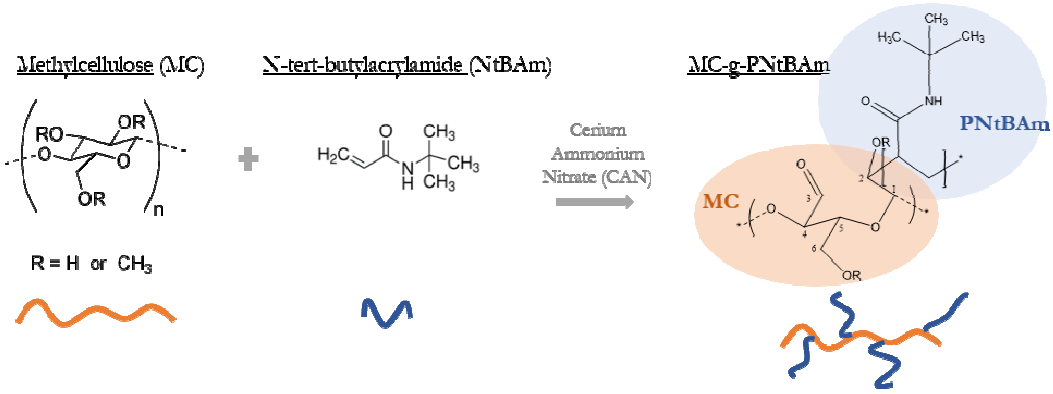

Figure 2-1: Synthesis of MC-g-PNtBAm copolymers. Grafting reaction of NtBAm on MC via cerium ammonium nitrate

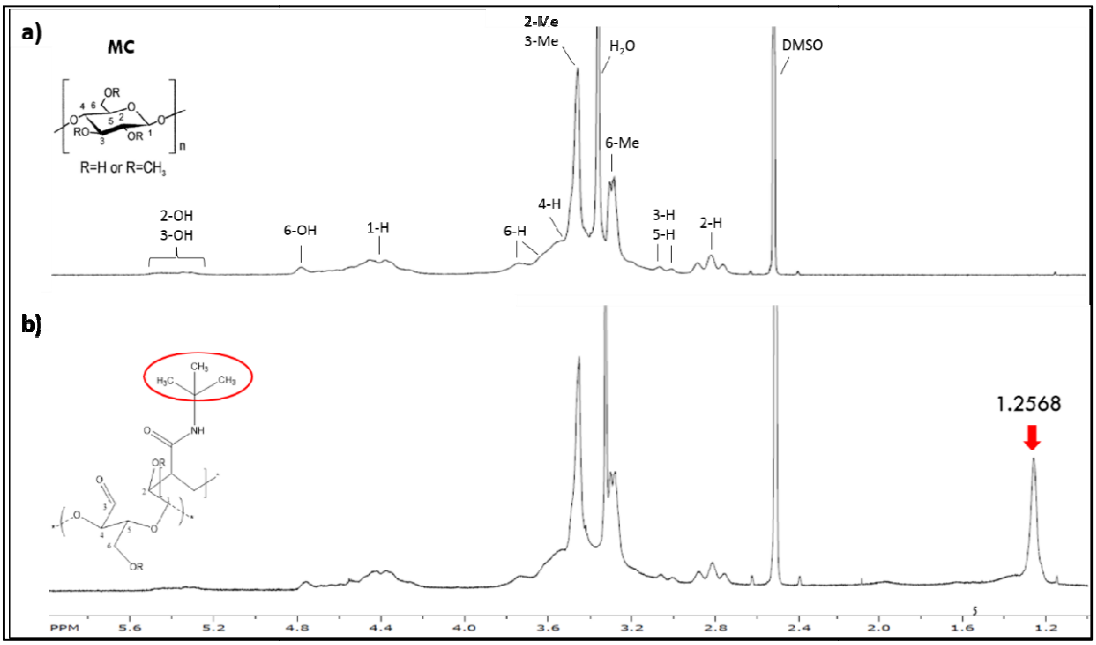

Figure 2-2: NMR spectra of a) MC, b) MC-g-PNtBAm

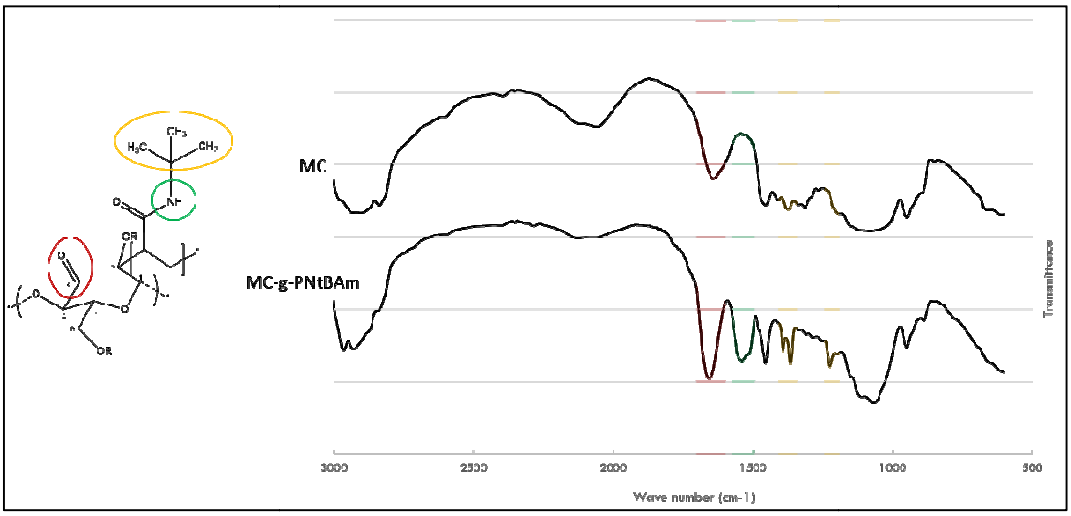

Figure 2-3: FT-IR spectra of MC and MC-g-PNtBAm

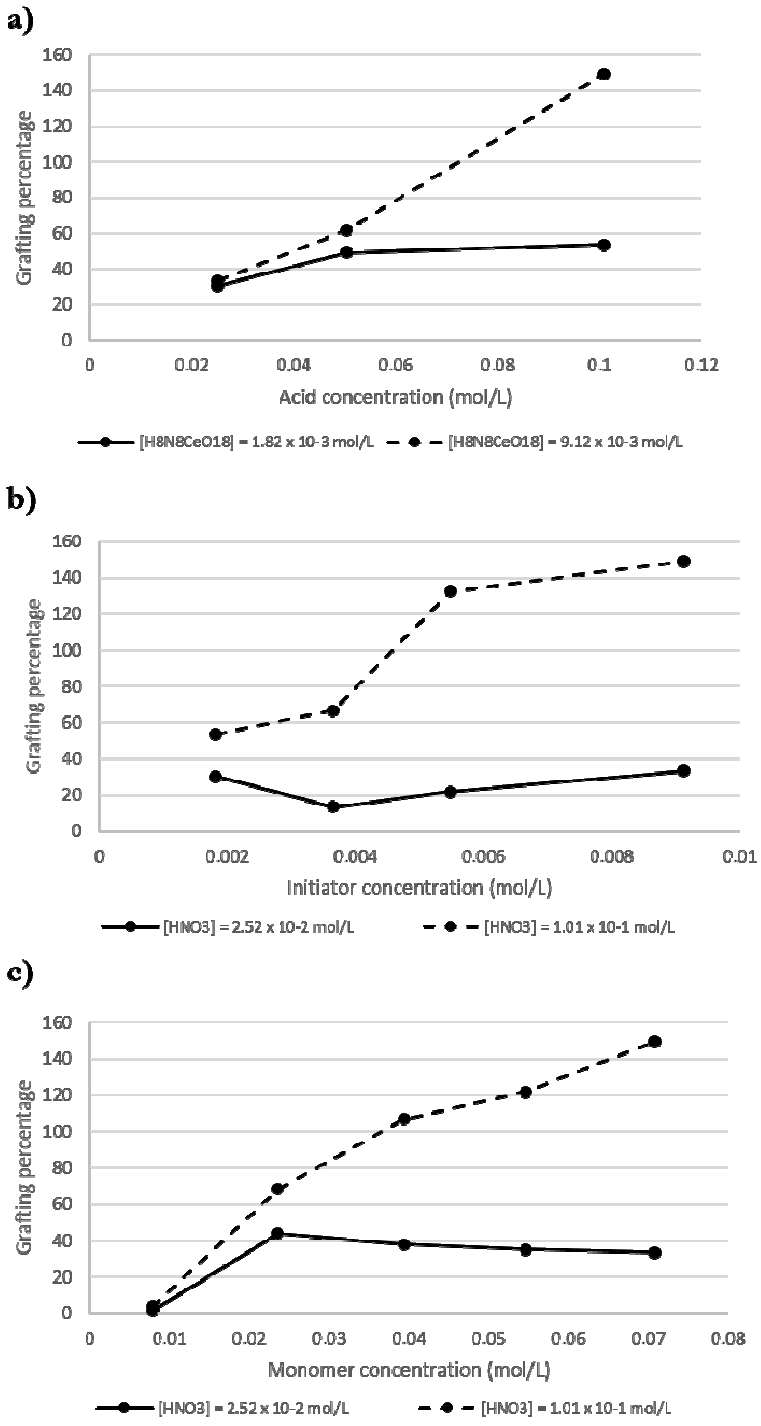

Figure 2-4: Degree of hydrophobization when increase in a) nitric acid concentration b) cerium ammonium nitrate concentration c) NtBAm concentration

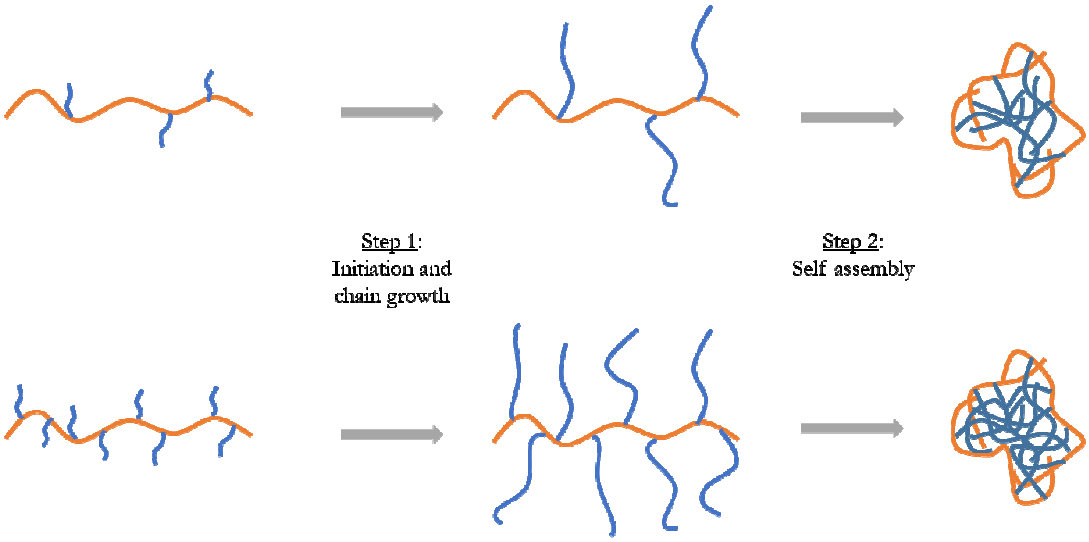

Figure 2-5: Effect of initiation on the degree of hydrophobization

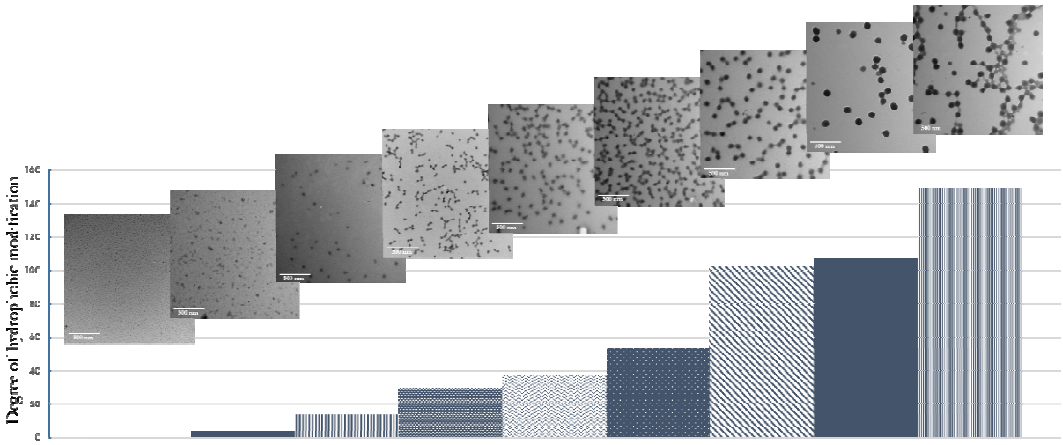

Figure 2-6: Morphology of the MC-g-PNtBAm nanogels with different degrees of hydrophobic modification.

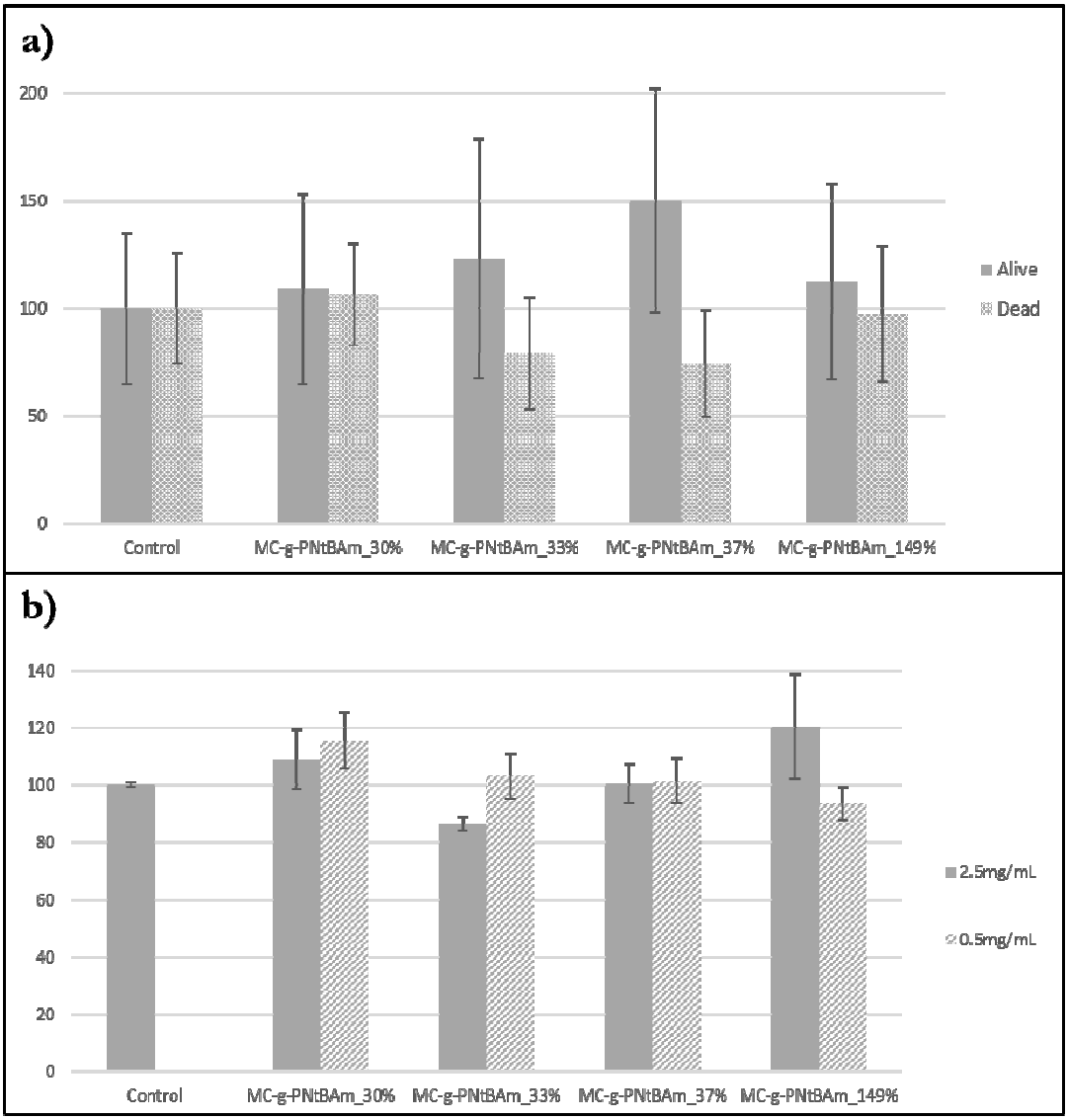

Figure 2-7: Comparison of a) cell viability in presence of 1.125 mg/mL MC-g-PNtBAm nanogels and b) metabolism in presence of 1.125 mg/mL and 0.225mg/mL MC-g-PNtBAm nanogels. Data expressed as a percentage relative to control comprising cells not exposed to the nanogels.n=6, error bars corresponding to the standard deviation.

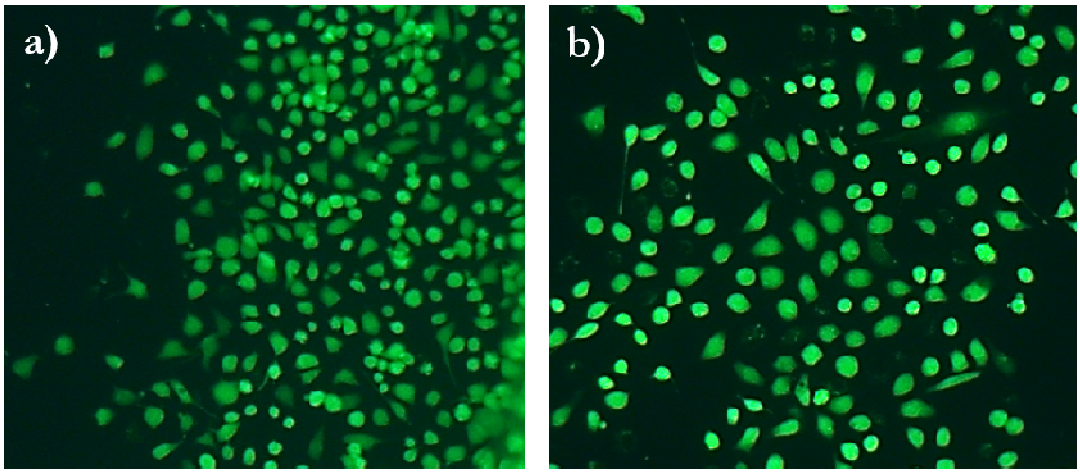

Figure 2-8: Cells after 48 hour incubation a) control b) with MC-g-PNtBAm_149%

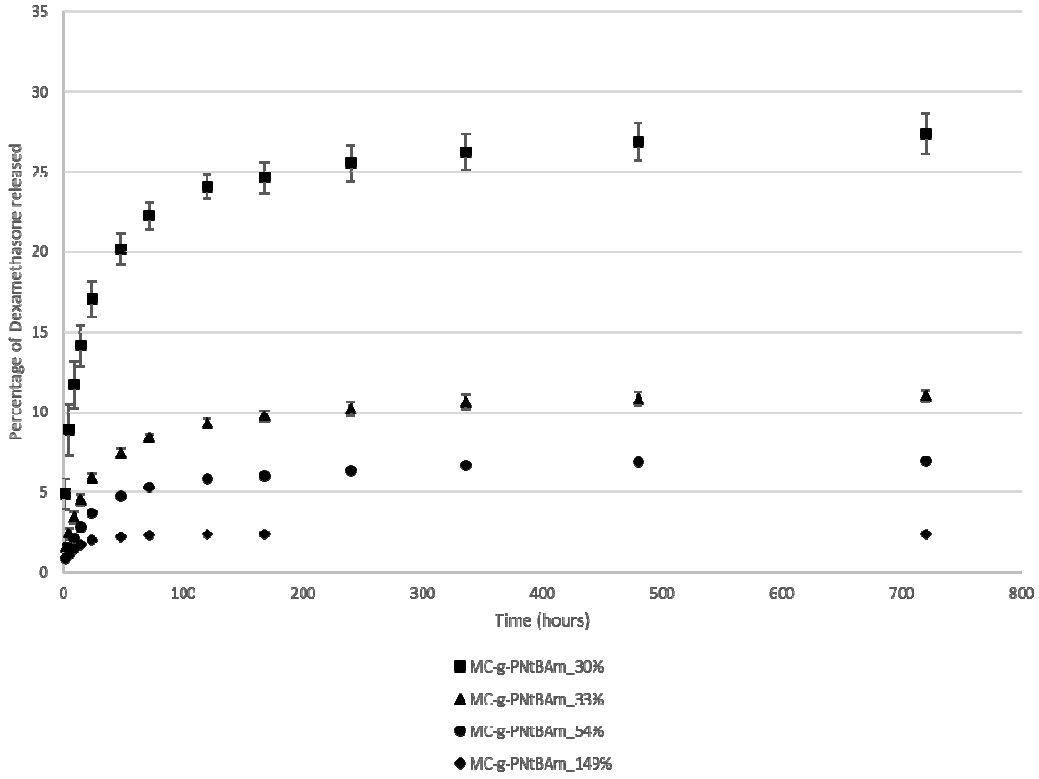

Figure 2-9: Release profiles of dexamethasone from MC-g-PNtBAm nanogels with different degrees of hydrophobic grafting.n=3 with the error bars corresponding to the standard deviation.

2.7 ACKNOWLEDGEMENTS

Funding support from NSERC and the CREATE Biointerface Training Program is gratefully acknowledged.

2.8 DISCLOSURES

The authors state no conflict of interest.

2.9 SUPPORTING INFORMATION

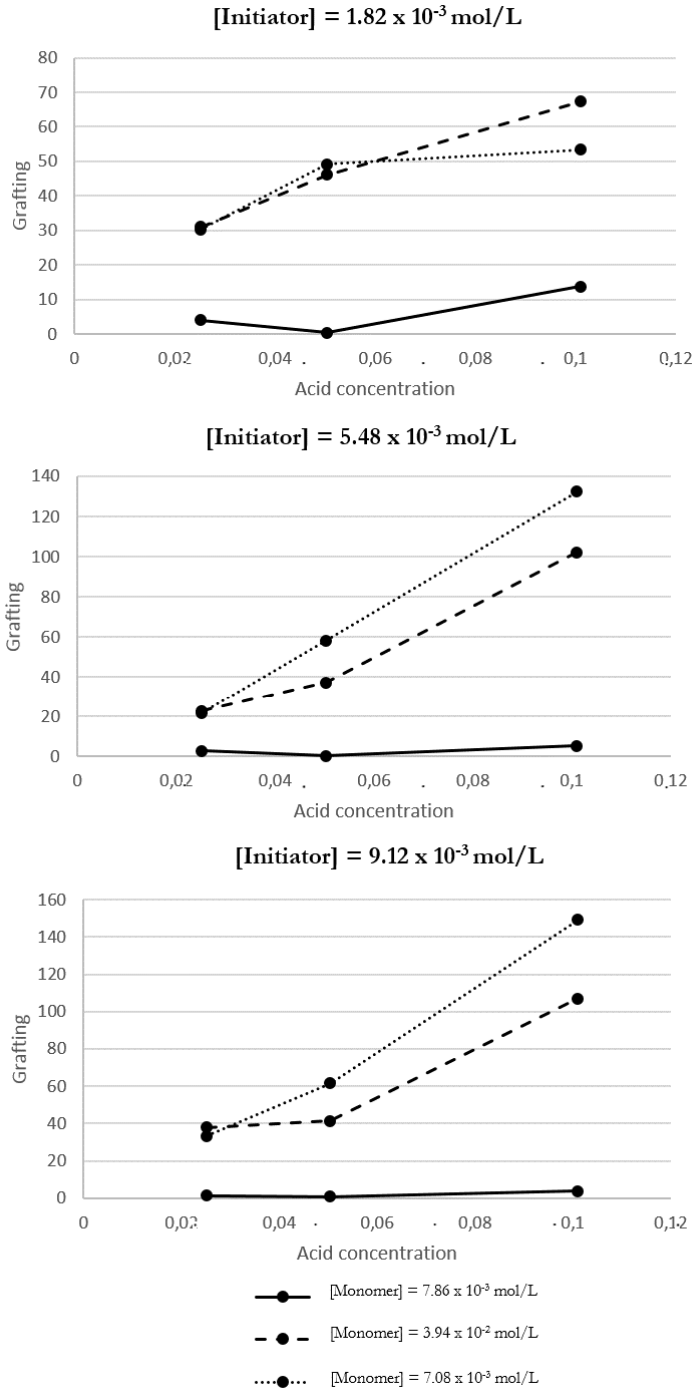

Figure A1: Influence of nitric acid concentration on hydrophobic grafting

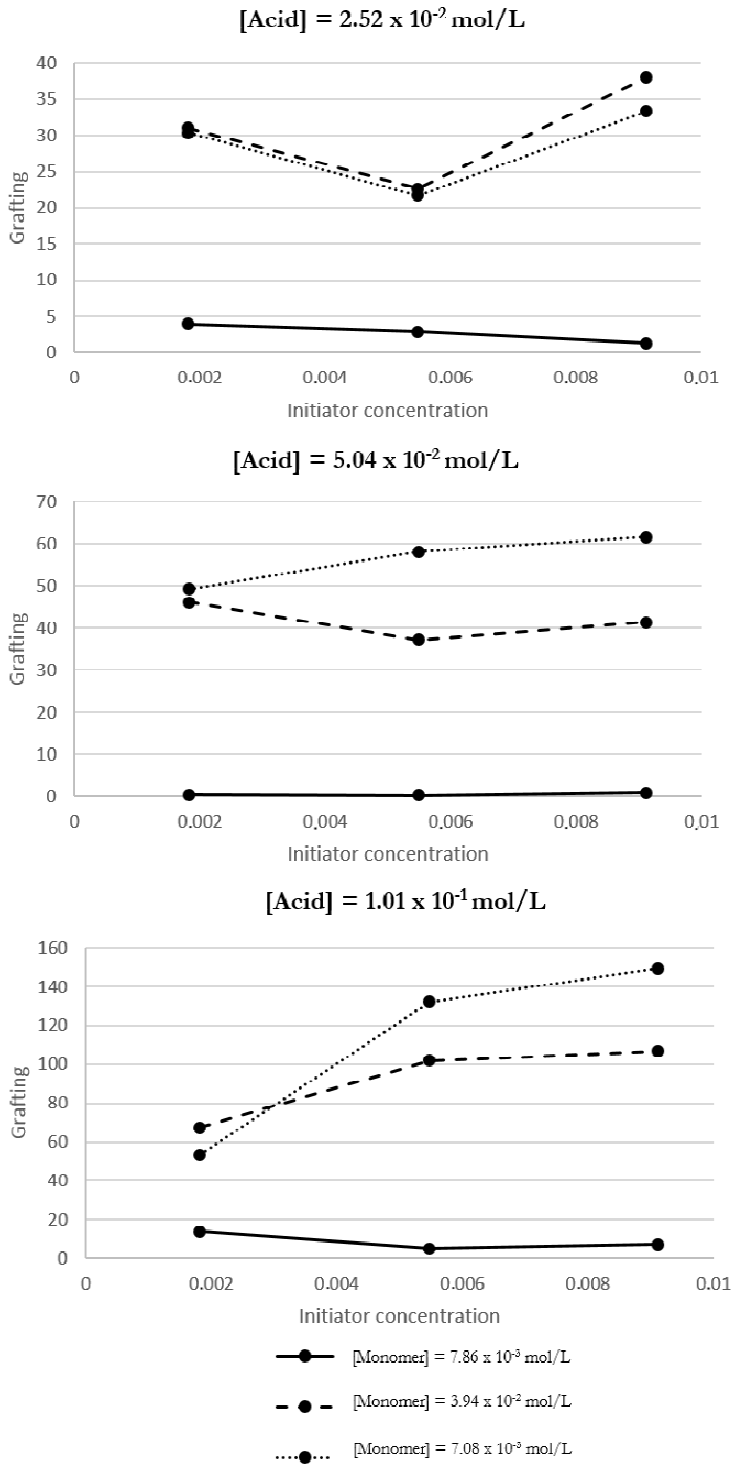

Figure A2: *Influence of cerium ammonium concentration on hydrophobic grafting*

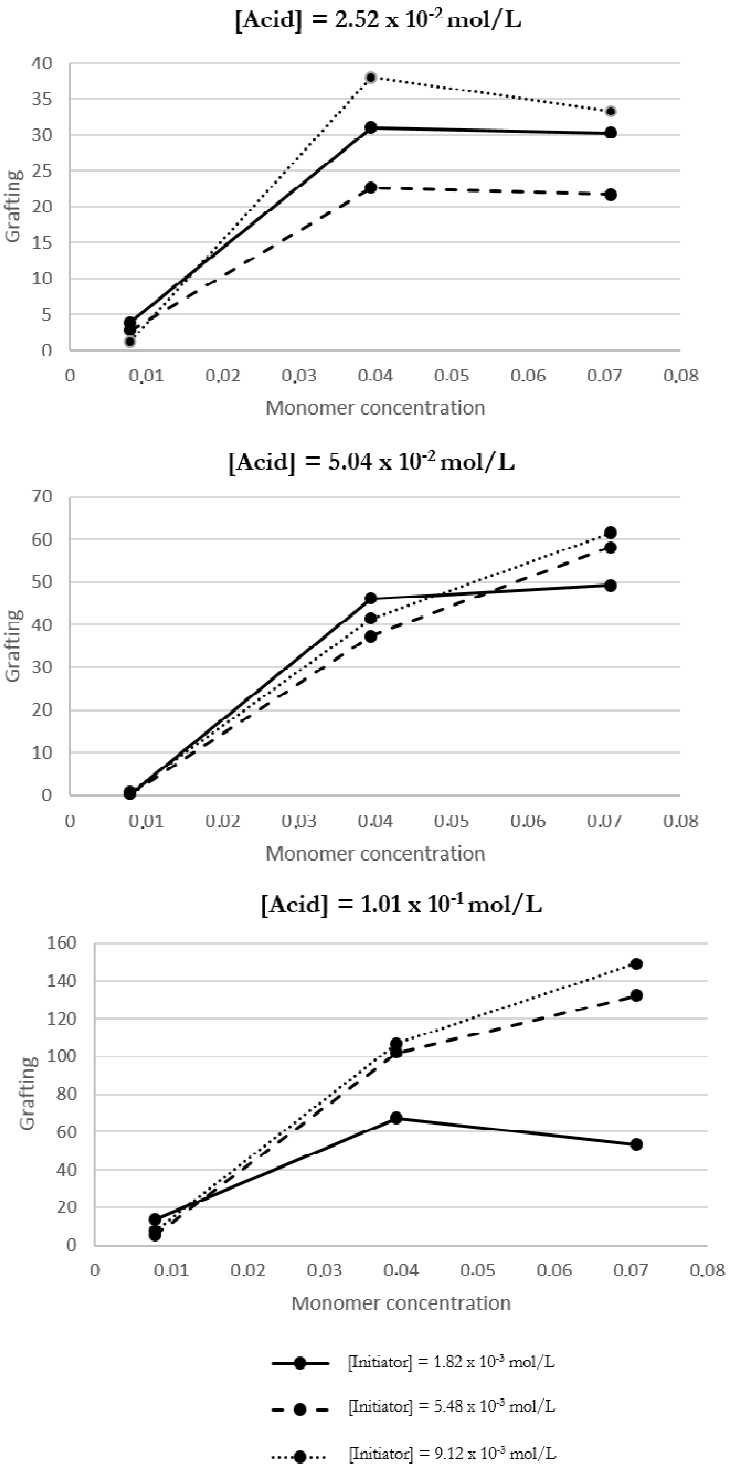

Figure A3: Influence of N-tert butylacrylamide concentration on hydrophobic grafting

BIBLIOGRAPHY

1. Jansook, P. *et al.* Cyclodextrin solubilization of carbonic anhydrase inhibitor drugs: Formulation of dorzolamide eye drop microparticle suspension. *Eur. J. Pharm. Biopharm.* **76,** 208–214 (2010).
2. Loftsson, T., Hreinsdóttir, D. & Stefánsson, E. Cyclodextrin microparticles for drug delivery to the posterior segment of the eye: aqueous dexamethasone eye drops. *J. Pharm. Pharmacol.* **59,** 629–635 (2007).
3. Diebold, Y. & Calonge, M. Applications of nanoparticles in ophthalmology. *Prog. Retin. Eye Res.* **29,** 596–609 (2010).
4. Gaudana, R., Jwala, J., Boddu, S. H. S. & Mitra, A. K. Recent perspectives in ocular drug delivery. *Pharm. Res.* **26,** 1197–216 (2009).
5. Bozdag, S. *et al.* In vitro evaluation of gentamicin- and vancomycin-containing minitablets as a replacement for fortified eye drops. *Drug Dev. Ind. Pharm.* **36,** 1259–1270 (2010).
6. Li, X., Zhang, Z. & Chen, H. Development and evaluation of fast forming nano-composite hydrogel for ocular delivery of diclofenac. *Int. J. Pharm.* **448,** 96–100 (2013).
7. Patton, T. F. & Robinson, J. R. Quantitative precorneal disposition of topically applied pilocarpine nitrate in rabbit eyes. *J. Pharm. Sci.* **65,** 1295–1301 (1976).
8. Qi, H. *et al.* Development of a poloxamer analogs/carbopol-based in situ gelling and mucoadhesive ophthalmic delivery system for puerarin. *Int. J. Pharm.* **337,** 178–187 (2007).
9. Urtti, a. *et al.* Controlled drug delivery devices for experimental ocular studies with timolol 2. Ocular and systemic absorption in rabbits. *Int. J. Pharm.* **61,** 241–249 (1990).
10. Nagarwal, R. C., Kant, S., Singh, P. N., Maiti, P. & Pandit, J. K. Polymeric nanoparticulate system: a potential approach for ocular drug delivery. *J. Control. Release* **136,** 2–13 (2009).
11. Sosnik, A., das Neves, J. & Sarmento, B. Mucoadhesive polymers in the design of nano-drug delivery systems for administration by non-parenteral routes: A review. *Prog. Polym. Sci.* **39,** 2030–2075 (2014).
12. Gan, L. *et al.* Recent advances in topical ophthalmic drug delivery with lipid-based nanocarriers. *Drug Discov. Today* **18,** 290–7 (2013).
13. Li, N. *et al.* Liposome coated with low molecular weight chitosan and its potential use in ocular drug delivery. *Int. J. Pharm.* **379,** 131–8 (2009).
14. Liu, R. *et al.* Thermosensitive in situ nanogel as ophthalmic delivery system of curcumin: development, characterization, in vitro permeation and in vivo pharmacokinetic studies. *Pharm. Dev. Technol.* **21,** 576–582 (2016).
15. Abd El-Rehim, H. a., Swilem, A. E., Klingner, A., Hegazy, E.-S. a S. a & Hamed, A. a. Developing the potential ophthalmic applications of pilocarpine entrapped into polyvinylpyrrolidone-poly(acrylic acid) nanogel dispersions prepared by γ radiation. *Biomacromolecules* **14,** 688–98 (2013).
16. Liu, S., Jones, L. & Gu, F. X. Nanomaterials for ocular drug delivery. *Macromol. Biosci.* **12,** 608–20 (2012).
17. Moya-Ortega, M. D., Alvarez-Lorenzo, C., Concheiro, A. & Loftsson, T. Cyclodextrin-based nanogels for pharmaceutical and biomedical applications. *Int. J. Pharm.* **428,** 152–163 (2012).
18. Oh, J. K., Drumright, R., Siegwart, D. J. & Matyjaszewski, K. The development of

microgels/nanogels for drug delivery applications. *Prog. Polym. Sci.* **33,** 448–477 (2008).

19. Samah, N. A., Williams, N. & Heard, C. M. Nanogel particulates located within diffusion cell receptor phases following topical application demonstrates uptake into and migration across skin. *Int. J. Pharm.* **401,** 72–78 (2010).
20. Sawada, S. I., Sasaki, Y., Nomura, Y. & Akiyoshi, K. Cyclodextrin-responsive nanogel as an artificial chaperone for horseradish peroxidase. *Colloid Polym. Sci.* **289,** 685–691 (2011).
21. Guo, Q., Wu, Z., Zhang, X., Sun, L. & Li, C. Phenylboronate-diol crosslinked glycopolymeric nanocarriers for insulin delivery at physiological pH. *Soft Matter* **10,** 911 (2014).
22. Kettel, M. J., Dierkes, F., Schaefer, K., Moeller, M. & Pich, A. Aqueous nanogels modified with cyclodextrin. *Polymer (Guildf).* **52,** 1917–1924 (2011).
23. Rafie, F. *et al.* In vivo evaluation of novel nanoparticles containing dexamethasone for ocular drug delivery on rabbit eye. *Curr. Eye Res.* **35,** 1081–1089 (2010).
24. Li, X. *et al.* Diclofenac/biodegradable polymer micelles for ocular applications. *Nanoscale* **4,** 4667 (2012).
25. Gupta, H. *et al.* Biodegradable levofloxacin nanoparticles for sustained ocular drug delivery. *J. Drug Target.* **19,** 409–17 (2011).
26. Ganguly, K., Chaturvedi, K., More, U. a., Nadagouda, M. N. & Aminabhavi, T. M. Polysaccharide-based micro/nanohydrogels for delivering macromolecular therapeutics. *J. Control. Release* **193,** 162–173 (2014).
27. Yanzhu Guo; Li Zhang; Haiming Li; Ying Han; Jinghui Zhou; Xiaohui Wang. Self-assembly and paclitaxel loading capacity of α-tocopherol succinate-conjugated hydroxyethyl cellulose nanomicelle. *Colloid Polym Sci* **294,** 135–143 (2016).
28. Moya-Ortega, M. D. *et al.* Dexamethasone eye drops containing γ-cyclodextrin-based nanogels. *Int. J. Pharm.* **441,** 507–15 (2013).
29. Nagarwal, R. C., Singh, P. N., Kant, S., Maiti, P. & Pandit, J. K. Chitosan nanoparticles of 5-fluorouracil for ophthalmic delivery: characterization, in-vitro and in-vivo study. *Chem. Pharm. Bull. (Tokyo).* **59,** 272–278 (2011).
30. Sinha, V. R. & Kumria, R. Polysaccharides in colon-specific drug delivery. *Int. J. Pharm.* **224,** 19–38 (2001).
31. Lemarchand, C., Gref, R. & Couvreur, P. Polysaccharide-decorated nanoparticles. *Eur. J. Pharm. Biopharm.* **58,** 327–341 (2004).
32. Akiyoshi, K. *et al.* Self-assembled hydrogel nanoparticle of cholesterol-bearing pullulan as a carrier of protein drugs: Complexation and stabilization of insulin. *J. Control. Release* **54,** 313–320 (1998).
33. Akiyoshi, K. & Sunamoto, J. Supramolecular assembly of hydrophobized polysaccharides. *Supramol. Sci.* **3,** 157–163 (1996).
34. Sawada, S.-I., Nomura, Y., Aoyama, Y. & Akiyoshi, K. Heat Shock Protein-like Activity of a Nanogel Artificial Chaperone for Citrate Synthase. *J. Bioact. Compat. Polym.* **21,** 487–501 (2006).
35. Gu, X. *et al.* A Novel Hydrophobized Polysaccharide / Oncoprotein Complex Vaccine Induces in Vitro and in Vivo Cellular and Humoral Immune Responses against HER2-expressing Murine Sarcomas. *Cancer Res.* **58,** 3385–3390 (1998).
36. Yoncheva, K., Vandervoort, J. & Ludwig, A. Development of mucoadhesive poly(lactide-co-glycolide) nanoparticles for ocular application. *Pharm. Dev. Technol.* **16,** 29–35 (2011).

37. Stella, B. *et al.* Nonpolymeric nanoassemblies for ocular administration of acyclovir: Pharmacokinetic evaluation in rabbits. *Eur. J. Pharm. Biopharm.* **80,** 39–45 (2012).
38. Arisz, P. W., Kauw, H. J. J. & Boon, J. J. Substituent distribution along the cellulose backbone in O-methylcelluloses using GC and FAB-MS for monomer and oligomer analysis. *Carbohydr. Res.* **271,** 1–14 (1995).
39. Bhowmik, M., Bain, M. K., Ghosh, L. K. & Chattopadhyay, D. Effect of salts on gelation and drug release profiles of methylcellulose-based ophthalmic thermo-reversible in situ gels. *Pharm. Dev. Technol.* **16,** 385–91 (2011).
40. Li, N., Yu, M., Deng, L., Yang, J. & Dong, A. Thermosensitive hydrogel of hydrophobically-modified methylcellulose for intravaginal drug delivery. *J. Mater. Sci. Mater. Med.* **23,** 1913–9 (2012).
41. Gupta, D., Tator, C. H. & Shoichet, M. S. Fast-gelling injectable blend of hyaluronan and methylcellulose for intrathecal, localized delivery to the injured spinal cord. *Biomaterials* **27,** 2370–9 (2006).
42. Ngadaonye, J. I., Cloonan, M. O., Geever, L. M. & Higginbotham, C. L. Synthesis and characterisation of thermo-sensitive terpolymer hydrogels for drug delivery applications. *J. Polym. Res.* **18,** 2307–2324 (2011).
43. H. Y. Liu, X. X. Z. Lower critical solution temperatures of N-substituted acrylamide. *Polymer (Guildf).* **40,** 6985–6990 (1999).
44. Moran, M. T., Carroll, W. M., Selezneva, I., Gorelov, A. & Rochev, Y. Cell growth and detachment from protein-coated PNIPAAm-based copolymers. *J. Biomed. Mater. Res.* (2007). doi:10.1002/jbm.a
45. Yldz, B., Işk, B. & Kş, M. Synthesis and characterization of thermoresponsive isopropylacrylamide-acrylamide hydrogels. *Eur. Polym. J.* **38,** 1343–1347 (2002).
46. Musial, W., Voncina, B., Pluta, J. & Kokol, V. The study of release of chlorhexidine from preparations with modified thermosensitive poly-N-isopropylacrylamide microspheres. *ScientificWorldJournal.* **2012,** 243707 (2012).
47. Muramatsu K Wada T, Hirai H, Miyawaki F, S. Y. Poly(N-isopropylacrylamide-co-N-tert-butylacrylamide)- grafted hyaluronan as an injectable and self-assembling scaffold for cartilage tissue engineering. *J. Biomed. Sci. Eng.* **5,** 639–646 (2012).
48. Hoffman, A. S. *et al.* Really smart bioconjugates of smart polymers and receptor proteins. *J. Biomed. Mater. Res.* **52,** 577–586 (2000).
49. Pourjavadi, A., Mahdavinia, G. R. & Omidian, H. Modified Chitosan . I . Optimized Cerium Ammonium Nitrate-Induced Synthesis of Chitosan- graft - Polyacrylonitrile. *J. Appl. Polym. Sci.* **88,** 2048–2054 (2003).
50. Zhu, Z. & Zhuo, R. Controlled Release of Carboxylic-Containing Herbicides by Starch-g-poly(butyl acrylate). *J. Appl. Polym. Sci.* **81,** 1535–1543 (2001).
51. Fanta, G. F., Burr, R. C. & Doane, W. M. Polymerization of Alkyl Acrylates and Alkyl Methacrylates with Starch. *J. Appl. Polym. Sci.* **25,** 2285–2294 (1980).
52. Mcdowall, D. J., Gupta, B. S. & Stannett, V. T. Grafting of Vinyl Monomers to Cellulose by Ceric Ion Initiation. *Prog. Polym. Sci.* **10,** 1–50 (1984).
53. Pulat, M. & Isakoca, C. Chemically induced graft copolymerization of vinyl monomers onto cotton fibers. *J. Appl. Polym. Sci.* **100,** 2343–2347 (2006).

54. Zahran, M. K. Grafting of Methacrylic Acid and Other Vinyl Monomers Onto Cotton Fabric Using Ce (IV) Ion–Cellulose Thiocarbonate Redox System. *J. Polym. Res.* **13,** 65–71 (2005).
55. Kaizerman, S., Mino, G. & Meinhold, L. F. The Polymerization of Vinyl Monomers in Cellulosic Fibers. *Text. Res. J.* **32,** 136–140 (1962).
56. A. Hebeish, A. Kaktouch, M. H. E.-R. Graft Copolymerization of Vinyl Monomers with modified cotton. II. Grafting of Acrylonitrile and Methyl Methacrylate on Acetylated Cotton. *J. Appl. Polym. Sci.* **15,** 11–24 (1971).
57. Gu, L., Gu, G. & Saadet, O. Graft Copolymerization of Acrylic Acid onto Cellulose : Effects of Pretreatments and Crosslinking Agent. *J. Appl. Polym. Sci.* **80,** 2267–2272 (2000).
58. Kubota, H. & Shiobara, N. Photografting of N-isopropylacrylamide on cellulose and temperature-responsive character of the resulting grafted celluloses. *React. Funct. Polym.* **37,** 219–224 (1998).
59. Chatterjee, S., Sarkar, S. & Bhattacharyya, S. N. Colloidal ferric oxide: a new photosensitizer for grafting acrylamide onto cellulose acetate films. *Polymer (Guildf).* **34,** 1979–1980 (1993).
60. Chiriac, A. P., Neamtu, I., Cazacu, G. & Simionescu, C. I. An investigation of the grafting of cellulose powder with acrylamide under a magnetic field. *Die Angew. Makromol. Chemie* **246,** 1–9 (1997).
61. Gupta, K. C. & Khandekar, K. Temperature-Responsive Cellulose by Ceric(IV) Ion-Initiated Graft Copolymerization of N-Isopropylacrylamide. *Biomacromolecules* **4,** 758–765 (2003).
62. Ahn, H. R. & Tak, T. M. Optimization grafting conditions and characterization of methyl cellulose grafted polyacrylonitrile copolymer. *Macromol. Res.* **22,** 318–323 (2014).
63. Hebeish, A. & Mehta, P. C. Cerium-Initiated Grafting of Acrylonitrile onto Cellulosic Materials. *J. Appl. Polym. Sci.* **12,** 1625–1647 (1968).
64. Okieimen, F. E. & OCBEIFUN, D. E. Graft Copolymerizations of Modified Cell ulose , Grafting of Acrylonitrile , and Methyl Methacry late on Carboxy Methyl Cellulose. *J. Appl. Polym. Sci.* **59,** 981–986 (1996).
65. Eromosele, I. C., Eromosele, C. O. & Zanna, H. K. Graft copolymerization of acrylic acid on methylcellulose by ceric ion/p-xylene redox pair. *J. Appl. Polym. Sci.* **84,** 500–504 (2002).
66. Griffith, M. Functional Human Corneal Equivalents Constructed from Cell Lines. *Science (80-.).* **286,** 2169–2172 (1999).
67. Akiyoshi, K., Deguchi, S., Tajima, H., Nishikawa, T. & Sunamoto, J. Microscopic Structure and Thermoresponsiveness of a Hydrogel Nanoparticle by Self-Assembly of a Hydrophobized Polysaccharide. *Macromolecules* **9297,** 857–861 (1997).
68. Verma, M. S., Liu, S., Chen, Y. Y., Meerasa, A. & Gu, F. X. Size-tunable nanoparticles composed of dextran-b-poly(D,L-lactide) for drug delivery applications. *Nano Res.* **5,** 49–61 (2012).
69. Qaddoumi, M. G. *et al.* The characteristics and mechanisms of uptake of PLGA nanoparticles in rabbit conjunctival epithelial cell layers. *Pharm. Res.* **21,** 641–648 (2004).
70. Funami, T. *et al.* Thermal aggregation of methylcellulose with different molecular weights. *Food Hydrocoll.* **21,** 46–58 (2007).
71. Akiyoshi, K., Deguchi, S., Moriguchi, N., Yamaguchi, S. & Sunamoto, J. Self-aggregates of hydrophobized polysaccharides in water. Formation and characteristics of nanoparticles. *Macromolecules* **26,** 3062–3068 (1993).

72. Saldías, C., Velásquez, L., Quezada, C. & Leiva, A. Physicochemical assessment of Dextran-g-Poly (ε-caprolactone) micellar nanoaggregates as drug nanocarriers. *Carbohydr. Polym.* **117,** 458–467 (2015).
73. Magenheim, B., Levy, M. Y. & Benita, S. A new in vitro technique for the evaluation of drug release profile from colloidal carriers - ultrafiltration technique at low pressure. *Int. J. Pharm.* **94,** 115–123 (1993).
74. Hwang, H. Y., Kim, I. S., Kwon, I. C. & Kim, Y. H. Tumor targetability and antitumor effect of docetaxel-loaded hydrophobically modified glycol chitosan nanoparticles. *J. Control. Release* **128,** 23–31 (2008).
75. Calejo, M. T., Kjøniksen, A. L., Maleki, A., Nyström, B. & Sande, S. A. Microparticles based on hydrophobically modified chitosan as drug carriers. *J. Appl. Polym. Sci.* **131,** 1–11 (2014).
76. Vafaei, S. Y. *et al.* Self assembled hyaluronic acid nanoparticles as a potential carrier for targeting the inflamed intestinal mucosa. *Carbohydr. Polym.* **144,** 371–381 (2016).
77. Yang, Y., Guo, Y., Sun, R. & Wang, X. Self-assembly and β-carotene loading capacity of hydroxyethyl cellulose-graft-linoleic acid nanomicelles. *Carbohydrate Polymers* **145,** 56–63 (2016).
78. Wang, M. *et al.* Facile One-Pot Synthesis of Self-Assembled Folate-Biotin-Pullulan Nanoparticles for Targeted Intracellular Anticancer Drug Delivery. **2016,** (2016).

CHAPTER 3: EFFECT OF METHYLCELLULOSE MOLECULAR WEIGHT ON THE PROPERTIES OF SELF-ASSEMBLING MC-G-PNTBAM NANOGELS.

Authors: Marion Jamard and Heather Sheardown

Objectives: Investigate the impact of the molecular weight of the hydrophilic methylcellulose backbone of the amphiphilic MC-g-PNtBAm copolymer on the characteristics and properties of the self-assembled nanogels.

Main Scientific contributions:

- Demonstrated tunability of the characteristics of the self-aggregates varying the molecular weight of methylcellulose.
- Showed control of the drug release kinetics varying the polysaccharide length.

ABSTRACT

The efficiency of drug delivery to the eye is limited by its clearance mechanisms. Nanocarriers, able to encapsulate bioactive compounds and slow down their release, may present a promising alternative to topical drop therapies. Previously, self-assemblies of methylcellulose hydrophobized with N-tert-butylacrylamide side chains (MC-g-PNtBAm) have been developed. The purpose of the current study was to investigate the impact of the methylcellulose backbone length on the properties of the nanogels. We synthesized MC-g-PNtBAm nanogels using 4 different molecular weights of MC with two degrees of hydrophobic modification. While no significant change could be observed at high degree of hydrophobization, properties were affected at a lower one. Increasing the molecular weight of MC improved the swelling capacity of the nanogels, increasing their size in water. An effect on the drug release was also noted. Nanogels prepared using MC with a molecular weight of 30 kDa did not retain as much dexamethasone and released it faster compared to those prepared using 230 kDa MC. Thus, besides the degree of hydrophobization, the length of MC chains provides another mean of tuning the properties of MC-g-PtBAm nanogels.

Keywords: Methylcellulose, hydrophobization, molecular weight, self-assembly, drug delivery/release

3.1 INTRODUCTION

Ocular diseases are most often treated by the topical application of a solution or suspension of the drug[1]. These topical therapies have the advantages of simplicity, safety and acceptance by patients. However, topical formulations have poor efficiency: less than 5% of the drug reaches the intraocular tissue as a result of the effective clearance mechanisms and intrinsic biological barriers of the eye[2]. In order to achieve therapeutic efficacy, relatively high concentrations of drug and frequent administration are necessary despite an increased potential for side effects due to systemic uptake and a higher incidence of patient noncompliance[3–5]. Improving the bioavailability of drugs to achieve optimal drug concentration at the target site is thus one of the biggest challenges in ocular drug delivery. By treating ophthalmic diseases in a localized and efficient manner, systemic uptake of the drug is limited.

Current advances in the development of nanocarriers have shown that these systems have promise in ocular drug delivery[6,7]. Their small size enables better diffusivity across membranes and thus improves corneal permeability[7–10]. They also present a high surface-to-volume ratio which may improve interaction with the ocular mucus membrane. Besides being able to entrap therapeutic agents, these systems may provide an additional barrier for the retention of the drug and to control its release. Such systems therefore have the potential to overcome the corneal barrier through increased residence time on the eye and prolonged activity, while still allowing for the topical delivery of therapeutics.

We recently synthesized self-assembling nanogels by grafting N-tert-butylacrylamide (NtBAm) hydrophobic side chains on methylcellulose[11] (MC) (MC-g-PNtBAm) via cerium

ammonium nitrate (CAN). The resulting nanogels were spherical and monodispersed with an average diameter of 140 nm in water. Able to efficiently entrap dexamethasone, they showed the ability to provide controlled release of their payload. Varying the degree of NtBAm grafting with the feed concentrations of monomer and initiator was found to affect the nanogel properties. Higher degrees of hydrophobization (DH) resulted in nanogels with lower swelling capacity and more prolonged release. Incubation with human corneal epithelial cells demonstrated the potential biocompatibility of the nanogels.

Previous studies on hydrophobized polysaccharides have investigatied the impact of the polysaccharide chain length on block structured copolymers, i.e. with the hydrophobic moiety attached to the end of the hydrophilic moiety[12–14], and a few studies have investigated its effect as the backbone of a comb-structured copolymer[15]. In the present work, we investigate the impact of the methylcellulose backbone length on the nanogel properties. MC-g-PNtBAm nanogel were synthesized using four molecular weights of MC ranging from 30 000 kg/mol to 230 000 kg/mol at two different degrees of hydrophobic modification.

3.2 MATERIALS AND METHODS

3.2.1 Materials

Methylcellulose (MC) Metholose SM-4, SM-25, SM-100 and SM-400 were purchased from Shin-Etsu (Totowa, NJ, USA). N-tert-butylacrylamide (NtBAm), Cerium ammonium nitrate (CAN) and dimethyl sulfoxide-d6 (DMSO-d6) were purchased from Sigma-Aldrich (Oakville ON), and Dexamethasone from Sigma Life Science (D1756) (St Louis, MO, USA). Phosphate buffered saline (PBS) 10 times concentrate was obtained from BioShop

(McMaster University ON). Nitric acid 70% was bought from EMD Chemical Inc. (Mississauga, ON).

3.2.2 Synthesis of MC-g-PNtBAm nanogels

The synthesis of MC-g-PNtBAm nanogels was performed following a method previously described[11]. Briefly, 250 mg of MC were dissolved in 50 mL water along with 200 mg of NtBAm. When dissolved, 0.5 mL of 70% nitric acid was incorporated into the solution. The mixture was purged with nitrogen for 30 minutes and either 50 mg or 250 mg of CAN dissolved in 1 mL of milliQ water was added to start the polymerization. The reaction was left stirring at room temperature for 24 hours, followed by extensive dialysis (Pre-wetted RC tubing 3.5kDa, Spectrum Laboratories, Ontario, Canada) to remove any unreacted compound. The compositions of the different formulations are summarized in Table 3-1.

Various molecular weights of MC were used with two different CAN concentrations to synthesize the nanogels as shown in Table 3-1. Nanogel nomenclature is based on the molecular weight of MC and the degree of hydrophobization, calculated as the average number of NtBAm monomer for 100 anhydroglucose units (AGU) of the MC (determined by ^{1}H NMR analysis[11]). For example, MC(165k)-g-PNtBAm_50% denotes a nanogel made with 165 kDa methylcellylose and 50 NtBAm units for 100 AGU.

3.2.3 ^{1}H NMR analysis

Freeze dried materials were dissolved in DMSO-d6 and analyzed by ^{1}H nuclear magnetic resonance (NMR, Bruker AVANCE 600 MHz NMR spectrometer).

3.2.4 Particle size measurements

Particle mean sizes were measured by single nanoparticle tracking using the Malvern NanoSight LM10.

3.2.5 Transmission electron microscopy study

Samples were diluted 40-fold with purified water and a 5 μL of the suspension was spread on 200 mesh Formvar coated cooper grids without staining and allowed to dry under ambient atmospheric conditions. Transmission electron microscopy (TEM, JEOL 1200EX TEMSCAN) with 80 kV electron beam was used to view and photograph the morphology of the nanogels.

3.2.6 Loading of dexamethasone

Dexamethasone was selected as a model ophthalmic drug for the release studies. To load dexamethasone into the nanogels, MC-g-PNtBAm synthesis was performed in a 0.01% w/v aqueous solution of dexamethasone, following the method described above. The suspension of loaded nanogels was then ultracentrifuged (Sorvall WX90) at 50,000 RPM for 30°C at 23°C. The amount of drug in the supernatant was measured by high performance liquid chromatography (HPLC, Waters 2707 Autosampler, 1525 Binary HPLC Pump, 2489 UV/Visible detector, Column Dionex. Model Acclaim (r) 120 C18 5μm 120A 4.6x250mm) with a 254 nm detection wavelength, injecting 10μL sample and using a 1mL/min isocratic flow rate of 40:60 (v/v) acetonitrile:water. The following equation was used to calculate the loading efficiency of dexamethasone into the nanogels:

$$Loading\ efficiency\ (\%) = 100 * \frac{Initial\ amount\ of\ drug - Amount\ of\ drug\ in\ supernatant}{Initial\ amount\ of\ drug}$$

3.2.7 In vitro release of dexamethasone

The in vitro release of dexamethasone from the nanogels was evaluated in phosphate buffered saline (PBS). 1 mL of a dispersion of drug-loaded particles (with a methylcellulose concentration of 4.5 mg/mL) in PBS was placed into a dialysis membrane (molecular weight cutoff 3500 Da, Spectra/Por, Spectrum laboratories) which was immersed into 5 mL of PBS maintained at 32 ± 1 °C by a shaking water bath to approximately mimic on eye conditions. Released dexamethasone was sampled by removing the release medium and replacing it with fresh pre-warmed PBS at selected time points. The HPLC method described above was used to determine the concentrations of dexamethasone in the releasate. All measurements were performed in triplicate and plotted as mean ± SD.

3.3 RESULTS AND DISCUSSION

3.3.1 Synthesis

The influence of the molecular weight of the MC backbone on the nanogel properties was investigated using four different molecular weights (M_w = 30 000 g/mol, 85 000 g/mol, 165 000 g/mol and 230 000g/mol). As the same mass was used for each, formulations all contained the same amount of anhydroglucose units (AGU). Two sets of materials were synthesized using two different initiator concentrations (1.82 x 10^{-3} mol/L and 9.12 x 10^{-3} mol/L - referred as low and high initiation respectively) while keeping constant NtBAm and nitric acid concentrations.

The amount of NtBAm grafted, referred to as the degree of hydrophobization (DH), was measured by ^{1}H-NMR to look into the influence of the MC chain length. As in previous work[11,16–19], DH was deduced from the ratio of relative peak integrations of protons belonging to the hydrogen in C2 position of MC and the CH_3 group of NtBAm. The values are listed in Table 3-2. As previously observed[11], higher CAN concentrations resulted in higher grafting of NtBAm. When looking at the influence of MC MW, it appeared that with similar levels of initiator present in the mixture, similar DH were achieved for all molecular weights. All formulations presented a degree of hydrophobization of 30% ± 2% at lower levels of initiator, and 49% ± 4% at higher levels of initiator, with no statistical difference ($p=0.1841$). Results thus indicate that the length of the polysaccharide backbone did not impact the degree of NtBAm grafting. A previous study reported higher grafting levels for shorter polysaccharides, due to reduced steric hindrance exposing more reactive groups[15]. No such effect was observed here. The longer MC backbones possessed more PNtBAm side chains, but the overall hydrophobic/hydrophilic balance remained the same.

3.3.2 Impact of MC molecular weight on particle size and morphology

At higher DH, the molecular weight of methylcellulose did not have an impact on the nanogel size in water, determined to be 180 nm ± 6 nm, while at a lower DH, increasing the molecular weight of MC significantly increased their size to up to 255 nm ± 10.5 nm (Figure 3-1). It has been previously shown that increasing DH decreased the swelling capacity of the nanogels[11,18,20]. It is thought that there is a higher frequency of hydrophobic chains along the polysaccharide backbone, induced by the higher feed ratio of initiator, supported by the fact that studies report that higher degrees of substitution result in nanogels of smaller sizes[19,21,22]

while longer hydrophobic chains result in larger particles[14,17,23]. The high frequency of hydrophobic side-chains tightens the aggregates and prevents the hydrophobic segments from expanding to uptake water. The nanogels are thus not able to swell as much in aqueous media at high DH. At lower DH however, the less numerous PNtBAm chains are separated by longer hydrophilic segments which are able to expand to take up water. The size of the assemblies thus increased with the MC molecular weight because of improved swelling capacity of the nanogels, in accordance with other studies[12,13,15].

The impact of hydrophobization has been previously reported to depend on the size of the polysaccharide chain[12,15]. This is likely due to the ratio between the length of the hydrophobic side chains relative to the length of the hydrophilic segment between each side chain. When in water, longer hydrophilic MC chains are able to expand to take up and trap water while still maintaining the cohesion of the nanogel mesh, as illustrated in Figure 3-2; shorter chains do not create a mesh able swell sufficiently to hold water molecules. However, at higher DH, the cosslinkingdensity prevents volume change of the hydrophilic chains, making a mesh that is too tight to expand, so the molecular weight of MC no longer has an impact.

TEM pictures showed that all formulations resulted in the formation of spherical particles (Figure 3-3). The diameters observed with TEM were smaller than those determined by Nanosight. These observations have been previously made and attributed to the different states of samples during analysis[11,18,24–26] – dry and shrunken for TEM, and suspended and swollen in water for Nanosight – as the high hydrophilicity of the polysaccharide increases the hydrodynamic diameter of the nanogels. TEM pictures reveal that particles are less monodispersed when the MC length is increased. Such observations have previously been

made and attributed to the larger polydispersity of the polysaccharide at high MW[15]. Their size in the dry state also seems to decrease when increasing the molecular weight of MC. The prevalence of intramolecular hydrophobic interactions due to the more numerous side-chains along the polysaccharide backbone might result in aggregate formation with fewer copolymer molecules, which would explain their smaller size when dehydrated.

3.3.3 Impact of MC molecular weight on Drug release

The impact of methylcellulose molecular weight on drug entrapment and release was studied using dexamethasone as a model hydrophobic drug. The highest and lowest methylcellulose chain lengths with both degrees of hydrophobic modification were selected for examination.

As previously observed[11], higher hydrophobic content induced higher loading efficiencies, due to stronger hydrophobic associations and/or the presence of increased hydrophobic domains (Table 3-3). The three phase release observed was in accordance with the previous study on MC-g-PNtBAm nanogels[11] (Figure 3-4). An initial burst stage attributed to the drug soaked in the outer hydrophilic part of the aggregates, is followed by a second slower diffusion phase corresponding to the dexamethasone that is more deeply entrapped. The final plateau stage is attributed to the high affinity of dexamethasone with the hydrophobic PNtBAm side chains[13].

At high levels of hydrophobic modification, both materials provided very high entrapment efficiencies and similar drug release rates. Those results indicate that molecular weight of methylcellulose had minimal impact on the entrapment and release properties of the nanogels at high DH. These observations are in accordance with the aggregate morphologies:

the impact of MC molecular weight is impeded by the strong association into tight networks by the numerous hydrophobic chains.

However, at lower levels of hydrophobic modification, the nanogels prepared using the lower molecular weight MC entrapped significantly less dexamethasone than those prepared with the higher MC molecular weight, and released it faster. Indeed, after the 30% of dexamethasone which was not entrapped came out of the dialysis bag, 20% of the payload in the nanogels was released over the next 15 days compared to only up to 10% in all of the other gels. Small MC chains are thought to be less subjected to entanglement, and therefore more mobile and are not able to retain as much drug, letting the dexamethasone diffuse through more easily. On the contrary, longer chains are more efficient at entrapping the drug when forming nanogels, and formed stable entangled networks impeding drug diffusion.

Noteworthy, while increasing the DH decreased the swelling capacity and the molecular weight of MC increased it, they both slowed down the release of dexamethasone. Therefore, the diffusion rate of the drug seems to be controlled by the quantity of hydrophobic moieties and the mobility of the molecules forming nanogel mesh. The length of the hydrophilic polysaccharide chain would determine the swelling ability and diffusion rate of the drug. Its impact on swelling is attributed to the ability of the longer MC chains to expand and uptake water while remaining aggregated. The same way the looseness of the mesh formed by shorter MC chains do not enable the uptake of water molecules, it also allows for diffusion of the drug from the hydrophobic domains to the outside media. A comparison of the stability of the different nanogel formulations would be interesting to further investigate this

analysis, as it has been reported that longer polysaccharide chains induced lower CACs thus better aggregate stability[15].

3.4 CONCLUSIONS

When grafting hydrophobic side chains along the methylcellulose chain, the molecular weight of the polysaccharide backbone was found to only have an effect on the nanogel properties at low degree of hydrophobization. Indeed, while no significant change was observed at high DH, increasing the MC length created larger and more swollen particles at lower DH. In terms of drug release, shorter chains resulted in lower entrapment efficiencies and faster release of dexamethasone. Changing the molecular weight of MC thus provides an additional lever to tune the properties of MC-g-PNtBAm nanogels.

3.5 TABLES

Table 3-1: Molecular weight of MC and CAN concentration used for the synthesis of MC-g-PNtBAm formulations

MC molecular weight (kg/mol)	30		85		165		230	
CAN concentration (mol/L)	1.82×10^{-3}	9.12×10^{-3}	1.82×10^{-3}	9.12×10^{-3}	1.82×10^{-3}	9.12×10^{-3}	1.82×10^{-3}	9.12×10^{-3}

Table 3-2: Degree of hydrophobization (DH) for various MC molecular weights and initiator concentrations.

MC molecular weight (kg/mol)	30	85	165	230
Low initiation	28.0%	32.0%	32.8%	30.1%
High initiation	50.8%	50.2%	43.2%	51.6%

Table 3-3: Entrapment efficiencies of dexamethasone. n=3 with error bars corresponding to the standard deviation.

MC molecular weight (kg/mol)	30	230
DH = 30%	71.61% ± 0.09%	98.96% ± 0.02%
DH = 50%	98.75% ± 0.09%	93.54% ± 0.03%

3.6 FIGURES

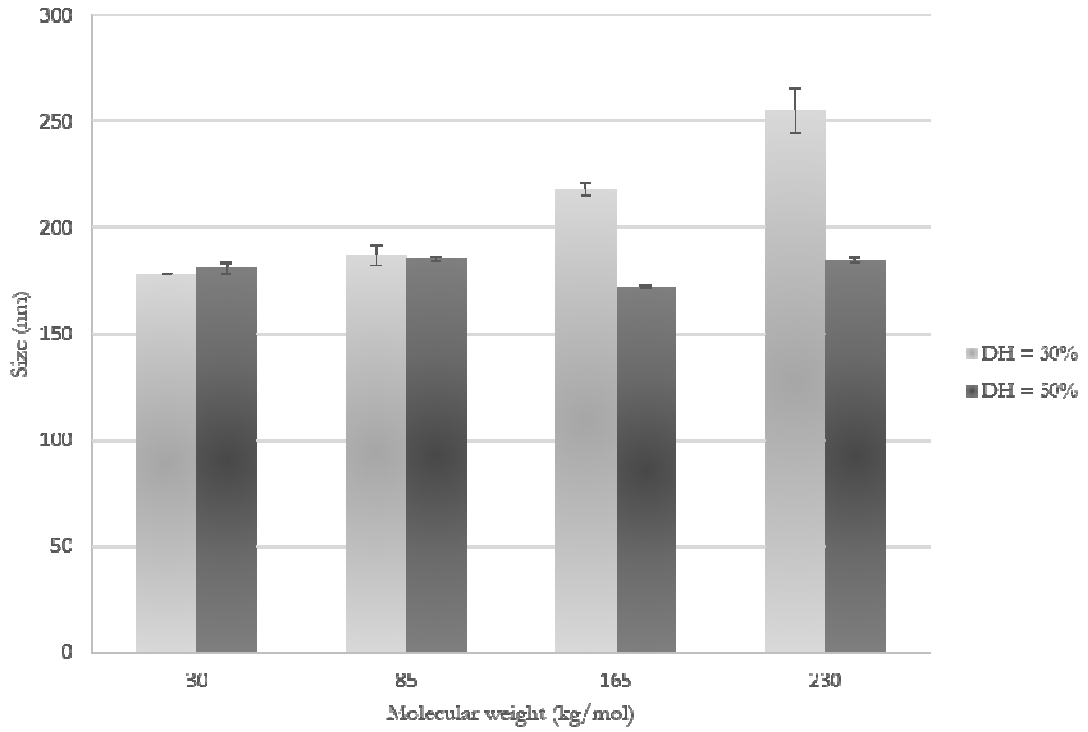

Figure 3-1: Hydrodynamic diameter of MC-g-PNtBAm nanogels varying the MC molecular weights at two different degrees of hydrophobization (DH), measured by particle tracking analysis. 3 measurements with the error bars corresponding to the standard deviation of the mean size.

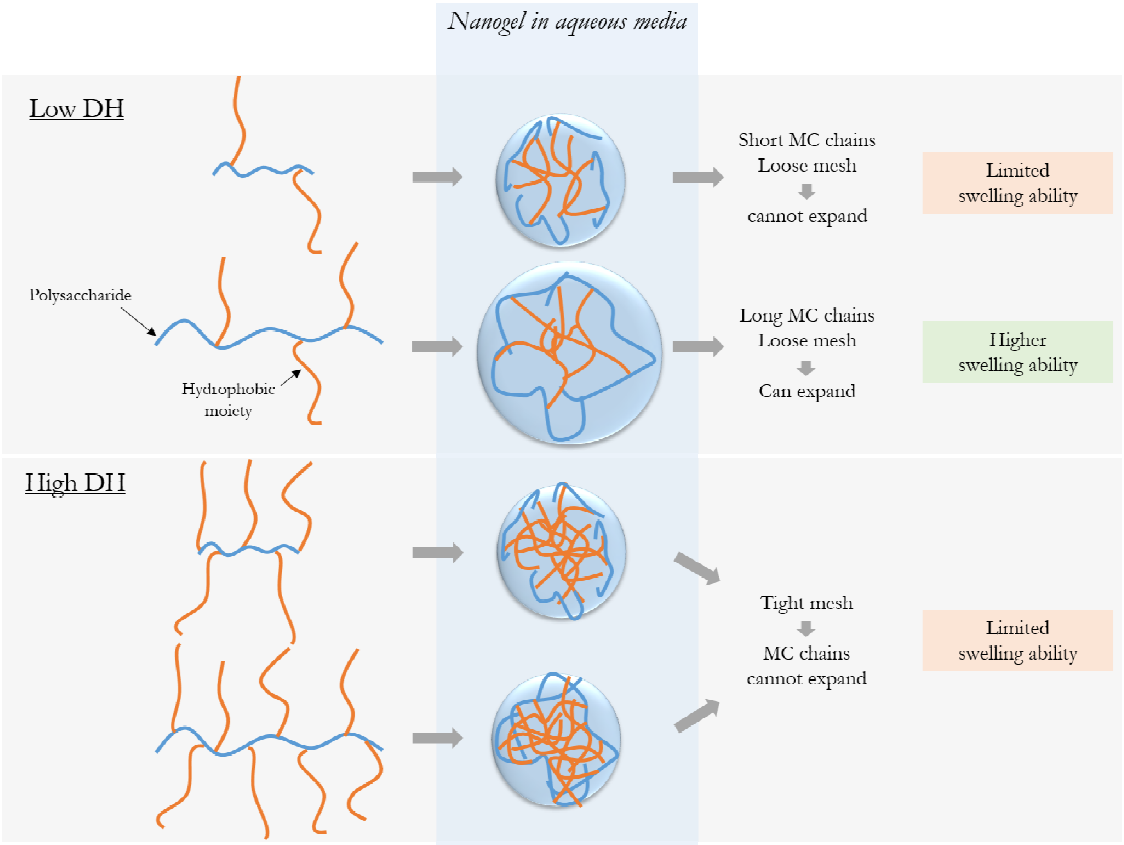

Figure 3-2: Scheme to illustrate the influence of MC molecular on the swelling ability of the nanogel (simplified with a single hydrophobic domain) at both degrees of hydrophobization. At high levels of hydrophobic modification, the tight mesh of the aggregates is unable to swell. Low levels of hydrophobic grafting create aggregates with a looser mesh, in which only longer MC chains can expend to uptake water while maintaining the cohesion of the nanogel.

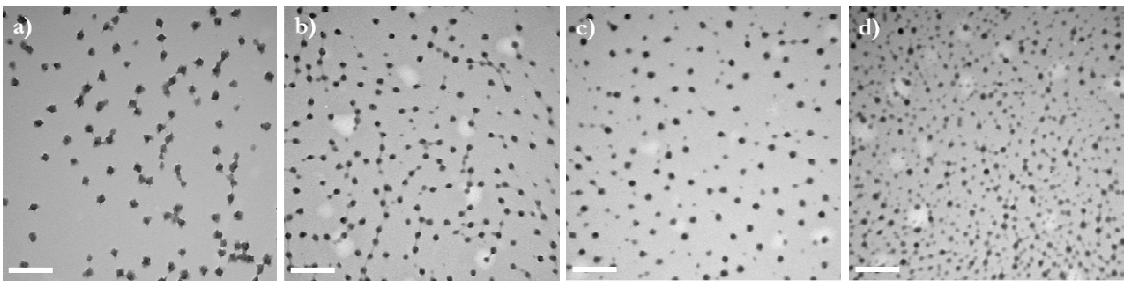

Figure 3-3: TEM pictures showing the morphology of nanogels with a DH of 30% and synthesized using various MC molecular weights: a) 30 kg/mol, b) 85 kg/mol, c) 165 kg/mol, d) 230 kg/mol 40% DH. The scale bars indicate 500 nm.

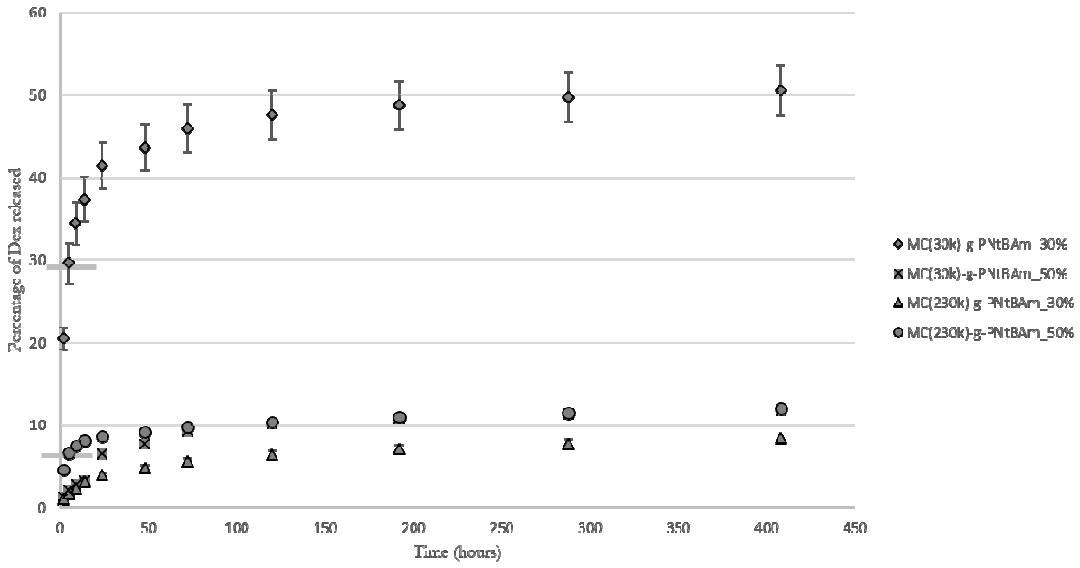

Figure 3-4: Dexamethasone release from MC-g-PNtBAm nanogels at 30% or 50% DH and synthesized using MC of 30 kg/mol or 230 kg/mol. The bars on the curves of MC(30k)-g-PNtBAm_30% and MC(230k)-g-PNtBAm_50% indicate the time point when the free drug in solution is released from the dialysis bag and the entrapped drug is being released.n=3 with the error bars corresponding to standard deviations.

ACKNOWLEDGEMENTS

Funding support from NSERC and the CREATE Biointerface Training Program is gratefully acknowledged.

3.7 DISCLOSURES

The authors state no conflict of interest.

BIBLIOGRAPHY

1. Urtti, A. Challenges and obstacles of ocular pharmacokinetics and drug delivery. *Adv. Drug Deliv. Rev.* **58,** 1131–1135 (2006).
2. Lee, V. H. & Robinsonx, J. R. Mechanistic and Quantitative Evaluation of Precorneal Pilocarpine Disposition in Albino Rabbits. **68,** (1979).
3. Salminen, L. Review: Systemic Absorption of Topically Applied Ocular Drugs in Humans. *J. Ocul. Pharmacol. Ther.* **6,** 243–249 (1990).
4. Baudouin, C. Side effects of antiglaucomatous drugs on the ocular surface. *Current opinion in ophthalmology* **7,** 80–6 (1996).
5. Arici, M. K., Arici, D. S., Topalkara, A. & Guler, C. Adverse effects of topical antiglaucoma drugs on the ocular surface. *Clin. Exp. Ophthalmol.* **28,** 113–117 (2000).
6. Liu, S., Jones, L. & Gu, F. X. Nanomaterials for ocular drug delivery. *Macromol. Biosci.* **12,** 608–20 (2012).
7. Wadhwa, S., Paliwal, R., Paliwal, S. R. & Vyas, S. P. Nanocarriers in Ocular Drug Delivery: An Update Review. *Curr. Pharm. Des.* **15,** 2724–2750 (2009).
8. Nagarwal, R. C., Kant, S., Singh, P. N., Maiti, P. & Pandit, J. K. Polymeric nanoparticulate system: a potential approach for ocular drug delivery. *J. Control. Release* **136,** 2–13 (2009).
9. Yaw-Chong Tong, Shwu-Fen Chang, Chia-Yang Liu, Winston W.-Y. Kao, Chong Heng Huang, J. L. Eye drop delivery of nano-polymericmicelle formulated genes with cornea-specific promoters. *J. Gene Med.* **10,** 610–618 (2008).
10. Zarbin, M. A., Montemagno, C., Leary, J. F. & Ritch, R. Nanomedicine in ophthalmology: The new frontier. *Am. J. Ophthalmol.* **150,** 144–162 (2010).
11. Jamard, M., Hoare, T. & Sheardown, H. Nanogels of Methylcellulose Hydrophobized with N-tert-butylacrylamide for Ocular Drug Delivery. (2016).
12. Nichifor, M., Mocanu, G. & Stanciu, M. C. Micelle-like association of polysaccharides with hydrophobic end groups. *Carbohydr. Polym.* **110,** 209–18 (2014).
13. Allen, C., Maysinger, D. & Eisenberg, A. Nano-engineering block copolymer aggregates for drug delivery. *Colloids Surfaces B Biointerfaces* **16,** 3–27 (1999).
14. Verma, M. S., Liu, S., Chen, Y. Y., Meerasa, A. & Gu, F. X. Size-tunable nanoparticles composed of dextran-b-poly(D,L-lactide) for drug delivery applications. *Nano Res.* **5,** 49–61 (2012).
15. Zhang, H., Cai, G., Tang, G., Wang, L. & Jiang, H. Synthesis, self-assembly, and cytotoxicity of well-defined trimethylated chitosan-O-poly(e-caprolactone): Effect of chitosan molecular weight. *J. Biomed. Mater. Res. - Part B Appl. Biomater.* **98 B,** 290–299 (2011).
16. Calce, E. *et al.* A biocompatible process to prepare hyaluronan-based material able to

self-assemble into stable nano-particles. *RSC Adv.* **5,** 29573–29576 (2015).

17. Nagahama, K., Mori, Y., Ohya, Y. & Ouchi, T. Biodegradable nanogel formation of polylactide-grafted dextran copolymer in dilute aqueous solution and enhancement of its stability by stereocomplexation. *Biomacromolecules* **8,** 2135–2141 (2007).
18. Yanzhu Guo; Li Zhang; Haiming Li; Ying Han; Jinghui Zhou; Xiaohui Wang. Self-assembly and paclitaxel loading capacity of α-tocopherol succinate-conjugated hydroxyethyl cellulose nanomicelle. *Colloid Polym Sci* **294,** 135–143 (2016).
19. Guo, Y., Wang, X., Shu, X., Shen, Z. & Sun, R. C. Self-assembly and paclitaxel loading capacity of cellulose-graft- poly(lactide) nanomicelles. *J. Agric. Food Chem.* **60,** 3900–3908 (2012).
20. Liu, S. *et al.* Phenylboronic acid modified mucoadhesive nanoparticle drug carriers facilitate weekly treatment of experimentallyinduced dry eye syndrome. *Nano Res.* **8,** 621–635 (2015).
21. Akiyoshi, K., Deguchi, S., Tajima, H., Nishikawa, T. & Sunamoto, J. Microscopic Structure and Thermoresponsiveness of a Hydrogel Nanoparticle by Self-Assembly of a Hydrophobized Polysaccharide. *Macromolecules* **9297,** 857–861 (1997).
22. Guo, Y., Wang, X., Shen, Z., Shu, X. & Sun, R. Preparation of cellulose-graft-poly(ε-caprolactone) nanomicelles by homogeneous ROP in ionic liquid. *Carbohydr. Polym.* **92,** 77–83 (2013).
23. Li, B., Wang, Q., Wang, X., Wang, C. & Jiang, X. Preparation, drug release and cellular uptake of doxorubicin-loaded dextran-b-poly(?-caprolactone) nanoparticles. *Carbohydr. Polym.* **93,** 430–437 (2013).
24. Balan, V., Redinciuc, V., Tudorachi, N. & Verestiuc, L. Biotinylated N-palmitoyl chitosan for design of drug loaded self-assembled nanocarriers. *Eur. Polym. J.* **81,** 284–294 (2016).
25. Vafaei, S. Y. *et al.* Self assembled hyaluronic acid nanoparticles as a potential carrier for targeting the inflamed intestinal mucosa. *Carbohydr. Polym.* **144,** 371–381 (2016).
26. Di Meo, C. *et al.* Highly versatile nanohydrogel platform based on riboflavin-polysaccharide derivatives useful in the development of intrinsically fluorescent and cytocompatible drug carriers. *Carbohydr. Polym.* **115,** 502–509 (2015).

CHAPTER 4: PHENYLBORONIC ACID FUNCTIONALIZATION OF MC-G-PNTBAM NANOGELS FOR IMPROVED MUCOADHESION

Authors: Marion Jamard, Nicole Mangiacotte, and Heather Sheardown

Objectives: Functionalization of the surface of MC-g-PNtBAm nanogels to increase their residence time on the ocular surface with the aim of improving drug permeation and thereby bioavailability.

Main Scientific contributions:

- Functionalized the surface of MC-g-PNtBAm nanogels with phenylboronic acid (PBA) at different coverage densities.
- Demonstrated the impact of the PBA layer on nanogel characteristics and on their performance as drug delivery systems, using a hydrophobic model drug.
- Showed the potential improvement of interaction with mucus through PBA functionalization of MC-g-PNtBAm nanogels.
- Demonstrated in vitro cytocompatibility of the PBA functionalized nanogels after 48-hour incubation with human corneal epithelial cells.

Author contributions:
Contributions of this work were as follows. Marion was responsible for synthesis and PBA surface functionalization of the nanogels and verification of their composition by ^{1}H-NMR and ATR FT-IR. She characterized their size and morphology by Nanosight and TEM, performed the cytocompatibility tests and drug release studies. Finally she was in charge of the paper write up. Nicole, following trouble-shooting of the method (with Marion), performed the zeta-potential measurements for the mucoadhesion study.

ABSTRACT

In order to overcome the limitations of topical ocular drug delivery, namely the effective barrier function of the corneal epithelial and the high rate of tear turnover, both of which lead to the need for frequent administration of relatively high concentrations of drug, self-assembling nanogels of hydrophobized methylcellulose (MC) have recently been synthesized. These materials have shown the ability to encapsulate and provide sustained release of their payload. In this study, the surface of the nanogels was functionalized with phenylboronic acid (PBA) in order to improve their mucoadhesive properties and prolong their retention on the ocular surface to increase drug absorption through the cornea. PBA grafting was performed via oxidation of the methylcellulose followed by a Schiff base reaction, and confirmed by XPS and ATR FT-IR. The effect of PBA coverage on the properties was studied for nanogels synthesized with two different molecular weights of methylcellulose. Oxidation was found to depolymerize methylcellulose, inducing a size reduction in the nanogels as well as a faster release of dexamethasone compared to unfunctionalized materials. Those made of higher molecular weight MC remained stable in solution at all coverages of PBA. PBA-grafting was found to enable greater entrapment efficiencies and decrease the initial release burst. Although the following diffusion phase was faster than for the unmodified nanogels, thought to be due to the shorter MC chains resulting from the oxidation step, the release of dexamethasone was sustained for over 12 days. Finally, zeta-potential measurements suggested better interaction of mucin with the nanogels synthesized

with shorter MC chain, indicative of mucoadhesion. PBA functionalized MC-g-PNtBAm nanogels showed great potential for ocular drug delivery.

Keywords: phenylboronic acid, surface functionalization, nanogel, mucoadhesion, ophthalmic, drug delivery/release

4.1 INTRODUCTION

The protective mechanisms of the eye result in a physical-biological barrier that protects the eye from foreign particulates. The surface of the cornea is protected by a gel-like layer composed of a tridimensional network of entangled mucins. These mucins present a physical barrier against foreign bodies and pathogens[1], as well as drugs. As well, induced lacrimation, tear turnover, and naso-lacrimal drainage cause rapid removal of drugs from the surface of the eye[2]. To be therapeutically effective, formulations require high dosage and frequent administration[3]. However, instead of reaching the targeted tissue, the drug may be absorbed into the systemic circulation leading to adverse effects. As a result, as little as 5% of topically administered drug reaches its intended target[4].

The development of nano-carriers as drug delivery devices is a promising approach with the potential to overcome these shortcomings without compromising the benefits of topical administration. Suspended in a liquid dosage, they provide a non-invasive method of delivering therapeutic agents to the target tissue in a controlled fashion[5–8]. We recently synthesized a hydrophobized methylcellulose (MC) copolymer, grafting side chains of N-tert-butylacrylamide (NtBAm) along the polysaccharide via cerium ammonium nitrate initiation. The resulting material, MC-g-PNtBAm, self-assembles in aqueous media to form nanogels[9]. The release of an entrapped compound from the gels can be tuned by simply adjusting the degree of hydrophobic grafting and the molecular weight of the methylcellulose backbone. While the methylcellulose on the surface may have mild mucoadhesive properties[10], we postulate modification of the MC-g-PNtBAm nanogel surface can lead to further targeting of the ocular surface, thus prolonging corneal retention. Increasing the residence time of the

drug carrier in the precorneal area would allow for greater penetration of the drug into the intraocular structures[11,12], which may be useful for addressing the bioavailability limitations of current topical formulations.

Indeed, prolonged residence time at the ocular surface and intimate contact of the drug delivery system with the mucosa are key to precorneal drug absorption[13,14]. They allow the carrier to better deliver its payload to the ocular surface and underlying tissues, enabling higher permeation and consequently increased bioavailability[15–17]. Prolonged retention depends on the interaction between the drug carrier and the mucin layer of tears. While following the same principles of intermolecular interactions[18], nanosystems seem to be more powerful than bulk techniques as their high surface-area-to-volume ratio increases the interface available to establish bonding, thereby allowing longer residence time than in larger structures[12,19]. Their nanoscale size also enables particles to penetrate the mucin mesh[20,21], whereas those with a size in the micrometer range are unable to penetrate and tend to remain at the top layers of the mucus[22] from which they are more easily cleared.

As the interaction depends on both the functionality and charge of carriers[3], several methods can be used to incorporate mucoadhesive properties. Mucoadhesive polymers can be chosen as matrix-forming materials[3,19,23] or the surface can be modified by attaching mucoadhesive polymers[10,24,25]. Taking advantage of the negatively charged mucin, the use of positively-charged systems to induce electrostatic interaction has been a common method of achieving mucoadhesion[26–30]. Also, hydrophobic nanosystems may show high ability to interact with hydrophobic domains of mucin[31]. Strategies such as thiol[32] and lectin[33] modification have also been investigated, but the instability of both modifications require special protection in

processing and storage. While different cellulose derivatives have been described as mucoadhesive polymers[34–36], methylcellulose presents only very mild ability to interact with mucin when diluted in water[37]. Alternatively, the surface of polymeric nanoparticles can be functionalized with ligands in order to selectively bind the ocular mucosa and increase the precorneal retention time of the drugs[3,10,24,25,38]. A strategy that has been widely employed to impart mucoadhesion in a variety of applications has been to graft phenylboronic acid[39–41]. Phenylboronic acid (PBA) contains a phenyl substituent and two hydroxyl groups attached to boron which can form a reversible covalent complex with the diol groups of sialic acid abundant on the mucin structures at physiological pH[42–46] (Figure 4-1).

Therefore in this study, we investigate the functionalization of the MC-g-PNtBAm nanogel surfaces with PBA to confer affinity to the ocular mucin with a goal of prolonging the residence time of the nanogels on the surface of the eye (Figure 4-2). We hypothesize that mucoadhesive nanogel drug carriers will significantly reduce the dosage and administration frequency used in the treatment of anterior segment eye diseases by enhancing the precorneal retention of the encapsulated agents. Oxidation of methylcellulose has been previously used to introduce aldehyde groups along the cellulosic chain to perform new reactions such as grafting of different molecules having one primary amine[47,48] or crosslinking with different polyamines such as diamines or chitosan[49]. This reaction was used herein to graft 3-amino phenylboronic acid (PBA) onto the surface of MC-g-PNtBAm nanogels. The amount of PBA functionalization on the MC surface was varied to analyze its effect on the nanogel characteristics and properties. The extent of their interaction with mucin was investigated in

order to find the optimal formulation at which desirable mucoadhesion is achieved, without compromising the colloidal stability of the nanogels or the drug delivery properties.

4.2 MATERIALS AND METHODS

4.2.1 Materials

Methylcellulose (MC) Metholose SM-4 and SM-100 were purchased from Shin-Etsu (Totowa, NJ, USA). N-tert-butylacrylamide (NtBAm), cerium ammonium nitrate (CAN) and dimethyl sulfoxide-d6 (DMSO-d6), 3-aminophenylboronic acid (PBA, sodium periodate, glycerol, sodium cyanoborohydride, dexamethasone and mucin (type II from porcine stomach) were purchased from Sigma-Aldrich (St Louis, MO, USA). Phosphate buffered saline (PBS) 10 times concentrate was obtained from BioShop (McMaster University - ON, Canada). Nitric acid 70% and potassium chloride were purchased from EMD Chemical Inc. (Mississauga, ON). Vybrant MTT cell proliferation assay kit and LIVE/DEAD viability/cytotoxicity kit as well as keratinocyte serum free medium were purchased from Life Technologies (Grand Island, NY, USA). Human corneal epithelial cells[50] (hCECs) were the kind gift of Dr. May Griffith.

4.2.2 MC-g-PNtBAm synthesis

MC-g-PNtBAm was synthesized as previously described[9]. Briefly, 250 mg of MC (95 kg/mol or 165 kg/mol) and 250 mg of recrystallized NtBAm were dissolved in 50 mL of water (0.5% w/v). When dissolved, 0.5 mL of 70% nitric acid was added to the solution which was then purged with nitrogen for 30 minutes. Finally, 150 mg of CAN dissolved in 1 mL of

purified water prepared in a Millipore Milli-Q system, was added and the reaction was left stirring at room temperature for 24 hours. The resulting solutions were extensively dialysized (Pre-wetted RC tubing 3.5kDa, Spectrum Laboratories) and freeze dried (Labconco 7752020).

4.2.3 PBA functionalization of the MC-g-PNtBAm nanogels

For functionalization of the nanogels, 100 mg of freeze dried MC-g-PNtBAm was dissolved in 5 mL of dimethyl sulfoxide (DMSO). Nanogels were formed by adding the mixture dropwise to 50 mL of water under stirred conditions. Protected from light in an amber vial, 9 mL of the nanogel suspension was added to 100 mg of sodium periodate ($NaIO_4$) dissolved 1 mL of water and periodate oxidation was carried out under stirring at room temperature for 2 hours, at which time the unreacted $NaIO_4$ was quenched with 0.1 mL of glycerol. Subsequently, 9 mL of an aqueous solution of phenylboronic acid at varying concentrations (Table 4-1) were added. 6 hours later, 60 mg of sodium cyanoborohydride ($NaCNBH_3$) dissolved in 1 mL water as a reducing agent was added. After 3 more hours of reaction, the mixture was extensively dialyzed against water to remove any unreacted solutes[39]. Unfunctionalized MC(30k)-g-PNtBAM and MC(165k)-g-PNtBAM nanogels were used as negative controls.

The compositions of the synthesized nanogels are summarized in Table 4-1.

4.2.4 GPC analysis

The impact of oxidation on methylcellulose molecular weight was studied by gel permeation chromatography (GPC). In an amber vial, 5mL of a 1% (w/v) solution of methylcellulose were added to an aqueous solution of sodium peroxide (100 mg in 5 mL). After 2, 6 and 24 hours, oxidation was stopped by quenching with glycerol. The molecular weight of molecular weight and polydispersity were measured by gel permeation chromatography (GPC) using a Waters system composed of a 590 HPLC pump, three Styragel columns (HR2, HR3, HR4), and a 410 refractive index detector. Samples were eluted in N,N-dimethylformamide containing 50 mM LiBr at a flow rate of 0.5 mL/min, and the system was calibrated using narrow dispersed polyethylene glycol (PEG) standards.

4.2.5 ATR FT-IR analysis

Freeze dried samples were measured by ATR FT-IR (Bruker Vertex 70 Bench and a diamond ATR module) in the range of 400 to 4000 cm^{-1}.

4.2.6 NMR analysis

Freeze dried materials dissolved in DMSO-d6 were analyzed by nuclear magnetic resonance (NMR, Bruker AVANCE 600 MHz NMR spectrometer).

4.2.7 XPS analysis

X-ray photoelectron spectroscopy (XPS) spectra were recorded using a Physical Electronics (PHI) Quantera II spectrometer equipped with an aluminum anode source for X-ray

generation and a quartz crystal monochromator for focusing the generated X-rays. A monochromatic Al K-α X-ray (1486.7 eV) source was operated at 50 W and 15 kV. The operating pressure did not exceed 2.0 $x10^{-8}$ Torr and a pass energy of 280 eV was used to obtain all survey (wide scan) spectra. All spectra were obtained at 45° take off angles, and a dual beam charge compensation system was used for neutralization of all samples. Data manipulation was performed using PHI MultiPak Version 9.4.0.7 software.

4.2.8 Particle size measurements

Nanogel suspensions were diluted with purified water and average particle sizes were measured by single nanoparticle tracking (Malvern NanoSight LM10).

4.2.9 Transmission electon microscopy study

After diluting the sample with purified water, 5 μL of the suspension was spread on 200 mesh Formvar coated cooper grids without staining and allowed to dry under ambient atmospheric conditions. The morphology of nanogel samples was viewed and photographed using transmission electron microscopy (TEM, JEOL 1200EX TEMSCAN) with 80kv electron beam.

4.2.10 Mucoadhesive evaluation by Zeta-potential measurements

Zeta-potential was used to measure interaction of the nanogels with negatively charged mucin and evaluate their potential mucoadhesiveness[23,51]. Triplicates of 2 mL samples were made from 0.1mL of the PBA functionalized nanogel solution (final MC-g-PNtBAm concentration of $4.5x10^{-2}$ mg/mL) with 0.4 mg/mL mucin and 25 mM potassium chloride.

Solutions were stored at 37°C for an hour in a shaking incubator. A sample of the nanogels that had not been functionalized and a sample without nanogels were used as controls. 5 zeta potential measurements were performed per sample with 15 runs per measurement (Brookhaven 90Plus Particle Size Analyzer).

4.2.11 Loading of dexamethasone

For drug loading, 5 mg of dexamethasone were added into the MC-g-PNtBAm and DMSO solution before reassembling. Encapsulation was performed during nanogel formation and particles were subsequently functionalized with PBA following the methods described above. Suspensions of loaded nanogels were then centrifuged at 15000 RPM for 20 minutes in Nanosep 10K Omega centrifugal units (10 kDa molecular weight cut-off, Pall Corporation) to separate the particles from free dexamethasone. Drug loading was calculated by measuring the amount of drug in the supernatant using high performance liquid chromatography (HPLC, Waters 2707 Autosampler, 1525 Binary HPLC Pump, 2489 UV/Visible detector, Column Dionex. Model Acclaim (r) 120 C18 5μm 120A 4.6x250mm). 254 nm detection wavelength, injecting 10μL sample and 1mL/min isocratic flow rate of 40:60 (v/v) acetonitrile:water were used in this experiment. Sample concentrations were deduced from a standard calibration curve of dexamethasone in 40:60 (v/v) acetonitrile:water.

The following formula was used to calculate loading efficiency of dexamethasone into the nanogel particles:

$$Loading\ efficiency\ (\%) = 100 * \frac{Initial\ amount\ of\ drug - Amount\ of\ drug\ in\ supernatant}{Initial\ amount\ of\ drug}$$

4.2.12 In vitro release of dexamethasone

The in vitro release of dexamethasone from the nanogels was evaluated in phosphate buffered saline (PBS). A dialysis bag (molecular weight cut-off 3500 Da, Spectra/Por, Spectrum laboratories) containing 1 mL of drug-loaded particles dispersed in PBS (MC-g-PNtBAm concentration of 0.81 was immersed into 5 mL of PBS maintained at 32 ± 1 °C by a shaking water bath. The release medium outside the bag was sampled at selected time points and replaced with fresh pre-warmed PBS. The Concentration of dexamethasone in the solutions was determined by HPLC. All measurements were performed in triplicate and plotted as mean ± SD.

4.2.13 Cell toxicity studies

The in vitro toxicity of the PBA grafted nanogels was assessed by performing an MTT assay and a Calcein AM – Ethidium homodimer-1 staining assay on human corneal epithelial cells (HCECs). Two different PBA coverages were used for these experiments: MC(165k)-g-PNtBAm_PBA50 and MC(165k)-g-PNtBAm_PBA100. 1% penicillin-streptomycin and overnight UV irradiation (254 nm) overnight were used to sterilize the nanogel suspensions. HCECs were seeded at a density of 5,000 cells/well human onto 96-well plates and cultured in 100 µL of keratinocyte serum free medium in a CO_2 incubator. 24 hours later, the spent medium was replaced with the nanogel formulations and diluted with culture medium to a final MC-g-PNtBAm concentration of 0.3 mg/mL. Cells were incubated at 37°C in the presence of the PBA grafted nanogels for 48 hours. Subsequently, the media containing the suspension was replaced with either 100µL of PBS and 10µL of MTT stock (5 mg/ml) or

100µL of calcein AM-ethidium homodimer-1 working solution (2µM calcein AM, 4µM ethicium homodimer-1). For the calcein AM – Ethidium homodimer-1 assay, the cells were incubated for 45 minutes at room temperature. For the MTT assay, the cells were incubated for 4 hours, and the supernatant was then replaced by 50µL of DMSO and incubated for an additional 10 minutes at 37°C. All the resultant solutions were measured in a microplate reader (Tecan Infinite 200 Pro) at 540 nm for the MTT assay, or 530 nm (emission) and 645 nm (excitation) for the Calcein and Ethidium assay.

4.3 RESULTS AND DISCUSSION

4.3.1 PBA Functionalization

For both formulations using 30 kg/mol MC and 165 kg/mol MC, MC-g-PNtBAm synthesis resulted in the grafting of 40 NtBAm per 100 anhydroglucose units on average (40%). This ratio is referred to as the degree of hydrophobization (DH) and was deduced from the ratio of relative peak integrations of protons belonging to the hydrogen in C2 position of MC and the CH_3 group of NtBAm, following a method used in previous studies[9,52].

Surface functionalization was performed through modification of the outer methylcellulose. The strategy used to graft MC with PBA involves a Schiff base reaction between the primary amine groups of the PBA and the carbonyl groups on the MC polymer chain (Figure 4-3, step 2). To generate a reactive MC support, MC was oxidized with sodium m-periodate, which yields carbonyl groups via a Malaprade-type reaction that preferentially breaks the C2-C3 bond of vicinal hydroxyl groups to form a 2,3-dialdehyde (Figure 4-3, step 1). This reaction has been reported to produce a reproducible degree of oxidation on the MC chain[53],

and no significant side reactions[54], but has also been reported to lead to depolymerization of methylcellulose[55]. Indeed, we performed GPC on MC solutions after different oxidation times and results showed a decrease in the MC molecular weight with increasing reaction time, confirming these observations (Table 4-2). As we have previously shown, the length of the polysaccharide was an important parameter defining the nanogel characteristics[52]. Therefore, the oxidation step will contribute to the changes in their properties, in addition to the PBA functionalization itself.

Grafting of PBA on the surface of MC-g-PNtBAm nanogels was confirmed on the NMR spectrum by the resonance signals of phenyl-ring protons at 7.0 - 8.0 ppm[56] (Figure 4-4). ATR FT-IR analysis (Figure 4-5) showed typical absorption peaks of the phenyl ring of PBA at 794 and 704 cm^{-1} [56]. Weakening of the peak band at 1645cm^{-1} assigned to C=O stretching[56] indicated fewer carbonyl groups due to grafting.

To compare the effect of PBA coverage on the nanogel properties, different feed concentrations were added to the reaction. The modification was performed on two types of nanogels with the same 40% degree of hydrophobization, but prepared with two different molecular weights of methylcellulose, 30 kDa and 165 kDa. When comparing nanogels made with different PBA feed concentrations, ATR FT-IR spectra showed increased intensity of the PBA peaks with increasing PBA initial concentration (Figure 4-6-a). Those results were confirmed by XPS measurements, with increased boron serving as an indication of increased PBA in the samples (Figure 4-6-b). The PBA functionalization was not impacted by the molecular weight of MC, as grafting was similar for both nanogel types at equal PBA feed concentrations. While ATR measurements testified to the presence of PBA in all of the

samples synthesized, with the lowest concentration of PBA, the XPS spectra gave no indication of its presence for the formulation with the lower feed. Such results are not surprising, as functionalization was only performed on the surface of the nanogels, meaning that the ratio of PBA compared to the bulk was quite low.

4.3.2 Size and morphology

Nanosight measurements of the size of the nanogel particles showed an overall decrease in particle size after functionalization (Figure 4-7). This was attributed to the oxidation step reducing its molecular weight. Previous results on the effect of molecular weight of MC demonstrated that shorter chains produced smaller nanogels because of decreased swelling capacity[52].

While the amount of PBA functionalization had no impact on the size of the nanogels prepared using high molecular weight MC, their size decreased upon PBA grafting for smaller molecular weight MC. A decrease in the particle size with PBA functionalization has been previously reported[39,57], and was interpreted as the possible result of a change in the packing density due to reduced hydrophilicity of the polysaccharide surface. At the highest PBA coverage with the low MC molecular weight only, the colloidal solution was observed to lose its stability. Indeed, while all nanogels exhibited a spherical morphology (Figure 4-8), TEM imaging demonstrated aggregation of the particles upon PBA grafting for MC(30k)-g-PNtBAm. A previous study observed that excess PBA on the surface may cause the particles to be too hydrophobic compromising stability[39]. However, despite their similar PBA grafting, nanogels made of the longer MC chains did not shrink or precipitate. Considering the size

difference of MC(30k)-g-PNtBAm and MC(165k)-g-PNtBAm nanogels at high PBA grafting, an equal amount of PBA functionalization would result in a denser coverage on smaller particles. Alternatively, it is possible that hydrophobic grafting would have a greater impact on shorter hydrophilic MC chains. Furthermore, oxidation likely had a more dramatic effect on MC(30k)-g-PNtBAm nanogels. Therefore, the PBA density must be tuned in order to balance between mucoadhesion and colloidal stability.

4.3.3 Cytocompatibility

In vitro cytotoxicity profiles of MC-g-PNtBAm_PBA were evaluated using live/dead and MTT assays. As shown in Figure 4-9, the PBA functionalization presented no cytotoxicity with corneal epithelial cells and the MTT assay demonstrated that the metabolism of the cells was not impacted by the presence of the mucoadhesive agent, indicating good cell biocompatibility. Other studies reported biocompatibilities of PBA molecules using both in vitro and in vivo assays[58–60].

4.3.4 Drug entrapment and release

MC(165k)-g-PNtBAm nanogels were chosen to perform the in vitro release study as they remained stable in solution at all PBA coverages. Lower encapsulation efficiencies were obtained loading by nanoprecipitation compared to entrapment during synthesis[9,52] (Table 4-3). This could be attributed to the presence of DMSO in solution at a 1:10 ratio during nanogel formation, as dexamethasone has a greater solubility in DMSO than in water[61]. However, it is most likely mainly the result of the lower nanogel concentration in solution, providing less hydrophobic domains to entrap the drug and inducing lower efficiencies. For

this drug loading method, low concentrations have been reported to ensure better dispersion of the copolymers to be able to separate into nanodomains upon addition into the non-solvent water[62].

PBA grafting was found to improve entrapment efficiency and increasing PBA concentration increased the encapsulation percentage of dexamethasone. Although the ungrafted nanogels and MC(165k)-g-PNtBAm_PBA(2.5) both showed similar encapsulation percentages, the PBA functionalization step induced a 9-hour difference in the measurements. Such delay would have been expected to induce lower entrapments due to release of drug in the meantime. This outcome could be attributed to a possible affinity between the dexamethasone and the PBA due to hydrophobic interaction. Indeed, the hydrophilicity of the MC network decreases upon PBA grafting as shown by the lower swelling ability, and thus would be expected to have higher affinity for the hydrophobic drug.

The dexamethasone release was plotted two different ways (Figure 4-10). Figure 4-10-a shows the cumulative release of all of the dexamethasone, encapsulated and free in solution, as all percentages are relative to the initial feed concentration of dexamethasone. Figure 4-10-b only shows the release of the dexamethasone from the nanogels, as the percentages are calculated relatively based on the amounts of drug encapsulated. While the latter gives a more realistic appreciation of the initial burst, the former enables a comparison of release rates, as all formulations are plotted relative to the same amount of dexamethasone.

Release profiles can be divided into 2 phases. The nanogels showed a burst release in the first 10 hours, corresponding to the dexamethasone freely suspended (Figure 4-10-a) and the dexamethasone which is loosely attached to the hydrophilic mesh of the nanogels[9,52,63] (Figure 4-10-b). It can be observed that the burst is decreased by PBA functionalization. It is expected as the grafting of PBA increased the affinity of dexamethasone for the MC hydrophilic network, and hence diffused more slowly to the aqueous media. This effect of PBA functionalization has been observed in a previous study[40].

The second phase of the release profile showed a slow diffusional release of dexamethasone from the hydrophobic domains[9,52,63]. When comparing the slopes (Figure 4-10-a), the functionalized nanogels released the drug faster than the unmodified ones. This may be the result of the shortening of the MC chains during the oxidation step. Indeed, our previous study on the effect of MC molecular weight showed that dexamethasone diffused more easily out of the hydrophobic domains through nanogels made of shorter MC chains[52]. Both PBA grafted nanogels featured similar release rates with 20% of the drug coming out between day 2 and day 12, MC(165k)-g-PNtBAm_PBA(5) reaching 100% earlier because of its lower entrapment efficiency. No impact of PBA coverage density could be observed in this phase of the release in accordance with other studies[39,59], which supports the hypothesis that the faster release could be attributed to the shorter MC chains. Overall, the study showed that dexamethasone release could be maintained for 12 days, which is significantly higher than other types of nanoparticles for topical ocular drug delivery[57,64–69]. Given that the turnover of the mucin layer of the tears occurs every 4-6 days and replacement of the corneal epithelial cells occurs every 4-8 days[3], this release period is appropriate.

4.3.5 Mucoadhesion

Mucin adsorption by nanoparticles dispersed in aqueous media was measured as a way to test their ability to bind to the mucosal surfaces of the body. This method provides an indirect evaluation of mucoadhesion in the sense that it is inferred from the interactions between the nanosystems and the mucosal fluid without evaluating the mucoadhesive force as such[12]. Mucins are the major component of the mucus[70]. Once in solution, they arrange themselves as nanosized structures and present a negative potential at physiological pH[71,72]. In this study, the mucoadhesive properties of PBA grafted nanogels were evaluated by measuring the changes of zeta-potential of mucin in presence of the particle, attributed to their interaction[23,51,72,73] (Figure 4-11).

All formulations presented a negative zeta-potential when suspended in mucus solution due to the presence of negatively charged mucin. The presence of MC(165k)-based nanogels, PBA grafted or not, did not have any impact on the zeta-potential of mucin solution, suggesting little or no interaction. However, the suspension with MC(30k)-based nanogels induced a decrease of the zeta potential, although no significant impact of PBA functionalization could be observed. Such negative shift has been previously reported and identified as a proof of particle-mucin interaction[72]. The different results obtained for each MC molecular weight regardless of functionalization could be due to the conformation of the polymer as it has been shown to play an important role in the intimate contact with mucus. For instance, random coil conformations show higher mucoadhesion than that spherical and rigid rod shape conformations[74]. Here, the mobile network composed of shorter methylcellulose chains could interact more easily with mucin compared to the

swollen mesh of entangled longer chains[52]. Besides, the high swelling ability of the nanogels synthesized with MC of higher molecular weight could also explain their lower mucoadhesion as neutral highly hydrophilic shells have been shown to inhibit the establishment of mucoadhesive forces[12,75,76]. Finally, the nanogel concentration might be another parameter affecting the results, and higher concentrations might give a more significant change in the measurements[73]. While the zeta-potential study may suggest mucin-particle interaction for some nanogels and provide insight to the underlying mechanisms of mucoadhesion of nanoparticulate systems, it fails to mimic the in vivo settings. For instance, while MC(30k)-g-PNtBAm_PBA(5) might provide higher mucin adsorption in vitro, their self-binding could create aggregates with diameters too high for diffusion through the mucus mesh[77]. A direct method of measuring mucoadhesion, such as in vivo testing, would be necessary to further investigate and compare the mucoadhesive performances of the different formulations.

4.4 CONCLUSION

Nanogels of hydrophobized methylcellulose were successfully functionalized with phenylboronic acid. Coverage density could be controlled by varying the feed concentration of PBA. PBA functionalization did not induce any cytotoxicity, and nanogels synthesized with methylcellulose of higher molecular weight remained stable after functionalization. The additional hydrophobic layer of PBA was found to reduce the initial burst release, while the shorter MC chains resulting from the oxidation step induced a faster diffusion rate compared with the unmodified nanogels. All formulations provided a sustained release of the drug for over 12 days. Zeta-potential measurements indicated interaction of mucin with the nanogels

synthesized with shorter MC chains, providing encouraging results to pursue the investigation on their mucoadhesive properties with in vivo experiments. With their ability to entrap and release in a controlled fashion, PBA functionalized MC-g-PNtBAm nanogels present promising properties to address the challenges of topical administration in the ocular environment.

4.5 TABLES

Table 4-1: Nomenclature and content of the formulations synthesized.

Formulation name	MC molecular weight (g/mol)	PBA solution concentration	PBA final concentration	Mass ratio PBA:MC-g-PNtBAm
MC(30k)-g-PNtBAm_PBA(1.25)	30 000	2.5 mg/mL	1.125 mg/mL	1.25:1
MC(30k)-g-PNtBAm_PBA(2.5)		5 mg/mL	2.25 mg/mL	2.5:1
MC(30k)-g-PNtBAm_PBA(5)		10 mg/mL	4.5 mg/mL	5:1
MC(165k)-g-PNtBAm_PBA(1.25)	165 000	2.5 mg/mL	1.125 mg/mL	1.25:1
MC(165k)-g-PNtBAm_PBA(2.5)		5 mg/mL	2.25 mg/mL	2.5:1
MC(165k)-g-PNtBAm_PBA(5)		10 mg/mL	4.5 mg/mL	5:1

Table 4-2: Molecular weight of methylcellulose after varying reaction times of periodate oxidation, measured by gel permeation chromatography.

Oxidation time	Mn	Mw	PDI
0 hour	26710	79359	2,97
2 hours	4903	12754	2,60
6 hours	2478	5391	2,18
24 hours	622	1809	2,90

Table 4-3: Loading efficiency of dexamethasone into MC(165k)-g-PNtBAm_PBA nanogels as a function of PBA coverage.

	Entrapment efficiencies (%)
MC(165k)-g-PNtBAm	48.0
MC(165k)-g-PNtBAm_PBA(2.5)	47.6
MC(165k)-g-PNtBAm_PBA(5)	61.2

4.6 FIGURES

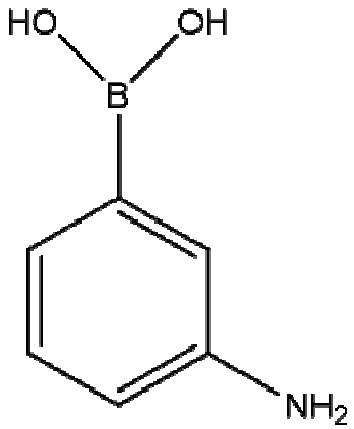

Figure 4-1: Structure of 3-aminophenylboronic acid.

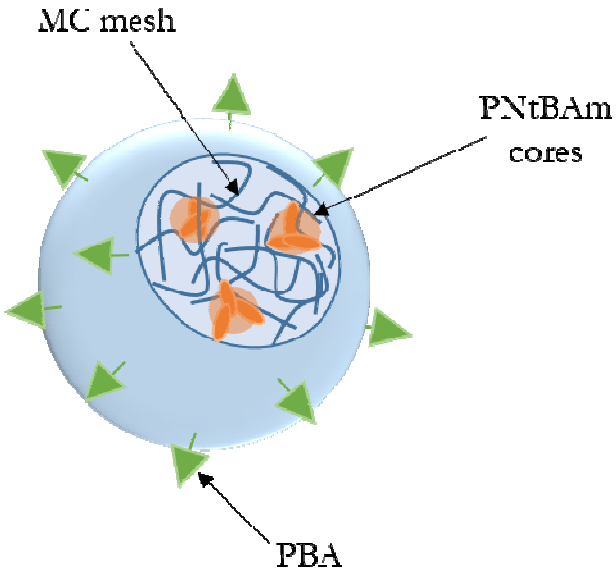

Figure 4-2: Structure of PBA functionalized MC-g-PNtBAm nanogels in aqueous solutions.

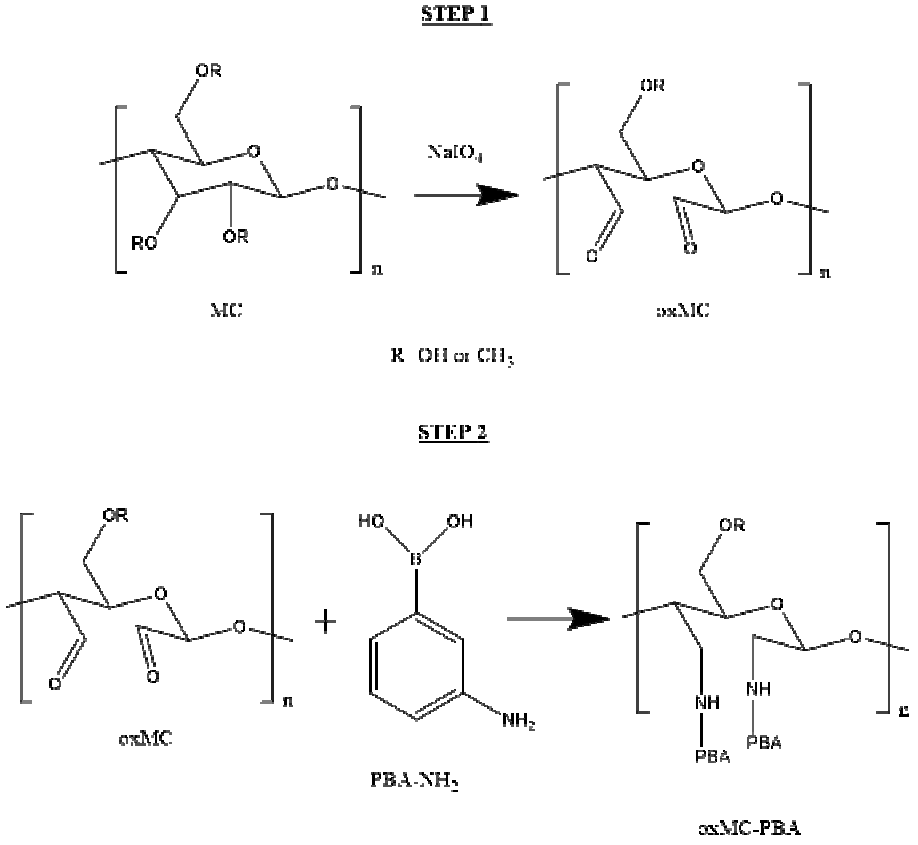

Figure 4-3: Scheme for tethering PBA to MC. Step 1: Sodium m-periodate ($NaIO_4$) oxidation via Malaprade-type reaction, which breaks the C2-C3 bond of vicinal hydroxyl groups to form 2,3-dialdehyde structure. Step 2: Reaction of aldehyde groups of oxidized MC structure with primary amine groups of 3-aminophenylboronic acid via Schiff base linkage.

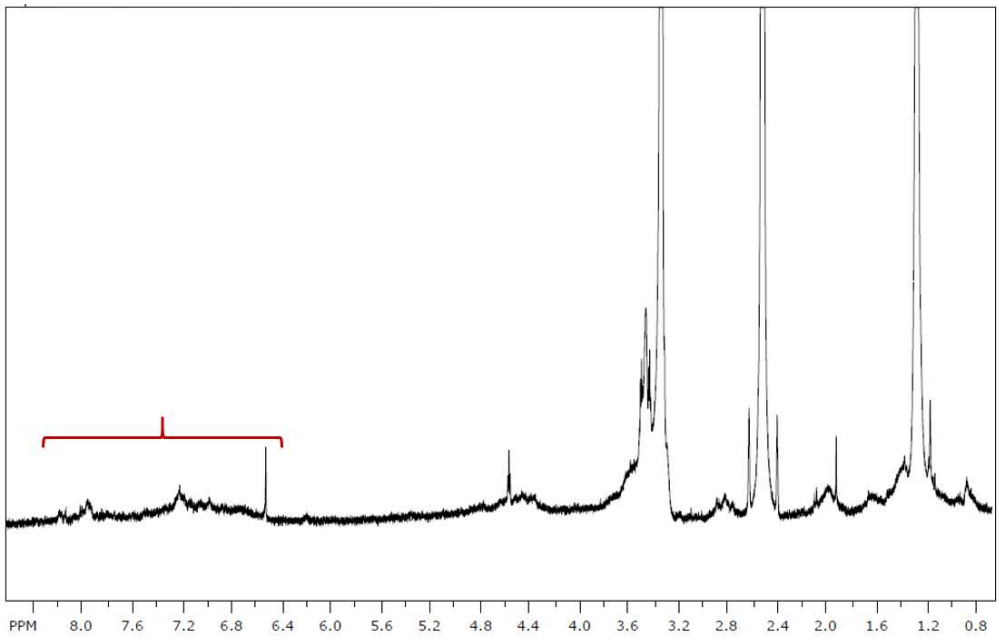

Figure 4-4: ^{1}H NMR spectrum of PBA functionalized MC-g-PNtBAm nanogels

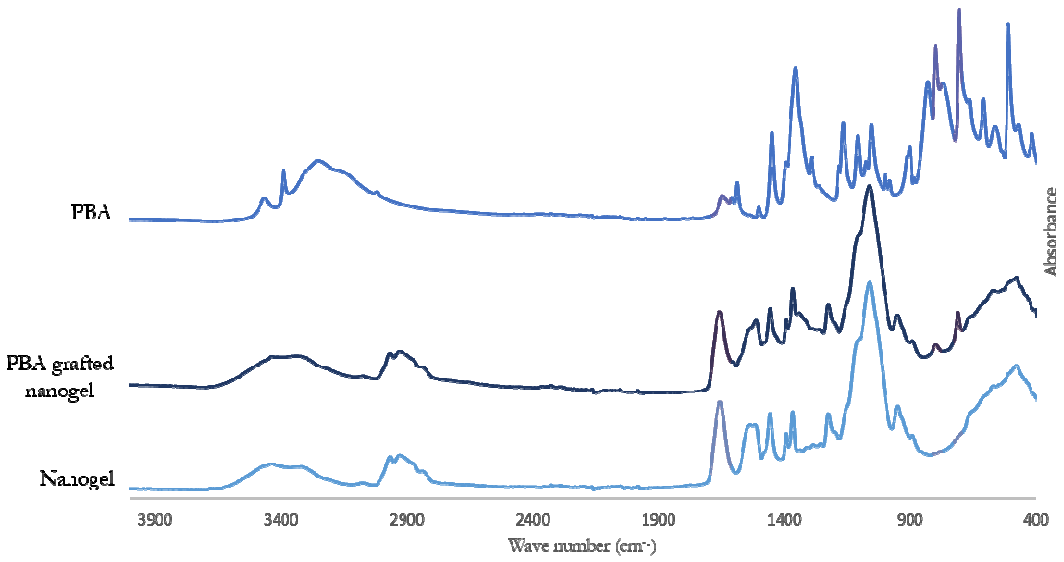

Figure 4-5: NMR spectrum of PBA, PBA functionalized MC-g-PNtBAm nanogels, MC-g-PNtBAm nanogels.

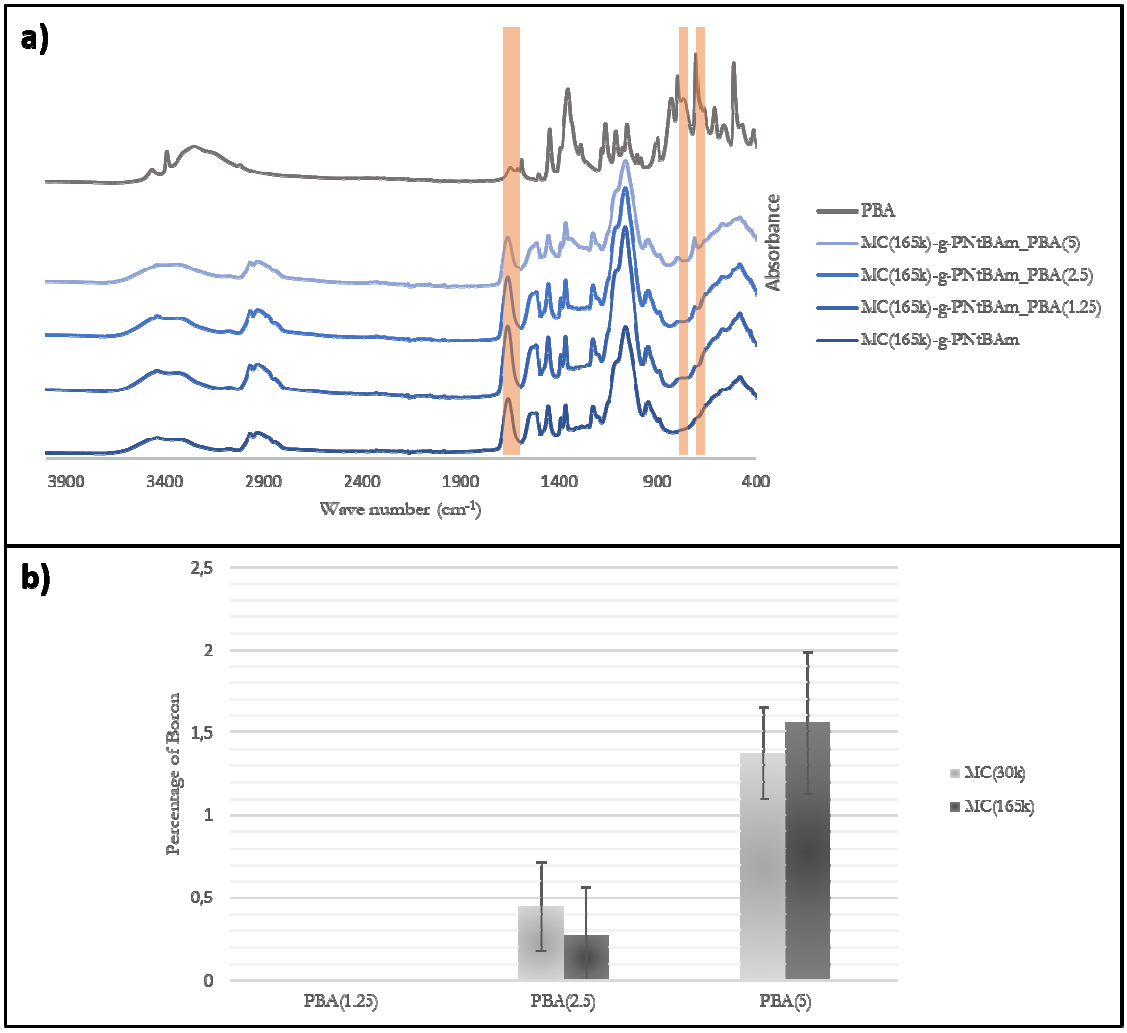

Figure 4-6: Comparaison of the PBA content a) ATR FT-IR spectra b) Boron quantification by XPS of all MC(x)-g-PNtBAm_PBA(y) formulations.

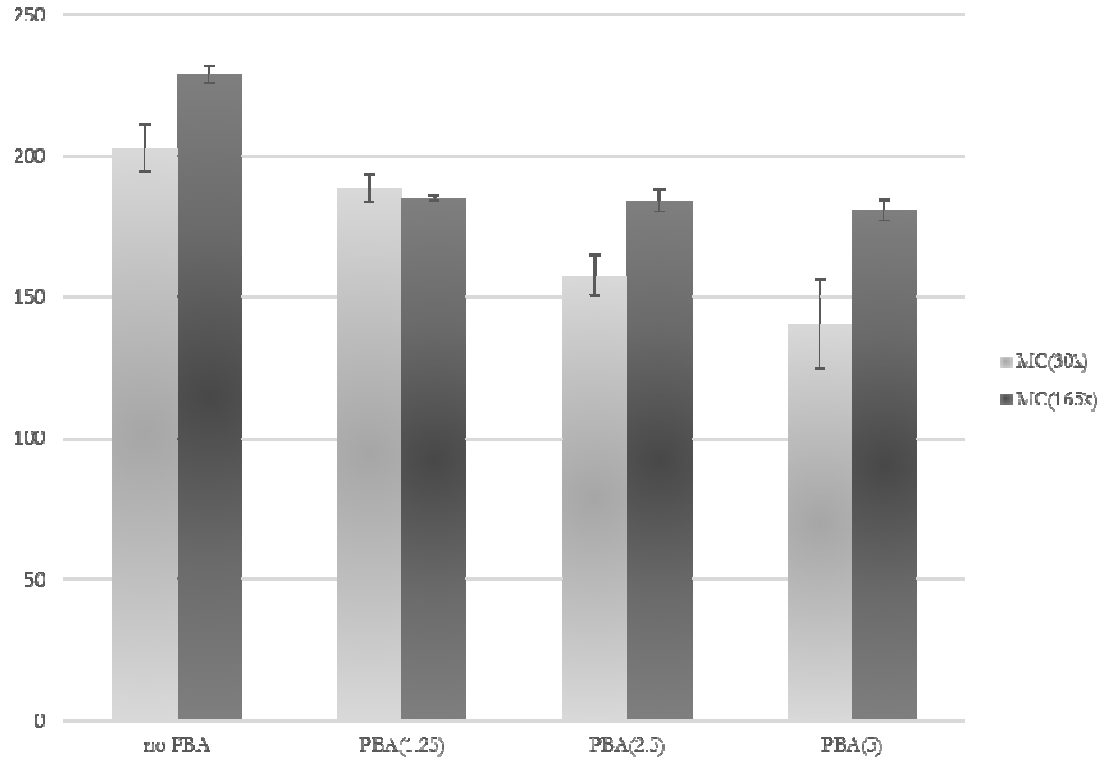

Figure 4-7: Influence of PBA coverage on the size of the nanogels synthesized using 30kg/mol or 165 kg/mol MC for the MC(x)-g-PNtBAm_PBA(y) formulations. 3 measurements per solution, error bars corresponding to the standard deviation of the mean size.

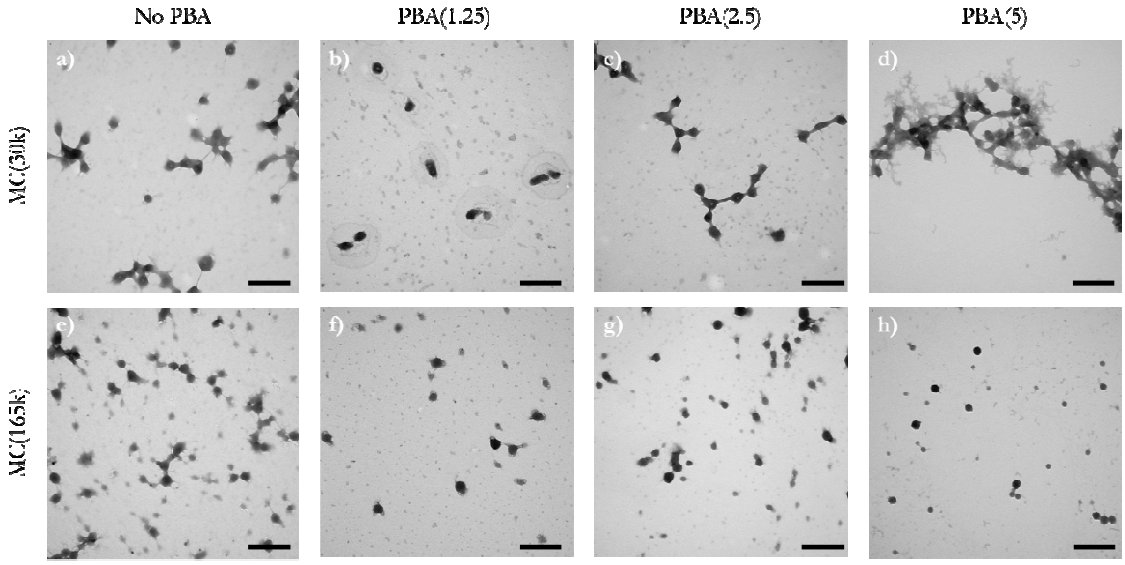

Figure 4-8: TEM pictures MC(x)-g-PNtBAm_PBA(y) nanogels. Scale bars indicate 500 nm.

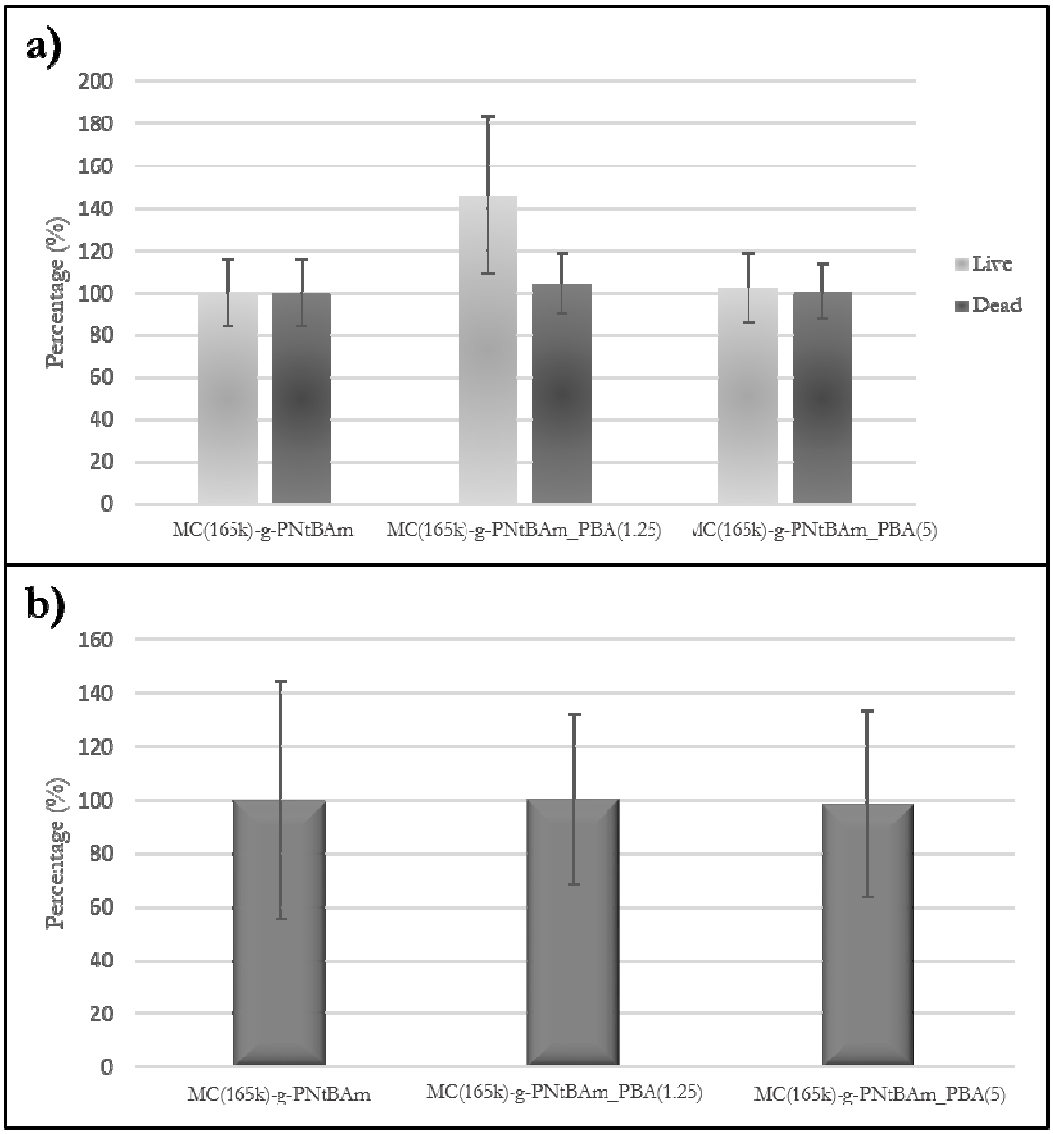

Figure 4-6: Comparison of a) cell viability and b) metabolism in presence of 0.3 mg/mL MC(165k)-g-PNtBAm_PBA nanogels at two different PBA coverages. Data expressed as a percentage relative to control comprising cells not exposed to the nanogels.n=6 with error bars corresponding to the standard deviation.

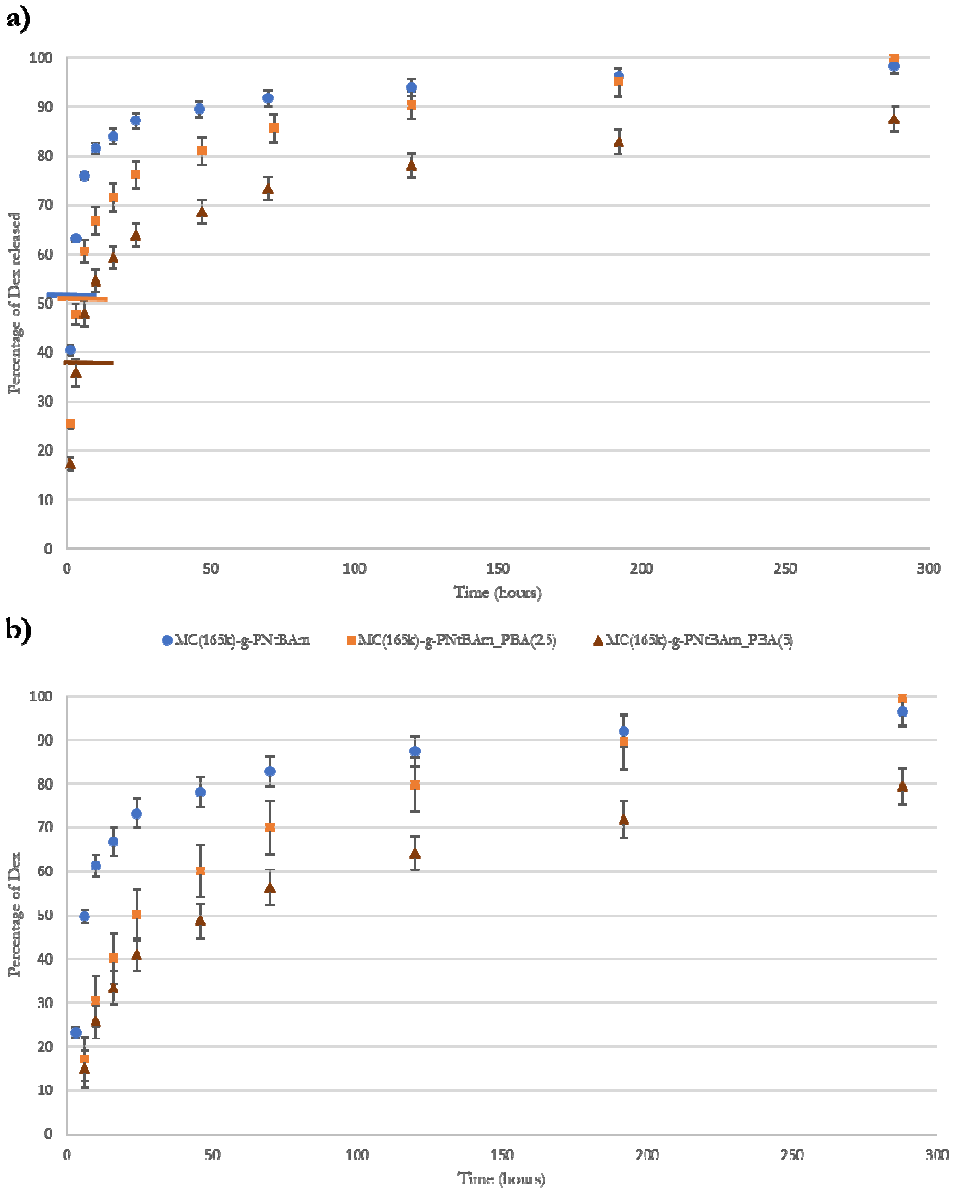

Figure 4-7: Dexamethasone release from MC(165k)-g-PNtBAm_PBA nanogels with two different PBA grafting coverages compared to not functionalized nanogels. a) Release plotted as a percentage relative to the total quantity of dexamethasone initially incorporated – 100% thus correspondi to the dexamethasone free in solution and encapsulated. The bars on the curves indicate the time point when the free drug in solution is released from the dialysis bag and the entrapped drug is being released. b) Release plotted as a percentage relative to the quantity of dexamethasone encapsulated – 100% corresponds to the amount of dexamethasone

encapsulated.n=3 with error bars corresponding to standard deviation.

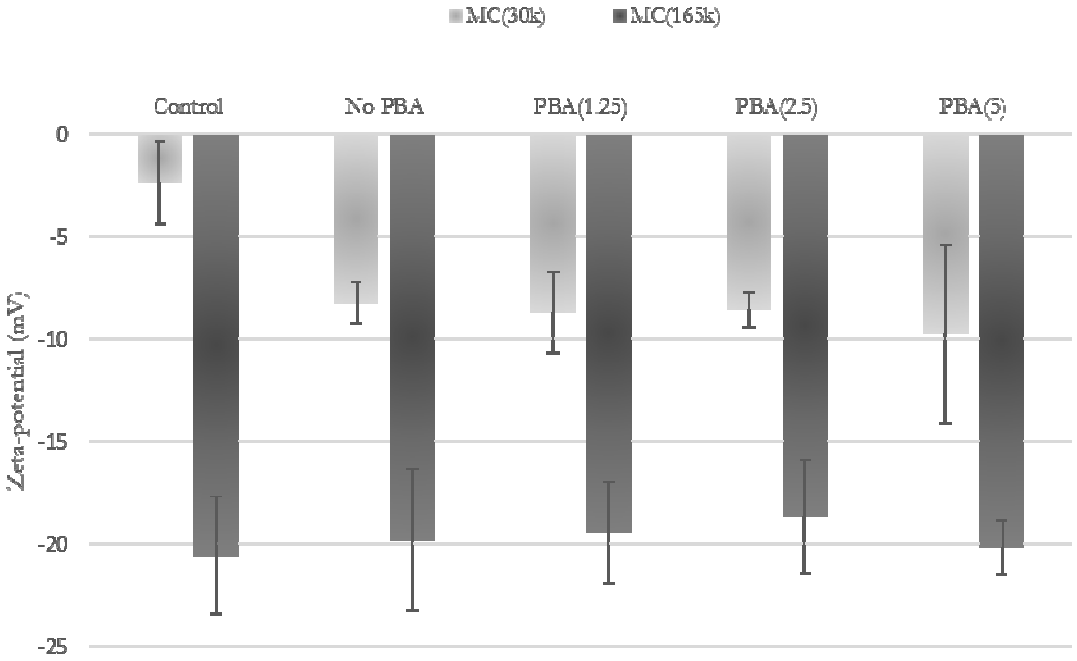

Figure 4-8: Zeta-potential of MC(x)-g-PNtBAm_PBA(y) formulations compared to a control solution of mucin.6 measurements per solution with error bars corresponding to the standard deviation.

4.7 ACKNOWLEDGEMENTS

Funding support from NSERC and the CREATE Biointerface Training Program is gratefully acknowledged. XPS measurements were performed by Danielle Covelli from the Biointerface Institute.

4.8 DISCLOSURES

The authors state no conflict of interest.

BIBLIOGRAPHY

1. Gipson, I. K. & Argüeso, P. Role of Mucins in the Function of the Corneal and Conjunctival Epithelia. *Int. Rev. Cytol.* **231,** 1–49 (2003).
2. Bucolo, C., Drago, F. & Salomone, S. Ocular drug delivery: A clue from nanotechnology. *Front. Pharmacol.* **3,** 1–3 (2012).
3. Ludwig, A. The use of mucoadhesive polymers in ocular drug delivery. *Adv. Drug Deliv. Rev.* **57,** 1595–639 (2005).
4. Gaudana, R., Jwala, J., Boddu, S. H. S. & Mitra, A. K. Recent perspectives in ocular drug delivery. *Pharm. Res.* **26,** 1197–216 (2009).
5. Diebold, Y. & Calonge, M. Applications of nanoparticles in ophthalmology. *Prog. Retin. Eye Res.* **29,** 596–609 (2010).
6. Liu, S., Jones, L. & Gu, F. X. Nanomaterials for ocular drug delivery. *Macromol. Biosci.* **12,** 608–20 (2012).
7. Cho, H. K., Cheong, I. W., Lee, J. M. & Kim, J. H. Polymeric nanoparticles, micelles and polymersomes from amphiphilic block copolymer. *Korean J. Chem. Eng.* **27,** 731–740 (2010).
8. Rameshkumar, P. & Ramaraj, R. Nanoparticles: Functionalization and Multifunctional Applications in Biomedical Sciences. *J. Appl. Electrochem.* **43,** 1005–1010 (2013).
9. Jamard, M., Hoare, T. & Sheardown, H. Nanogels of Methylcellulose Hydrophobized with N-tert-butylacrylamide for Ocular Drug Delivery. (2016).
10. Khutoryanskiy, V. V. Advances in mucoadhesion and mucoadhesive polymers. *Macromol. Biosci.* **11,** 748–64 (2011).
11. Haas, J. & Lehr, C.-M. Developments in the area of bioadhesive drug delivery systems. *Expert Opin. Biol. Ther.* **2,** 287–298 (2002).
12. das Neves, J. *et al.* Mucoadhesive nanomedicines: characterization and modulation of mucoadhesion at the nanoscale. *Expert Opin. Drug Deliv.* **8,** 1085–104 (2011).
13. Achouri, D., Alhanout, K., Piccerelle, P. & Andrieu, V. Recent advances in ocular drug delivery. *Drug Dev. Ind. Pharm.* **39,** 1599–617 (2013).
14. Nagarwal, R. C., Kant, S., Singh, P. N., Maiti, P. & Pandit, J. K. Polymeric nanoparticulate system: a potential approach for ocular drug delivery. *J. Control. Release* **136,** 2–13 (2009).
15. Sakuma, S. *et al.* Mucoadhesion of polystyrene nanoparticles having surface hydrophilic polymeric chains in the gastrointestinal tract. *Int. J. Pharm.* **177,** 161–172 (1999).
16. Sarmento, B. *et al.* Alginate/chitosan nanoparticles are effective for oral insulin delivery. *Pharm. Res.* **24,** 2198–2206 (2007).
17. Sarmento, B., Ribeiro, A., Veiga, F., Ferreira, D. & Neufeld, R. Oral bioavailability of

insulin contained in polysaccharide nanoparticles. *Biomacromolecules* **8,** 3054–3060 (2007).

18. Peppas, N. a & Huang, Y. Nanoscale technology of mucoadhesive interactions. *Adv. Drug Deliv. Rev.* **56,** 1675–87 (2004).
19. Sosnik, A., das Neves, J. & Sarmento, B. Mucoadhesive polymers in the design of nano-drug delivery systems for administration by non-parenteral routes: A review. *Prog. Polym. Sci.* **39,** 2030–2075 (2014).
20. Lai, S. K. *et al.* Rapid transport of large polymeric nanoparticles in fresh undiluted human mucus. *Proc. Natl. Acad. Sci. U. S. A.* **104,** 1482–1487 (2007).
21. Lai, S. K., Wang, Y.-Y., Hida, K., Cone, R. & Hanes, J. Nanoparticles reveal that human cervicovaginal mucus is riddled with pores larger than viruses. *Proc. Natl. Acad. Sci. U. S. A.* **107,** 598–603 (2010).
22. Ponchel, G., Montisci, M. J., Dembri, A., Durrer, C. & Duchêne, D. Mucoadhesion of colloidal particulate systems in the gastro-intestinal tract. *Eur. J. Pharm. Biopharm.* **44,** 25–31 (1997).
23. De Campos, A. M., Diebold, Y., Carvalho, E. L. S., Sánchez, A. & Alonso, M. J. Chitosan nanoparticles as new ocular drug delivery systems: in vitro stability, in vivo fate, and cellular toxicity. *Pharm. Res.* **21,** 803–810 (2004).
24. du Toit, L. C., Pillay, V., Choonara, Y. E., Govender, T. & Carmichael, T. Ocular drug delivery - a look towards nanobioadhesives. *Expert Opin. Drug Deliv.* **8,** 71–94 (2011).
25. Sogias, I. a., Williams, A. C. & Khutoryanskiy, V. V. Why is chitosan mucoadhesive? *Biomacromolecules* **9,** 1837–1842 (2008).
26. Li, N., Zhuang, C.-Y., Wang, M., Sui, C.-G. & Pan, W.-S. Low molecular weight chitosan-coated liposomes for ocular drug delivery: in vitro and in vivo studies. *Drug Deliv.* **19,** 28–35 (2012).
27. Mahmoud, A. a, El-Feky, G. S., Kamel, R. & Awad, G. E. a. Chitosan/sulfobutylether-β-cyclodextrin nanoparticles as a potential approach for ocular drug delivery. *Int. J. Pharm.* **413,** 229–36 (2011).
28. Abdelbary, G. Ocular ciprofloxacin hydrochloride mucoadhesive chitosan-coated liposomes. *Pharm. Dev. Technol.* **16,** 44–56 (2011).
29. Li, N. *et al.* Liposome coated with low molecular weight chitosan and its potential use in ocular drug delivery. *Int. J. Pharm.* **379,** 131–8 (2009).
30. De Campos, a M., Sánchez, a & Alonso, M. J. Chitosan nanoparticles: a new vehicle for the improvement of the delivery of drugs to the ocular surface. Application to cyclosporin A. *Int. J. Pharm.* **224,** 159–68 (2001).
31. Ensign, L. M., Cone, R. & Hanes, J. Oral drug delivery with polymeric nanoparticles: The gastrointestinal mucus barriers. *Adv. Drug Deliv. Rev.* **64,** 557–570 (2012).
32. Kumar, R. & Sinha, V. R. Thiomer: A potential carrier for therapeutic delivery. *React. Funct. Polym.* **73,** 1156–1166 (2013).

33. Bies, C., Lehr, C. M. & Woodley, J. F. Lectin-mediated drug targeting: History and applications. *Adv. Drug Deliv. Rev.* **56,** 425–435 (2004).

34. Roy, S., Pal, K., Anis, A., Pramanik, K. & Prabhakar, B. Polymers in Mucoadhesive Drug-Delivery Systems: A Brief Note. *Des. Monomers Polym.* **12,** 483–495 (2009).

35. Serra, L., Dom??nech, J. & Peppas, N. A. Engineering design and molecular dynamics of mucoadhesive drug delivery systems as targeting agents. *Eur. J. Pharm. Biopharm.* **71,** 519–528 (2009).

36. Carvalho, F., Bruschi, M., Evangelista, R. & Gremiao, M. Mucoadhesive drug delivery systems. *Brazilian J. Pharm. Sci.* **46,** 1–17 (2010).

37. Madsen, F., Eberth, K. & Smart, J. D. A rheological examination of the mucoadhesive/mucus interaction: the effect of mucoadhesive type and concentration. *J. Control. Release* **50,** 167–78 (1998).

38. Carvalho, F. *et al.* Mucoadhesive drug delivery systems. *J. Pharm. Bioallied Sci.* **3,** 89–100 (2011).

39. Liu, S., Jones, L. & Gu, F. X. Development of mucoadhesive drug delivery system using phenylboronic acid functionalized poly(D,L-lactide)-b-dextran nanoparticles. *Macromol. Biosci.* **12,** 1622–6 (2012).

40. Zhang, X., Wang, Y., Zheng, C. & Li, C. Phenylboronic acid-functionalized glycopolymeric nanoparticles for biomacromolecules delivery across nasal respiratory. *Eur. J. Pharm. Biopharm.* **82,** 76–84 (2012).

41. Li, C., Liu, Z., Yan, X., Lu, W. & Liu, Y. Mucin-controlled drug release from mucoadhesive phenylboronic acid-rich nanoparticles. *Int. J. Pharm.* **479,** 261–264 (2015).

42. Liu, A. *et al.* Quantum dots with phenylboronic acid tags for specific labeling of sialic acids on living cells. *Anal. Chem.* **83,** 1124–1130 (2011).

43. Matsumoto, A., Sato, N., Kataoka, K. & Miyahara, Y. Noninvasive Sialic Acid Detection at Cell Membrane by Using Phenylboronic Acid Modified Self-Assembled Monolayer Gold Electrode. *J. Am. Chem. Soc.* **131,** 12022–12023 (2009).

44. Ivanov, A. E. *et al.* Boronate-containing polymer brushes: Characterization, interaction with saccharides and mammalian cancer cells. *J. Biomed. Mater. Res. - Part A* **88,** 213–225 (2009).

45. Zheng, C. *et al.* Amphiphilic glycopolymer nanoparticles as vehicles for nasal delivery of peptides and proteins. *Eur. J. Pharm. Sci.* **49,** 474–482 (2013).

46. Cambre, J. N. & Sumerlin, B. S. Biomedical applications of boronic acid polymers. *Polymer (Guildf).* **52,** 4631–4643 (2011).

47. Yalpani, M. & Hall, L. D. Some chemical and analytical aspects of polysaccharide modifications. III. Formation of branched-chain, soluble chitosan derivatives. *Macromolecules* **17,** 272–281 (1984).

48. Hall, L. D. & Holme, K. R. Tailored-rheology: chitosan derivatives with branched

pendant sugar chains. *J. Chem. Soc. Chem. Commun.* 217 (1986). doi:10.1039/c39860000217

49. Rinaudo, M. New way to crosslink chitosan in aqueous solution. *Eur. Polym. J.* **46,** 1537–1544 (2010).
50. Griffith, M. *et al.* Functional Human Corneal Equivalents Constructed from Cell Lines. *Science (80-.).* **286,** 2169–2172 (1999).
51. Bhatta, R. S. *et al.* Mucoadhesive nanoparticles for prolonged ocular delivery of natamycin: In vitro and pharmacokinetics studies. *Int. J. Pharm.* **432,** 105–12 (2012).
52. Jamard, M. & Sheardown, H. Effect of Methylcellulose Molecular Weight on the properties of Self-Assembling MC-g-PNtBAm Nanogels. (2016).
53. Chang, P.-C. *et al.* Thermoreversible laminin-functionalized hydrogel for neural tissue engineering. *J. Biomed. Mater. Res. A* **81,** 771–780 (2007).
54. Margutti, S. *et al.* Physical–chemical characterisation of acrylic polymers grafted on cellulose. *Polymer (Guildf).* **43,** 6183–6194 (2002).
55. Rinaudo, M. Periodate oxidation of methylcellulose: Characterization and properties of oxidized derivatives. *Polymers (Basel).* **2,** 505–521 (2010).
56. Guo, Q., Wu, Z., Zhang, X., Sun, L. & Li, C. Phenylboronate-diol crosslinked glycopolymeric nanocarriers for insulin delivery at physiological pH. *Soft Matter* **10,** 911 (2014).
57. Liu, S. *et al.* Phenylboronic acid modified mucoadhesive nanoparticle drug carriers facilitate weekly treatment of experimentallyinduced dry eye syndrome. *Nano Res.* **8,** 621–635 (2015).
58. Otsuka, H., Uchimura, E., Koshino, H., Okano, T. & Kataoka, K. Anomalous binding profile of phenylboronic acid with N-acetylneuraminic acid (Neu5Ac) in aqueous solution with varying pH. *J. Am. Chem. Soc.* **125,** 3493–3502 (2003).
59. Deshayes, S. *et al.* Phenylboronic acid-installed polymeric micelles for targeting sialylated epitopes in solid tumors. *J. Am. Chem. Soc.* **135,** 15501–15507 (2013).
60. Cheng, C., Zhang, X., Wang, Y., Sun, L. & Li, C. Phenylboronic acid-containing block copolymers: synthesis, self-assembly, and application for intracellular delivery of proteins. *New J. Chem.* **36,** 1413 (2012).
61. Gulyaeva, N., Zaslavsky, A., Lechner, P., Chait, A. & Zaslavsky, B. Relative hydrophobicity of organic compounds measured by partitioning in aqueous two-phase systems. *J. Chromatogr. B Biomed. Sci. Appl.* **743,** 187–194 (2000).
62. Hornig, S., Bunjes, H. & Heinze, T. Preparation and characterization of nanoparticles based on dextran-drug conjugates. *J. Colloid Interface Sci.* **338,** 56–62 (2009).
63. Hwang, H. Y., Kim, I. S., Kwon, I. C. & Kim, Y. H. Tumor targetability and antitumor effect of docetaxel-loaded hydrophobically modified glycol chitosan nanoparticles. *J. Control. Release* **128,** 23–31 (2008).
64. Li, N., Zhuang, C.-Y., Wang, M., Sui, C.-G. & Pan, W.-S. Low molecular weight

chitosan-coated liposomes for ocular drug delivery: *In vitro* and *in vivo* studies. *Drug Deliv.* **19,** 28–35 (2012).

65. Yuan, X. b., Li, H. & Yuan, Y. b. Preparation of cholesterol-modified chitosan self-aggregated nanoparticles for delivery of drugs to ocular surface. *Carbohydr. Polym.* **65,** 337–345 (2006).

66. Hermans, K., Van Den Plas, D., Schreurs, E., Weyenberg, W. & Ludwig, A. Cytotoxicity and anti-inflammatory activity of cyclosporine a loaded plga nanoparticles for ocular use. *Pharmazie* **69,** 32–37 (2014).

67. Shen, J. *et al.* Thiolated nanostructured lipid carriers as a potential ocular drug delivery system for cyclosporine A: Improving in vivo ocular distribution. *Int. J. Pharm.* **402,** 248–53 (2010).

68. Aksungur, P. *et al.* Development and characterization of Cyclosporine A loaded nanoparticles for ocular drug delivery: Cellular toxicity, uptake, and kinetic studies. *J. Control. Release* **151,** 286–94 (2011).

69. Başaran, E., Yenilmez, E., Berkman, M. S., Büyükköroğlu, G. & Yazan, Y. Chitosan nanoparticles for ocular delivery of cyclosporine A. *J. Microencapsul.* **2048,** 1–9 (2013).

70. Ferez-Vilar, J. & Hill, R. L. The structure and assembly of secreted mucins. *J. Biol. Chem.* **274,** 31751–31754 (1999).

71. Bansil, R. & Turner, B. S. Mucin structure, aggregation, physiological functions and biomedical applications. *Curr. Opin. Colloid Interface Sci.* **11,** 164–170 (2006).

72. Takeuchi, H. *et al.* Novel mucoadhesion tests for polymers and polymer-coated particles to design optimal mucoadhesive drug delivery systems. *Adv. Drug Deliv. Rev.* **57,** 1583–94 (2005).

73. Taylor, M. J., Tanna, S. & Sahota, T. The role of mucoadhesion of trimethyl chitosan and PEGylated trimethyl chitosan nanocomplexes in insulin uptake. *J. Pharm. Sci.* **99,** 4215–4227 (2010).

74. Fiebrig, I., Harding, S. E., Rowe, A. J., Hyman, S. C. & Davis, S. S. Transmission electron microscopy studies on pig gastric mucin and its interactions with chitosan. *Carbohydr. Polym.* **28,** 239–244 (1995).

75. Ensign, L. M., Schneider, C., Suk, J. S., Cone, R. & Hanes, J. Mucus penetrating nanoparticles: Biophysical tool and method of drug and gene delivery. *Adv. Mater.* **24,** 3887–3894 (2012).

76. Lai, S. K., Wang, Y. Y. & Hanes, J. Mucus-penetrating nanoparticles for drug and gene delivery to mucosal tissues. *Adv. Drug Deliv. Rev.* **61,** 158–171 (2009).

77. Cu, Y. & Saltzman, W. M. Controlled surface modification with poly(ethylene)glycol enhances diffusion of PLGA nanoparticles in human cervical mucus. *Mol. Pharm.* **6,** 173–81 (2010).

CHAPTER 5: PEG FUNCTIONALIZED METHYLCELLULOSE BASED NANOGELS WITH POTENTIAL FOR IMPROVED MUCUS TRANSPORT

Authors: Marion Jamard, Nicole Mangiacotte, Jianfeng Zhang and Heather Sheardown

Objectives: PEGylation of the surface of MC-g-PNtBAm nanogels to improve their transport through the ocular mucus layer to limit their clearance and allow intimate contact with the cornea for improved drug adsorption.

Main Scientific contributions:

- Functionalized the surface of MC-g-PNtBAm nanogels with poly(ethylene glycol) at different coverage densities.
- Demonstrated the impact of the PEG layer on nanogel characteristics and on their performance as drug delivery systems, using two model drugs with different degrees of hydrophobicity, indicating improvement of the nanogels through PEGylation for the sustain delivery of less hydrophobic compounds.
- Showed the dependence of interaction with mucus on PEG coverage density of MC-g-PNtBAm nanogels
- Demonstrated in vitro cytocompatibility of the PEGylated nanogels after 48-hour incubation with human corneal epithelial cells.

Author contributions:
Contributions of this work were as follows. Marion was responsible for synthesis and PBA surface functionalization of the nanogels, verification of their composition by ^{1}H-NMR and ATR FT-IR, and quantification (with Jianfeng) of the PEG content. She characterized their size and morphology by Nanosight and TEM, performed the cytocompatibility tests and drug release studies. Finally she was in charge of the paper write up. Nicole, following trouble-shooting of the method (with Marion), performed the zeta-potential measurements for the mucoadhesion study. Jianfeng suggested the PEG quantification method and helped Marion with the synthesis of rhodamine-labelled PEG.

ABSTRACT

The efficient clearance mechanisms of the eye limit ocular drug delivery, requiring the frequent instillation of more concentrated formulations. To address this issue, we recently developed methylcellulose-based self-assembling nanogels and demonstrated their ability to efficiently encapsulate a hydrophobic model drug and control its release. In this work, those nanogels were functionalized with chains of poly(ethylene glycol) (PEG) with the aim of improving their transport to the deeper layers of the mucus. PEG was grafted using a Schiff base reaction onto oxidized methylcellulose at different coverage densities monitored by the polymer feed ratio. PEG-functionalized nanogels with sizes ranging from 130 nm to 155 nm were found to maintain their spherical shape, stability and cytocompatibility. Drug release studies with both dexamethasone and dexamethasone phosphate showed that PEG-grafting improved encapsulation efficiencies and slowed the diffusion of the drug. Finally, zeta-potential measurements showed that interaction with mucin changed upon PEGylation coverage of the nanogels, suggesting that these systems have great potential for further development as ocular drug delivery systems.

Keywords: poly(ethylene glycol), surface functionalization, nanogel, ophthalmic, mucoadhesion, drug delivery/release

5.1 INTRODUCTION

Particulate systems have many advantages in drug delivery, including protection of the payload, enhanced solubility and sustained release of the drug cargo[1]. Suspended in topical formulations, they have generated great interest for ocular drug delivery[2]. In addition, due to their nanometric size, particles may also be taken up by cells or continue their migration through the surrounding tissues. The necessity for them to rapidly reach epithelial cells is particularly important for therapeutic agents requiring intracellular delivery or targeting deeper tissue layers. However, their efficacy is limited as they are rapidly cleared from the surface of the eye when only adhering to the superficial layers of mucus[3]. The corneal surface is protected by a layer of corneal epithelial cells which are lubricated by a mucous layer[4]. The dense porous mesh formed by highly crosslinked mucin fibers[5] results in a characteristic gel-like, cohesive and viscoelastic structure[4]. The gel-forming properties are important for entrapping foreign particles and bacteria which are discharged to the drainage system during blinking[6]. However this layer might also clear particle-based drug delivery systems, potentially preventing them from remaining on the ocular surface for a sufficiently long time period to be effective, thus reducing the efficiency of drug delivery to the target site.

In order to improve precorneal retention of nanocarriers, surface chemistry, charge and size of nanosystems have been modified in order to maximize their mucoadhesive behavior, and target the ocular surface moieties[2,7–9]. In a different approach, mucus-inert nanosystems, which were shown to be able to avoid interaction with mucus and featured interesting properties, have been examined[10]. Indeed, after initial administration, particles interact and diffuse through the mucus differently according to their size and adhesive properties[11]. Steric

hindrance prevents particles with sizes on the order of microns from diffusing through the mucus layer. Even in the case of bonding with the mucin chains, these particles will remain in the outer mucus layer. Smaller particles can diffuse through the mucus layer, but the diffusion of adhesive particles will be slowed by interactions with mucin and retained at the external layer. Furthermore, those with sizes below 100 nm in diameter have decreased diffusion rates, probably due to retention in pockets of the mucin mesh. Non-adhesive nanoparticles of around 200-500 nm in diameter, however, have shown the ability to diffuse rapidly and reach the epithelial lining to further undergo cell uptake or tissue penetration. In parallel, clearance mechanisms progressively remove the particles located on the luminal side of mucus[11,12].

Poly(ethylene glycol) (PEG) is a biocompatible poly(ether)[13] lacking side functional groups, such as amine or carboxylic acid, which are able to specifically interact with the components of mucin[14]. Numerous studies from the Hanes group[15–17] suggested that PEGylated particles with a diameter of up to 500 nm show minimal adhesive interaction and were able to diffuse through mucus[5]. Previous literature also indicates that PEG coating causes mucoadhesion[18–21], presumably by an interpenetrating polymer network effect between the PEG chains and the mucus mesh[19,22,23] or by hydrogen bonding[24]. When studying the effect of PEG molecular weight and the degree of surface coverage on diffusion through mucus, both appropriate density of the hydrophilic uncharged surface (Hanes et al. reported PEG conjugation with 65–70% of the carboxy groups on the surface of polystyrene nanoparticles[25]) to minimize hydrophobic and ionic bonding as well as short chains to reduce the possibility for entanglement with mucin fibers were necessary[14,25,26]. Low grafting density or long PEG

chains resulted in mucoadhesive particles[25]. Thus, coverage by a dense layer of short molecular weight poly(ethylene glycol) chains has been found to allow particles to penetrate mucus[5]. Other groups have confirmed these observations for nanosystems densely modified with short PEG chains[14,27,28], and PEGylation has been performed on different types of nanocarriers to confer mucus-penetration properties[25,29,30]. Besides demonstrating rapid penetration through healthy human mucus, they also showed the same properties with human mucus in diseased states[15,16,31]. In addition, PEG has also been added on the surface of nanoparticles to improve their stability in physiological environments including precorneal tear fluid[32–38]. By altering the hydrophobicity of the surface of the nanocarrier, a PEG coating has been shown to confer protection from protein opsonisation[39], plasma protein absorption[40] in addition to prolonging circulation[41,42].

We have previously synthesized self-assembling nanogels by grafting hydrophobic chains of N-tert-polybutylacrylamide (NtBAm) onto methylcellulose[43] (MC). The MC-g-PNtBAm nanogels showed efficient entrapment and sustained release of a model hydrophobic drug. The release rate was tunable by modifying the degree of hydrophobic grafting and the molecular weight of the MC, allowing for an optimum drug concentration at the site of interest with a minimal initial burst. However, for the nanogels to fulfill their goal, their payload must be delivered to the target tissue before clearance of the carriers. The particles thus have to overcome the mucus barrier by penetrating sufficiently deep into the more slowly cleared layers of mucus to improve epithelial distribution and retention time[44]. In this study, the MC-g-PNtBAm nanogels were modified with short chains of 2000 g/mol methoxy poly(ethylene glycol) amine (PEG-NH_2) as a means of generating mucus

penetrating nanoparticles, and the impact of surface coverage on morphology and properties was examined.

5.2 MATERIALS AND METHODS

5.2.1 Materials

Methylcellulose (MC) Metholose SM-15 were bought from Shin-Etsu (Totowa, NJ, USA). N-tert-butylacrylamide (NtBAm), cerium ammonium nitrate (CAN) and dimethyl sulfoxide-d6 (DMSO-d6), methoxypolyethylene glycol amine (2000 g/mol), poly(ethylene glycol) diamine (2000 g/mol), sodium periodate, glycerol, sodium cyanoborohydride, rhodamine B isothiocyanate (Rho-NCS) and mucin (type II from porcine stomach) were purchased from Sigma-Aldrich (Oakville ON). Dexamethasone phosphate and Dexamethasone were obtained from Sigma Life Science (St Louis, MO, USA). Phosphate buffered saline (PBS) (10 times concentrate) was obtained from BioShop (McMaster University – Hamilton ON). Nitric acid 70% and potassium chloride were purchased from EMD Chemical Inc. (Mississauga, ON). Vybrant MTT cell proliferation assay kit and LIVE/DEAD viability/cytotoxicity kit were purchased from Molecular Probes by Life Technologies (Eugene, OR, USA) and cell growth media – Keratinocyte-SFM came from Gibco by Life Technologies (Grand Island, NY, USA). Human corneal epithelium cells (hCECs) were the kind gift of Dr. May Griffith.

5.2.2 MC-g-PNtBAm synthesis

MC-g-PNtBAm was synthesized as previously described[43]. Briefly, 250 mg of MC and 250 mg of recrystallized NtBAm were dissolved in 50 mL of water (0.5% w/v). When dissolved, 0.3 mL of 70% nitric acid was added to the solution. The mixture was purged with nitrogen for 30 minutes. Finally, 50 mg of CAN dissolved in 1 mL of purified water prepared in a Millipore Milli-Q system, was added to the solution to start the polymerization. The reaction was left stirring at room temperature for 24 hours, followed by extensive dialysis (pre-wetted RC tubing 3.5kDa, Spectrum Laboratories) to remove any unreacted compound, and freeze dried (Labconco 7752020).

5.2.3 PEG functionalization of the MC-g-PNtBAm nanogels

100 mg of freeze dried MC-g-PNtBAm were dissolved in 5mL DMSO. The mixture was then added dropwise to 50 mL of water under stirred conditions to trigger the self-assembly of the nanogels. Protected from light in an amber vial, 100 mg of sodium periodate ($NaIO_4$) dissolved 1 mL of water, 9 mL of nanogel suspension were mixed and periodate oxidation was carried out under stirring at room temperature. After 2 hours, the unreacted $NaIO_4$ was quenched with 0.1 mL glycerol. Subsequently, various amounts of 2000 g/mol methoxypolyethylene glycol amine (reported in Table 5-1) diluted in 1mL of water were added followed by 30 mg of sodium cyanoborohydride ($NaCNBH_3$) dissolved in 1 mL water after 6 hours of reaction. Three hours following the incorporation of the reducing agent, the mixture was extensively dialyzed against water to remove any unreacted compounds[46].

Reassembled MC-g-PNtBAM nanogels which did not undergo the functionalization steps were used as a negative control (MC-g-PNtBAm_PEG0).

5.2.4 ATR FT-IR analysis

ATR FT-IR spectra of freeze dried samples were measured (Bruker Vertex 70 Bench and a diamond ATR module) in the range of 400 to 4000 cm^{-1}.

5.2.5 NMR analysis

Freeze dried materials (Labconco 7752020) were dissolved in DMSO-d6 and analyzed by nuclear magnetic resonance (NMR, Bruker AVANCE 600 MHz NMR spectrometer).

5.2.6 PEG quantification

Mono-labeled PEG was synthesized as followed. Poly(ethylene glycol) diamine was dissolved in DCM at 30% w/v and Rho-NCS (1:1 molar ratio with PEG) was dissolved in DCM. The Rho-NCS was slowly added drop-wise to the PEG solution under nitrogen. The reaction was left for 24 hours, protected from light. Then, DCM was evaporated under reduced pressure. While some diamine PEG molecules might be labeled at both ends and some molecules might not be labeled, it is assumed that the amount of mono-labeled PEG would be significant.

A mixture of 90% methoxypoly(ethylene glycol) amine and 10% Rho-NCS labeled PEG was used to functionalize the nanogels following the method described above with the same final PEG concentrations. The solutions were extensively dialyzed, and the derivation degree was

assessed by fluorescence with a microplate reader (Tecan Infinite 200 Pro) at 540 nm excitation and 625 nm emission, using a calibration curve of Rho-NCS labeled PEG aqueous solutions. Pictures were taken with an upright fluorescence microscope (Olympus, BX53).

5.2.7 Particle size measurements

Single nanoparticle tracking (Malvern NanoSight LM10) was used to measure the particles mean size in aqueous media.

5.2.8 Transmission electon microscopy (TEM)

After diluting the sample with purified water, 5 μL of the suspension was spread on 200 mesh Formvar coated cooper grids without staining and allowed to dry under ambient atmospheric conditions. The morphology of nanogel samples was viewed and photographed using transmission electron microscopy (TEM, JEOL 1200EX TEMSCAN) with 80kv electron beam.

5.2.9 Zeta-potential measurements

In this study, the mucoadhesive properties were evaluated by measuring the changes in zeta-potential on interaction with negatively charged mucin[47,48]. 2 mL samples were prepared from 0.1 mL of the PEG grafted nanogel solution (final nanogel concentration of 7.9 x 10^{-2} mg/mL) with 0.4 mg/mL mucin and 25 mM potassium chloride. Following an hour of incubation at 37°C in a shaking incubator, zeta potential was determined (Brookhaven 90Plus Particle Size Analyzer). Samples of unmodified nanogels as well as solutions without

nanogels were used as controls. Samples were made in triplicate with 5 zeta potential measurements per sample and 15 runs per measurement.

5.2.10 Drug loading

To load the drug into the nanogels, 5 mg or 10 mg of dexamethasone or dexamethasone phosphate (Dex-P) respectively were added to the DMSO along with the MC-g-PNtBAm before reassembling. Nanogel formation and PEG functionalization were performed as described above. Suspensions of loaded nanogels were then centrifuged at 15000 RPM for 20 minutes in Nanosep 10K Omega centrifugal units (10 kDa molecular weight cut-off, Pall Corporation) to separate the particles from the free drug in solution. The amount of drug in the supernatant was measured by high performance liquid chromatography (HPLC, Waters 2707 Autosampler, 1525 Binary HPLC Pump, 2489 UV/Visible detector, Column Dionex. Model Acclaim (r) 120 C18 5μm 120A 4.6x250mm) 254 nm detection wavelength, injecting 10μL sample and using 1mL/min isocratic flow rate of 40:60 (v/v) acetonitrile:water. A standard calibration curve of dexamethasone in 40:60 (v/v) acetonitrile:water allowed sample concentration determination.

The loading efficiency of dexamethasone into the nanogel particles was calculated as follow:

$$Loading\ efficiency\ (\%) = 100 * \frac{Initial\ amount\ of\ drug - Amount\ of\ drug\ in\ supernatant}{Initial\ amount\ of\ drug}$$

5.2.11 In vitro drug release

The in vitro release of dexamethasone or Dex-P from the nanogels was evaluated following the same method. A 1 mL dispersion of drug-loaded particles was placed into a dialysis bag (molecular weight cutoff 3500 Da, Spectra/Por, Spectrum laboratories) immersed into 5 mL of PBS maintained at 32 ± 1 °C by a shaking water bath. At selected time intervals, the outside medium was removed and replaced with fresh pre-warmed PBS. Concentrations of drug in the releasate were determined by HPLC. All measurements were performed in triplicate and plotted as mean ± SD.

5.2.12 Cell toxicity studies

The viability of human corneal epithelial cells was assessed by the MTT assay and Calcein AM – Ethidium homodimer-1 staining assay to assess the in vitro toxicity of the materials prepared. Experiments were performed on nanogels with two different PEG grafting densities MC-g-PNtBAm_PEG50 and MC-g-PNtBAm_PEG100. PEG grafted nanogels were sterilized by 1% of penicillin-streptomycin and UV irradiation (254 nm) overnight. 5,000 cells/well human corneal epithelial cells (HCECs) were seeded onto 96-well plates and cultured in 100 μL of keratinocyte serum free medium for 24 hours in a CO_2 incubator. The spent medium was then replaced with nanogel formulations and diluted with culture medium to a final methylcellulose concentration of 0.52 mg/mL. Cells were incubated at 37°C in the presence of the PEG functionalized nanogels or controls for 48 hours. Subsequently, for the calcein AM – Ethidium homodimer-1 assay, the nanogel containing media was replaced with 100μL of calcein AM-ethidium homodimer-1 working solution (2 μM calcein AM, 4μM

ethicium homodimer-1), and the cells were incubated for 45 minutes at room temperature. The resultant solutions were measured in a microplate reader (Tecan Infinite 200 Pro) at 530 and 645 nm. For the MTT assay, the nanogel containing media was replaced with 100 μL of PBS and 10 μL of MTT stock solution (5 mg/ml). Following 4 hours of incubation, the supernatant was replaced by 50 μL of DMSO and incubated at 37°C for 10 minutes. The resultant solutions were measured in a microplate reader at 540 nm. Cell viability was expressed as percentage of absorbance relative to the control comprising cells not exposed to the nanogels.

5.3 RESULTS AND DISCUSSION

5.3.1 Synthesis

In order to functionalize the nanogels, active sites were created on the methylcellulose at their surface using periodate oxidation. This approach selectively oxidizes the adjacent hydroxyl groups (C2–OH and C3–OH) of cellulose opening the sugar ring, creating aldehyde groups in the C2 and C3 positions[49]. Oxidation was followed by a Schiff base reaction between the newly formed carbonyl groups along the MC backbone and the primary amine end groups of the methoxy poly(ethylene glycol) amine (PEG-NH_2) chains (Figure 5-1).

Grafting of PEG adds a layer of 2000 g/mol hydrophilic chains on the surface which may jeopardize the hydrophilic/hydrophobic balance that maintains the MC-g-PNtBAm copolymers as nanogels. Thus, MC-g-PNtBAm nanogels with a very high degree of hydrophobization (DH) of 100 NtBAm monomer for 100 anhydroglucose units[43] were chosen to perform PEG functionalization. This ratio was deduced from the ratio of relative

peak integrations of protons belonging to the hydrogen in C2 position of MC and the CH_3 group of NtBAm, following a method used in previous studies[43,50].

Analysis by ^{1}H-NMR showed the appearance of a distinctive peak at 3.5 ppm corresponding to the repeat unit of PEG[51,52] (Figure 5-2), thus confirming successful grafting onto the surface of MC-g-PNtBAm nanogels. By comparing the IR spectra of the unmodified and modified nanogels (Figure 5-3), the latter ones showed new or more intense peaks at 960 cm^{-1}, 1105 cm^{-1}, and 2871 cm^{-1}, which were respectively ascribed to CH_2 rock and C-C stretch, C-O and C-C stretch, and the CH_2 symmetric stretch of PEG[53,54]. These observations confirm that the PEG chains were effectively grafted on the nanogel surface. ATR FT-IR showed an increase in the peak intensity with an increased feed ratio of PEG, but more accurate quantification was necessary to support these observations.

5.3.2 PEG quantification

In order to investigate the correlation between the initial PEG concentration and the amount grafted, the same reaction was performed using fluorescently labeled PEG. For varying concentrations, 10% of the incorporated PEG was functionalized with rhodamine. While some of the PEG would be functionalized at both ends with the rhodamine, while other PEG chains would remain unfunctionalized, it was assumed that the amount of monofunctionalized PEG would be significant and on approximately the same order as the unfunctionalized and bifunctionalized PEG. The fluorescence of the formulation was found to increase with an increasing amount of PEG in the solution as expected (Figure 5-4). As the ratio of fluorescent PEG was consistent throughout the formulations, these results

indicate increased PEGylation when increasing its initial PEG concentration. The coverage density of PEG on the nanogels can thus be tuned by varying the feed concentration. However, due to the fact that the amount of monofunctionalized PEG in the mixture is not known, a PEG density is not reported.

5.3.3 Size and morphology

TEM pictures (Figures 5-5) showed spherical particles indicating that the hydrophilic/hydrophobic balance allowing self-assembling into nanogels was not disturbed with the grafting of hydrophilic PEG chains, probably due to the high degree of hydrophobization of the MC-g-PNtBAm maintaining the cohesion of the aggregates. No significant change in their morphology could be observed with increasing PEG coverage density, and the colloids remained stable for all formulations as expected[14].

Size analysis using Nanosight revealed that the PEG functionalized nanogels were smaller than the unmodified ones (Figure 5-5). Previous studies reported that periodate oxidation induced depolymerisation of methylcellulose[5556] leading to size reduction of the nanogels attributed to a decrease in the swelling capacity[55]. No trend was observed when examining the impact of the amount of PEG grafted on the nanogel size in water. All formulations resulted in nanogels with a size of approximately 147 nm ± 13 nm in diameter. As the density of the PEG layer changed with the length of the PEG chains themselves remaining the same, the thickness of the hydrophilic outer layer did not vary as expected.

As discussed above, previous studies showed that the enhanced ability to penetrate mucus was not linear with size reduction[15,25]. Mucus-inert nanoparticles with diameters of 200-500

nm were able to travel faster across mucin compared to their 100 nm counterparts physically entrapped into smaller channels. The size of the current PEGylated nanogels falls in between the reported data, and further investigation on the effect of the diameter for those specific particles should be carried out, tuning the size of the MC-g-PNtBAm nanogels modifying the DH and molecular weight of MC to generate particles of the desired size[50].

5.3.4 Cytotoxicity

MC-g-PNtBAm nanogels have been previously shown to be cytocompatible[43]. Since the intended application of these nanogels is in a topical ophthalmic formulation, in vitro biocompatibility was assessed human corneal epithelial cells. The nanogels were tested for 2 different degrees PEGylation MC-g-PNtBAm_PEG50 and MC-g-PNtBAm_PEG100. After incubating for 48h, the relative cell viability was higher than the control for all of the nanogels, indicating that their presence did not negatively impact cell viability (Figure 5-6-a). Percentages above 100% are due the fact that the data is expressed relative to the control. The MTT assay verified that there was no negative effect on the metabolism (Figure 5-6-b) and indicated that the cells continued to proliferate in the presence of the material at a similar rate.

5.3.5 Drug release

5.3.5.1 Dexamethasone

To encapsulate Dexamethasone, MC-g-PNtBAm was dissolved in DMSO along with the drug and the solution was then added dropwise to stirring water inducing self-assembly of the nanogels and entrapment of the drug. Drug loading by nanoprecipitation resulted in a

much lower encapsulation efficiency of 37% (Table 5-2) compared to loading during synthesis which reached efficiencies above 95%[43,50]. This difference is most likely mainly due to a lower nanogel concentration as 250 mg of MC were used (along with varying amounts of NtBAm monomer) when entrapping during synthesis versus only 100 mg of MC-g-PNtBAm copolymer when entrapping for nanoprecipitation. Thus, there is less nanogel in solution and fewer hydrophobic PNtBAm domains to encapsulate the drug. Less copolymer was used when loading by nanoprecipitaion because low concentrations have been reported to ensure better dispersion and separation into nanodomains upon addition into the non-solvent water[57].

PEG functionalization of the nanogel surface was performed subsequently to encapsulation. Surprisingly, following this extra 9-hour-long step, higher entrapment efficiencies were obtained (Table 5-2). As PBA functionalization of the nanogel following a similar method did not induce such a drastic change[55], those results are attributed to the presence of the PEG chains on the surface. The presence of hydrophilic PEG in the aqueous media for functionalization might have affected the partitioning balance of dexamethasone in favor of the nanogel.

The high degree of hydrophobization of the MC-g-PNtBAm nanogels resulted in an extremely slow release of dexamethasone for all formulations (Figure 5-7): 26.3% released from the MC-g-PNtBAm nanogels (aside from the initial burst corresponding to the 63% of free drug in solution) and only 2% in 8 days for the PEG functionalized ones. PEGylation thus induced slower release from the nanogels with dexamethasone, as expected from an additional hydrophilic layer hindering the diffusion of the hydrophobic drug. However, no

significant difference could be observed upon increased density of the PEG layer, possibly because the release might be too slow and mainly controlled by the high DH to observe the effect of coverage.

Noteworthy, unlike a previous study on phenylboronic acid functionalization of MC-g-PNtBAM nanogels[55], the depolymerization of methylcellulose by the oxidation step did not induce a faster release. This is most likely due to the high degree of hydrophobization which has been shown to prevail over the impact of short MC chains[50].

5.3.5.2 Dexamethasone Phosphate

In order to obtain a faster release and enable the observation of the impact of PEGylation, dexamethasone-phosphate (Dex-P) as a slightly more hydrophilic model drug was used.

As with dexamethasone, the loading efficiency increased upon PEGylation of the nanogels (Table 5-2). These results are consistent with the hypothesis that PEG improves encapsulation. Lower efficiencies were reached compared to dexamethasone as expected as Dex-P, being less hydrophobic, has lower affinity for the hydrophobic PNtBAm domains compared to dexamethasone. For the same reason, although still very slow, the release was faster than that observed for dexamethasone (Figure 5-8). All of the Dex-P was released from the unmodified particles within 24 hours, while 12.9% of the drug remained in the system after 8 days (24.1% released among the 37% entrapped).

The Dex-P release was plotted two different ways (Figure 5-8). Figure 5-8-a shows the cumulative release of the total amount of drug, encapsulated and free in solution, as all

percentages are relative to the initial feed concentration of Dex-P. Figure 5-8-b only shows the drug released from the nanogels, with the percentages calculated relative to the amounts of drug encapsulated. While the latter gives a more realistic appreciation of the initial burst, the former enables to compare the release rates, as all formulations are plotted relative to the same amount of dex-P.

With Dex-P, the impact of PEG functionalization was more clearly highlighted as it resulted in lengthening the release of the drug from the nanogels from 1 to over 8 days. Including the free drug in solution, 78.6% and 72.8% of the total Dex-P was released from MC-g-PNtBAm_PEG(50) and MC-g-PNtBAm_PEG(100) respectively within 8 days (Figure 5-8-a). Thus, 21.4% and 27.2% of the drug remained in the nanogels, indicating that 45.8% and 44.3% of their payload was released in a week (Figure 5-8-b). The additional hydrophilic layer created by PEGylation may hinder the diffusion of the more hydrophobic drug. This outcome is consistent with the effect of PEG on entrapment efficiencies, and indicates an improvement for the nanogels with PEGylation for the delivery of less hydrophobic molecules. Denser hydrophilic coverage did not significantly impact the release rate as MC-g-PNtBAm_PEG(50) and MC-g-PNtBAm_PEG(100) showed similar kinetics, as observed with PBA functionalization[55]. The release study was carried out over 8 days, as the turnover of the mucin layer of the tears occurs every 4-6 days and replacement of the corneal epithelial cells occurs every 4-8 days[58].

5.3.6 Interaction with mucus

Interaction of mucus with the nanogels was investigated in vitro using zeta-potential. Mucin is negatively charged at most physiological pHs and lowering of the zeta-potential of a mucin solution with colloids has been reported to show the association of the particles with mucin[47,48,59]. The presence of unmodified MC-g-PNtBAm nanogels increased the zeta-potential of mucin solution from -10.2 ± 0.6 mV to -8.2 ± 4.8 mV (Figure 5-9). A positive shift has been previously reported and attributed to particle-mucin interaction[59]. A low amount of surface PEGylation further increased the zeta potential, while functionalization with a denser coverage of PEG had the reverse impact. Those results suggest that PEG grafting increased interaction with mucin to a certain point and then created the reverse effect, although still demonstrating association. Those findings are in accordance with previous studies which reported that partial PEG coverage resulted in mucoadhesive particles while denser coverage created mucus-inert ones[14,25,60]. According to current results, PEGylation did not screen interaction to the extent of providing mucin-inert particles. It is possible that less adhesion would be observed with shorter PEG chains. Besides, shorter PEG chains might allow denser coverage because of reduced steric hindrance[14]. However, while penetration may be better, particles which do not interact with mucus may also avoid uptake by cells[61–63]. Therefore, in vivo testing needs to be carried out to further investigate the performances of PEG functionalized nanogels and determine which of the formulations would provide the best results under in vivo conditions.

5.4 CONCLUSIONS

In this study, we functionalized the MC-g-PNtBAm nanogels with 2000g/mol PEG chains with the aim of improving mucus penetration ability. Different coverage densities were obtained varying the feed concentration of PEG-NH_2. Hydrophilic/hydrophobic balance allowing nanogel morphology was maintained as well as colloid stability, and the cytocompatibility of the nanogels was not impaired by PEG functionalization. Drug release studies with both dexamethasone and dexamethasone phosphate showed that drug loading was significantly improved after PEG grafting, and that the additional hydrophilic layer provided an extra barrier to prolong drug release. While both PEG grafted and unmodified nanogels provided prolonged release of dexamethasone, the hydrophobic model drug, only PEGylated particles enabled sustained release of Dex-P, the more hydrophilic model drug, over 8 days. Zeta-potential measurements showed that PEG functionalized nanogels interacted with mucin and that the extent of the interaction could be controlled tuning PEG coverage.

5.5 TABLES

Table 5-1: PEG feed mass, concentration and ratio to MC-g-PNtBAm nanogel for each formulation.

Formulation name	PEG feed mass	Final PEG concentration in solution		Mass ratio PEG:MC-g-PNtBAm
MC-g-PNtBAm	0 mg			
MC-g-PNtBAm_PEG20	20 mg	1.6 mg/mL	$8.0x10^{-7}$ mol/mL	1.11:1
MC-g-PNtBAm_PEG50	50 mg	6.0 mg/mL	$2.0x10^{-6}$ mol/mL	2.77:1
MC-g-PNtBAm_PEG100	100 mg	8.0 mg/mL	$4.0x10^{-6}$ mol/mL	5.55:1
MC-g-PNtBAm_PEG200	200 mg	16.0 mg/mL	$8.0x10^{-6}$ mol/mL	11.11:1

Table 5-2: Entrapment efficiencies of dexamethasone and dexamethasone phosphate of different nanogel formulations.

Formulation	Dexamethasone entrapment efficiency (%)	Dexamethasone phosphate entrapment efficiency (%)
MC-g-PNtBAm	37.0	11.6 ± 5.8
MC-g-PNtBAm_PEG(50)	99.7	39.5 ± 5.9
MC-g-PNtBAm_PEG(100)	99.9	48.9 ± 3.5

5.6 FIGURES

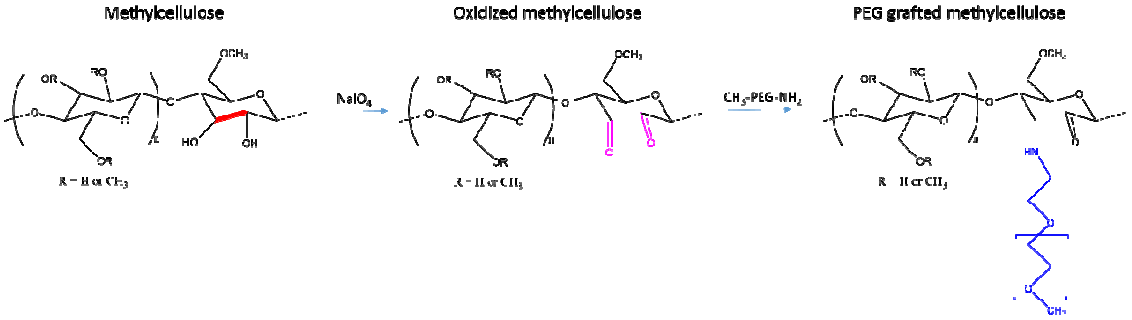

Figure 5-1: Reaction scheme of PEG grafting onto methylcellulose. Sodium m-periodate (NaIO4) oxidation via Malaprade-type reaction breaking the C2-C3 bond of vicinal hydroxylgroups from the AGU of methycellulose, followed by the reaction of the newly formed aldehyde groups od oxidized MC with primary amine groups of methoxy-poly(ethylene glycol) amine via Schiff base linkage.

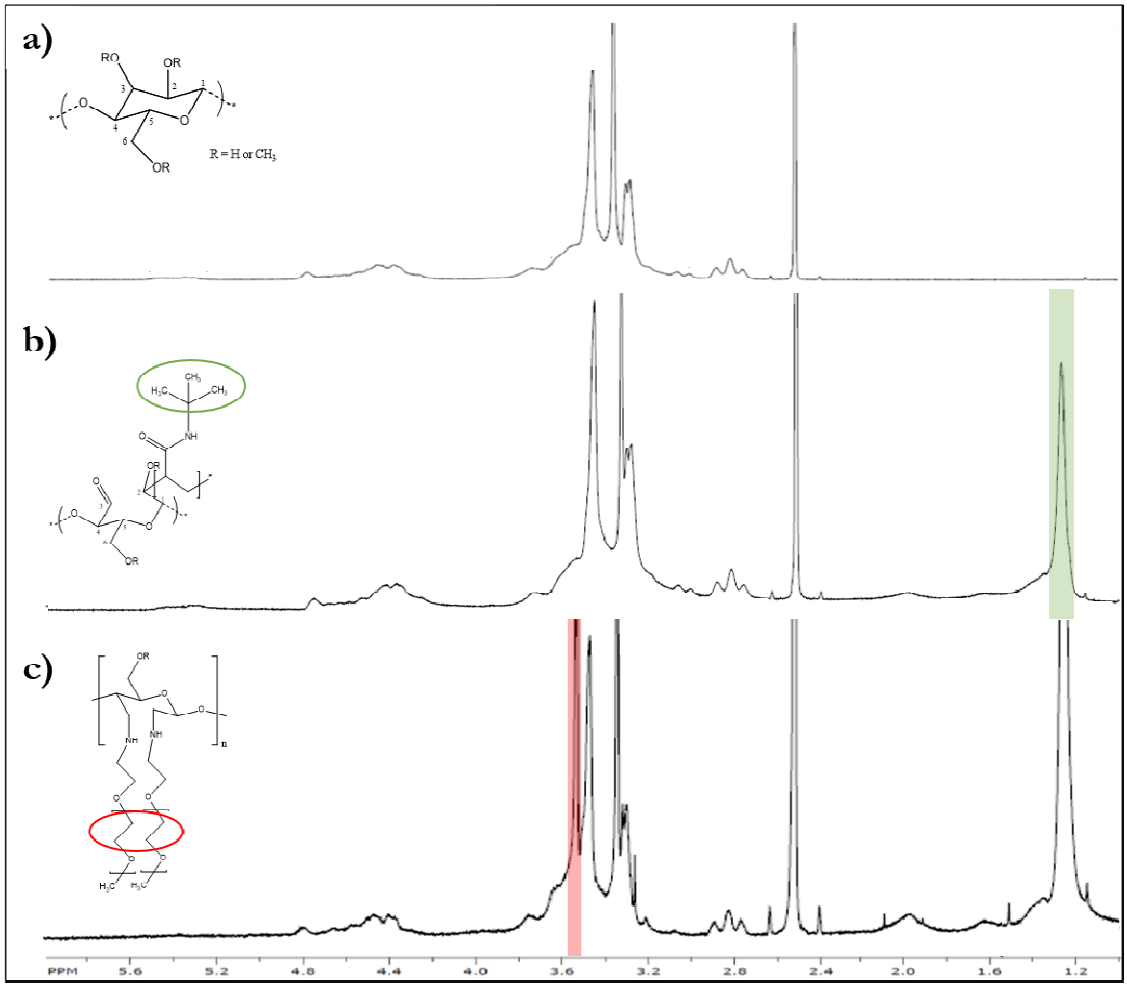

Figure 5-2: ^{1}H-NMR spectra of (a) methylcellulose, (b) MC-g-PNtBAm, (c) PEG functionalized MC-g-PNtBAm.

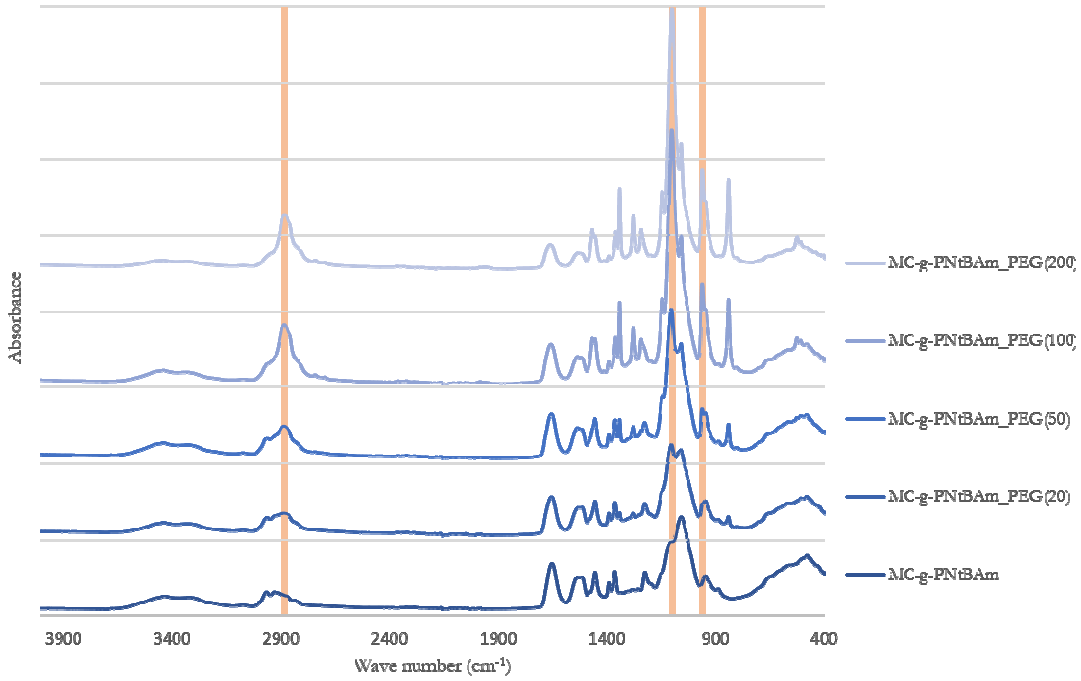

Figure 5-3: ATR FT-IR spectra of MC-g-PNtBAm_PEG(x) formulations at different PEG grafting densities, compared to unmodified MC-g-PNtBAm.

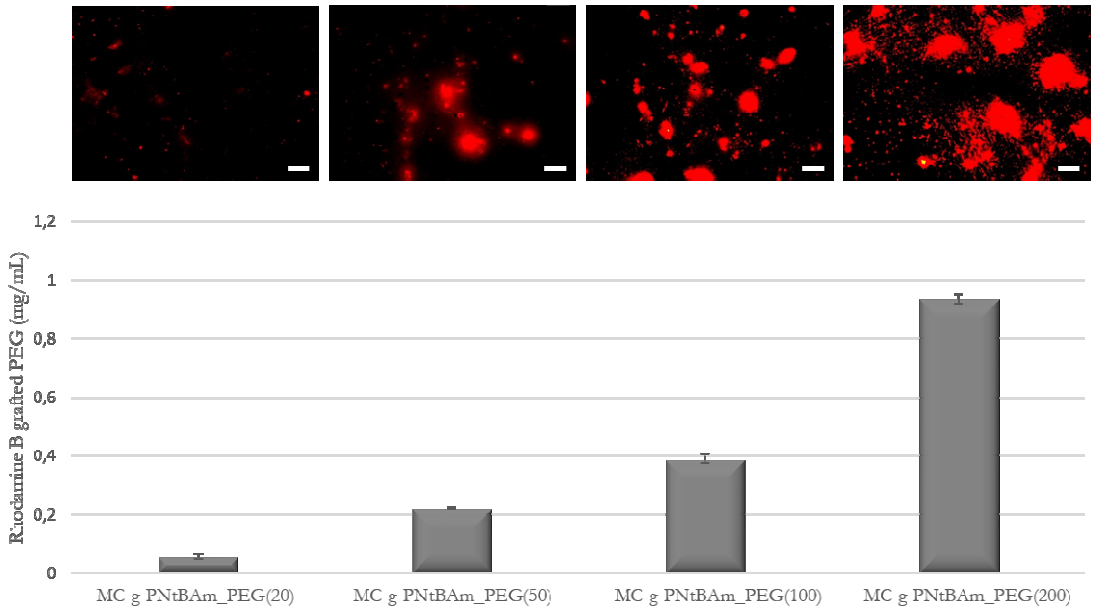

Figure 5-4: Quantification of PEG grafted on thesurface on the nanogel as a function of feed mass by fluorescence. Scale bars = 50 μm.

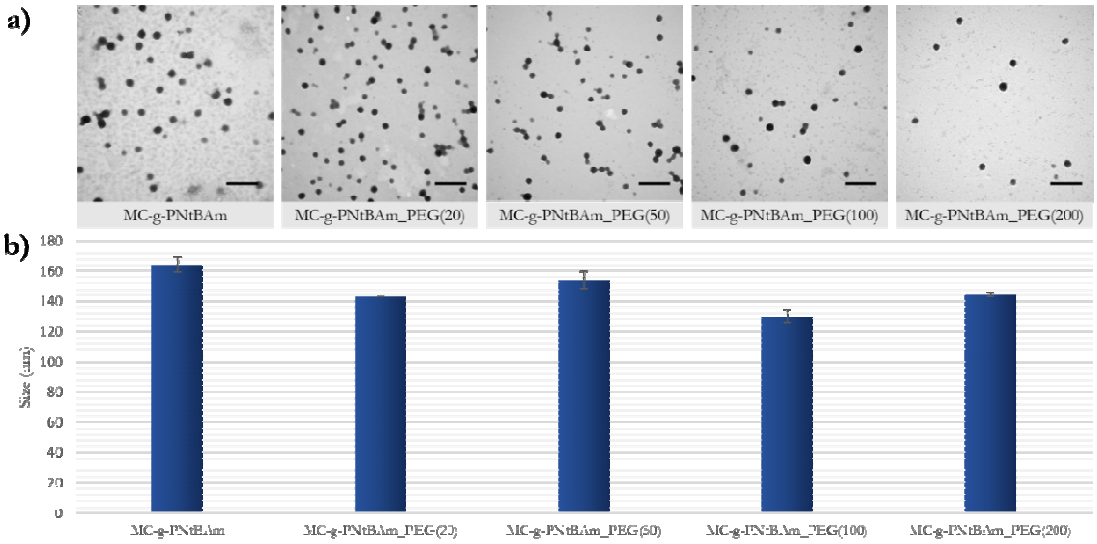

Figure 5-5: (a) TEM pictures, scale bars represent 500nm and (b) size of PEG functionalized MCg-PNtBAm nanogels.3 measurements per solution, error bars corresponding to the standard deviation of the mean size.

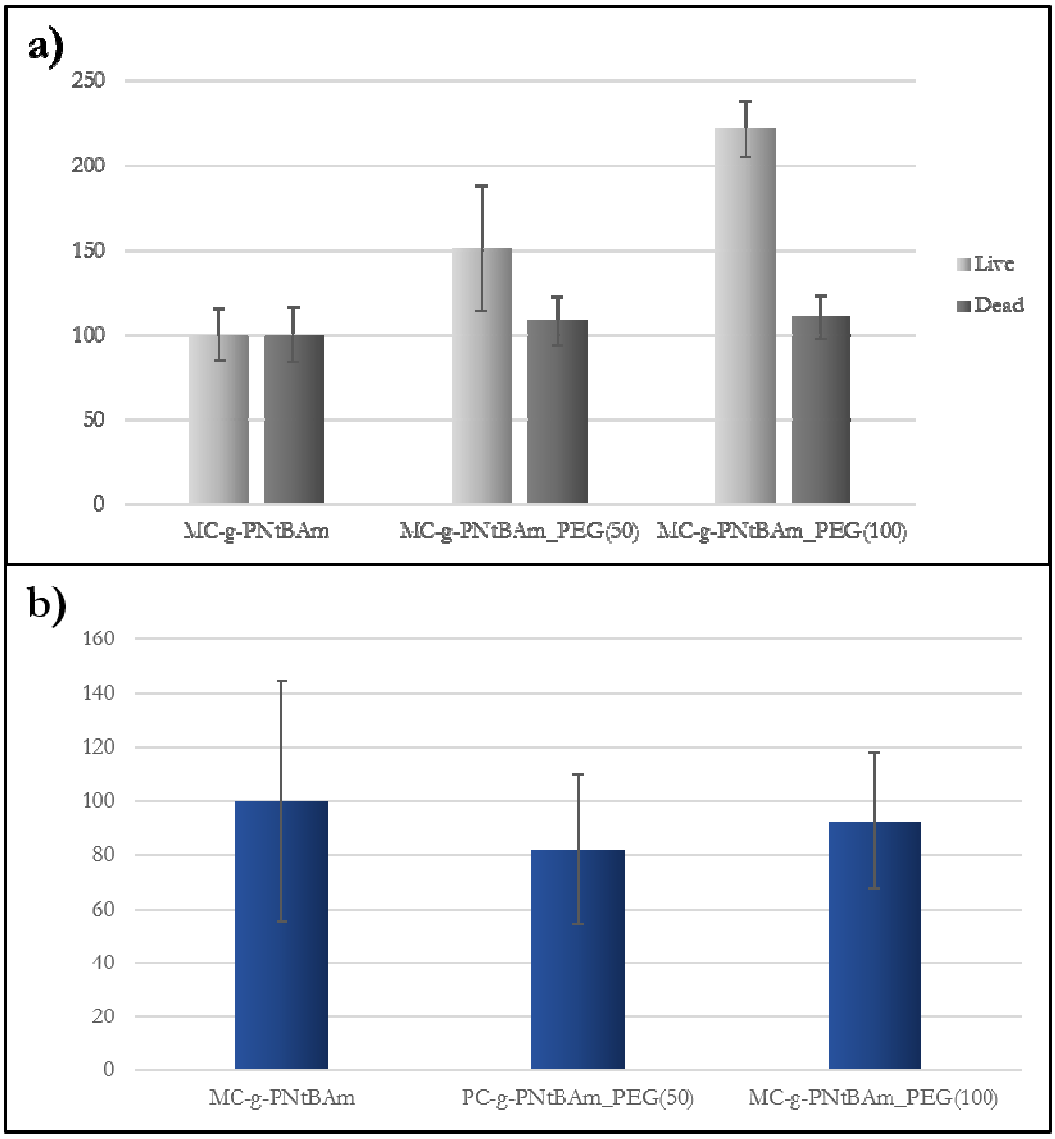

Figure 5-6: Comparison of human corneal epithelial cell a) viability and b) metabolism in presence of PEG functionalized MC-g-PNtBAm nanogels with 2 different PEG densities. Data expressed as a percentage relative to control comprising cells not exposed to the nanogels.n=6, error bars corresponding to the standard deviation.

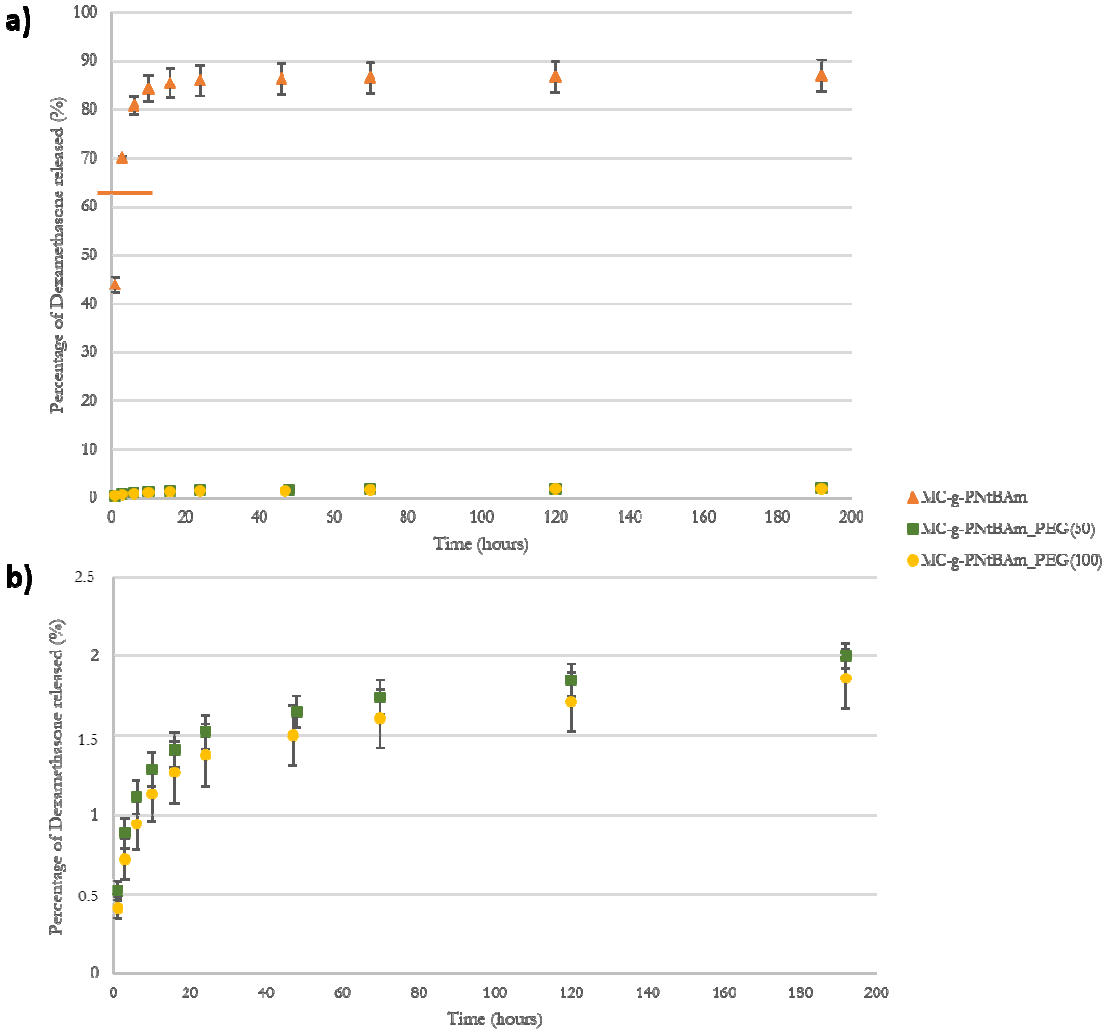

Figure 5-7: Dexamethasone release from the nanogel formulations. a) Comparison of the release from PEG functionalized nanogels with unmodified nanogels. The bar on the release curve of MC-g-PNtBAm indicates the end of the release of the free drug in solution. The bars on the curve of MC-g-PNtBAm indicate the time point when the free drug in solution is released from the dialysis bag and the entrapped drug is being released. b) Zoom on the release to compare the release from PEG functionalized nanogels at two grafting densities. n=3, error bars corresponding to the standard deviation.

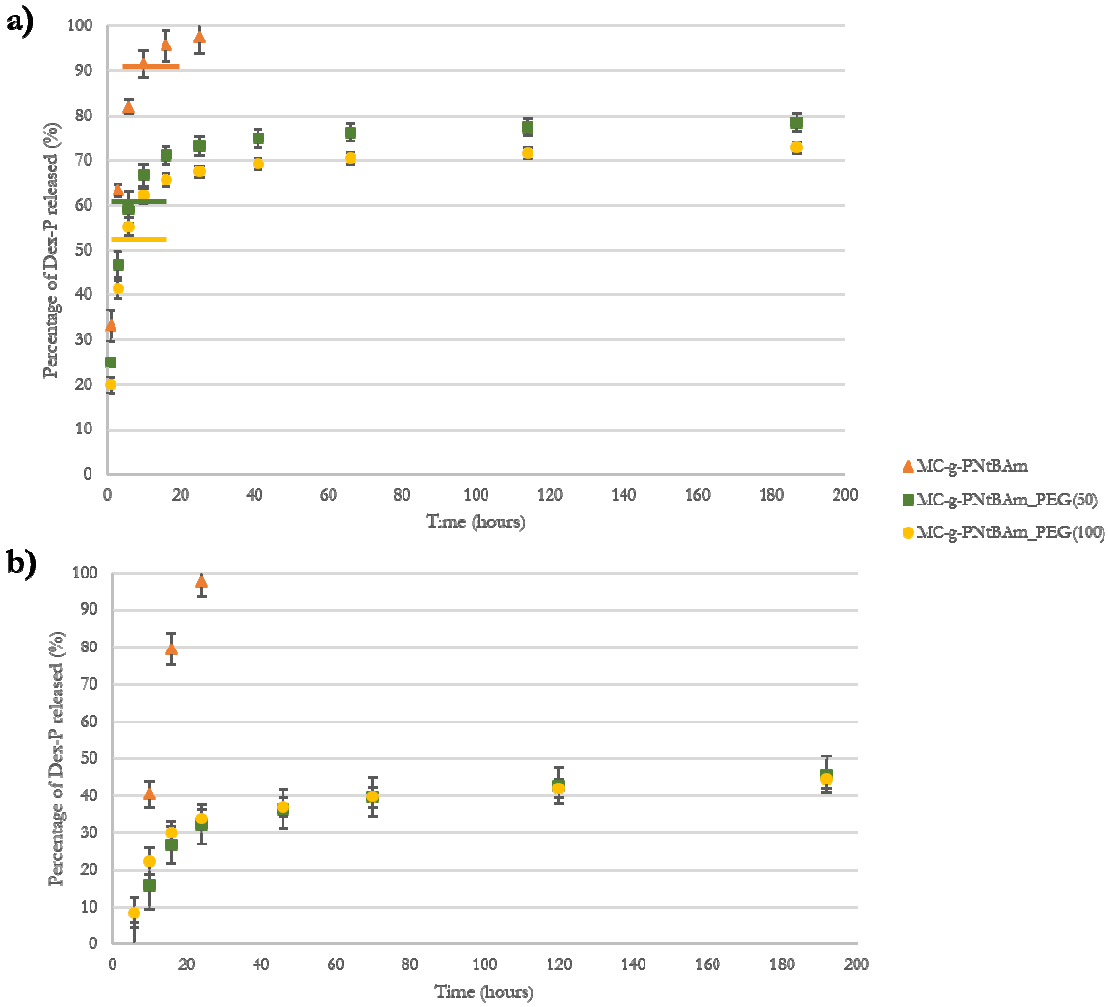

Figure 5-8: Dexamethasone phosphate release from MC-g-PNtBAm_PEG nanogels with two different PEG grafting coverages compared to not functionalized nanogels. a) Release plotted as a percentage relative to the total quantity of dex-P initially incorporated – 100% thus correspondi to the dex-P free in solution and encapsulated. The bars on the curves indicate the time point when the free drug in solution is released from the dialysis bag and the entrapped drug is being released. b) Release plotted as a percentage relative to the quantity of dex-P encapsulated – 100% corresponds to the amount of dexamethasone encapsulated. n=3, error bars corresponding to the standard deviation.

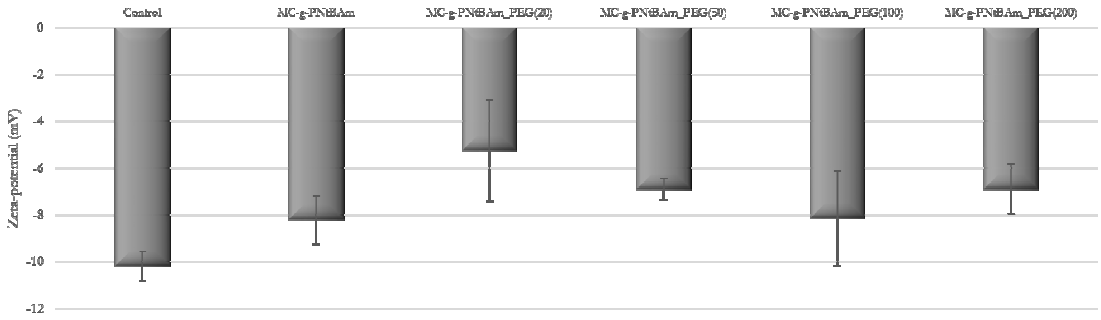

Figure 5-9: Zeta-potential of MC-g-PNtBAm nanogels with different degrees of PEG functionalization, compared to a control of mucin solution.6 measurements per solution, error bars corresponding to the standard deviation.

5.7 ACKNOWLEDGEMENTS

Funding support from NSERC and the CREATE Biointerface Training Program is gratefully acknowledged. Photographs in Figure 5-4 were taken by Banafshe Rastegari.

5.8 DISCLOSURES

The authors state no conflict of interest.

BIBLIOGRAPHY

1. de la Fuente, M., Csaba, N., Garcia-Fuentes, M. & Alonso, M. J. Nanoparticles as protein and gene carriers to mucosal surfaces. *Nanomedicine (Lond).* **3,** 845–857 (2008).
2. Diebold, Y. & Calonge, M. Applications of nanoparticles in ophthalmology. *Prog. Retin. Eye Res.* **29,** 596–609 (2010).
3. Ensign, L. M., Schneider, C., Suk, J. S., Cone, R. & Hanes, J. Mucus penetrating nanoparticles: Biophysical tool and method of drug and gene delivery. *Adv. Mater.* **24,** 3887–3894 (2012).
4. Bansil, R. & Turner, B. S. Mucin structure, aggregation, physiological functions and biomedical applications. *Curr. Opin. Colloid Interface Sci.* **11,** 164–170 (2006).
5. Lai, S. K., Wang, Y. Y. & Hanes, J. Mucus-penetrating nanoparticles for drug and gene delivery to mucosal tissues. *Adv. Drug Deliv. Rev.* **61,** 158–171 (2009).
6. Stern, M. E. *et al.* Autoimmunity at the ocular surface : pathogenesis and regulation. *Mucosal Immunol.* **3,** 425–442 (2010).
7. Liu, S., Jones, L. & Gu, F. X. Nanomaterials for ocular drug delivery. *Macromol. Biosci.* **12,** 608–20 (2012).
8. Cho, H. K., Cheong, I. W., Lee, J. M. & Kim, J. H. Polymeric nanoparticles, micelles and polymersomes from amphiphilic block copolymer. *Korean J. Chem. Eng.* **27,** 731–740 (2010).
9. Rameshkumar, P. & Ramaraj, R. Nanoparticles: Functionalization and Multifunctional Applications in Biomedical Sciences. *J. Appl. Electrochem.* **43,** 1005–1010 (2013).
10. das Neves, J., Amiji, M. & Sarmento, B. Mucoadhesive nanosystems for vaginal microbicide development: Friend or foe? *Wiley Interdiscip. Rev. Nanomedicine Nanobiotechnology* **3,** 389–399 (2011).
11. Sosnik, A., das Neves, J. & Sarmento, B. Mucoadhesive polymers in the design of nano-drug delivery systems for administration by non-parenteral routes: A review. *Prog. Polym. Sci.* **39,** 2030–2075 (2014).
12. das Neves, J. *et al.* Mucoadhesive nanomedicines: characterization and modulation of mucoadhesion at the nanoscale. *Expert Opin. Drug Deliv.* **8,** 1085–104 (2011).
13. Zalipsky, S. Functionalized poly(ethylene glycol) for preparation of biologically relevant conjugates. *Bioconjug. Chem.* **6,** 150–165 (1995).
14. Cu, Y. & Saltzman, W. M. Controlled surface modification with poly(ethylene)glycol enhances diffusion of PLGA nanoparticles in human cervical mucus. *Mol. Pharm.* **6,** 173–81 (2010).
15. Lai, S. K. *et al.* Rapid transport of large polymeric nanoparticles in fresh undiluted human mucus. *Proc. Natl. Acad. Sci. U. S. A.* **104,** 1482–1487 (2007).
16. Tang, B. C. *et al.* Biodegradable polymer nanoparticles that rapidly penetrate the

human mucus barrier. *Proc. Natl. Acad. Sci. U. S. A.* **106,** 19268–19273 (2009).

17. Ensign, L. M. *et al.* Ex vivo characterization of particle transport in mucus secretions coating freshly excised mucosal tissues. *Mol. Pharm.* **10,** 2176–2182 (2013).
18. Sahlin, J. J. & Peppas, N. A. Enhanced hydrogel adhesion by polymer interdiffusion: Use of linear poly(ethylene glycol) as an adhesion promoter. *J. Biomater. Sci.* **8,** 421–436 (1997).
19. Bures, P., Huang, Y., Oral, E. & Peppas, N. A. Surface modifications and molecular imprinting of polymers in medical and pharmaceutical applications. **72,** 25–33 (2001).
20. Peppas, N. a. Molecular calculations of poly(ethylene glycol) transport across a swollen poly (acrylic acid)/mucin interface. *J. Biomater. Sci. Polym. Ed.* **9,** 535–542 (1998).
21. Sasaki, H., Nagano, T., Sakanaka, K. & Kawakami, S. One-side-coated insert as a unique ophthalmic drug delivery system. **92,** 241–247 (2003).
22. De Ascentiis, A., DeGrazia, J. L., Bowman, C. N., Colombo, P. & Peppas, N. A. Mucoadhesion of poly(2-hydroxyexthyl methacrylate) is improved when linear poly(ethylene oxide) chains are added to the polymer network. *J. Control. release* **33,** 197–201 (1995).
23. Huang, Y., Leobandung, W., Foss, a & Peppas, N. a. Molecular aspects of muco- and bioadhesion: tethered structures and site-specific surfaces. *J. Control. Release* **65,** 63–71 (2000).
24. Efremova, N. V., Huang, Y., Peppas, N. A. & Leckband, D. E. Direct measurement of interactions between tethered poly(ethylene glycol) chains and adsorbed mucin layers. *Langmuir* **18,** 836–845 (2002).
25. Wang, Y. Y. *et al.* Addressing the PEG mucoadhesivity paradox to engineer nanoparticles that 'slip' through the human mucus barrier. *Angew. Chemie - Int. Ed.* **47,** 9726–9729 (2008).
26. Yang, M. *et al.* Biodegradable nanoparticles composed entirely of safe materials that rapidly penetrate human mucus. *Angew. Chemie - Int. Ed.* **50,** 2597–2600 (2011).
27. Svensson, O., Thuresson, K. & Arnebran, T. Interactions between drug delivery particles and mucin in solution and at interfaces. *Langmuir* **24,** 2573–2579 (2008).
28. Wu, S. Y., Chang, H. I., Burgess, M. & McMillan, N. A. J. Vaginal delivery of siRNA using a novel PEGylated lipoplex-entrapped alginate scaffold system. *J. Control. Release* **155,** 418–426 (2011).
29. Kim, A. J. *et al.* Use of single-site-functionalized PEG dendrons to prepare gene vectors that penetrate human mucus barriers. *Angew. Chemie - Int. Ed.* **52,** 3985–3988 (2013).
30. Cu, Y., Booth, C. J. & Saltzman, W. M. In vivo distribution of surface-modified PLGA nanoparticles following intravaginal delivery. *J. Control. Release* **156,** 258–264 (2011).

31. Suk, J. S. *et al.* Rapid transport of muco-inert nanoparticles in cystic fibrosis sputum treated with N-acetyl cysteine. *Nanomedicine (Lond).* **6,** 365–375 (2011).

32. Bazile, D. *et al.* Stealth Me.PEG-PLA nanoparticles avoid uptake by the mononuclear phagocytes system. *J. Pharm. Sci.* **84,** 493–498 (1995).

33. Dhar, S., Gu, F. X., Langer, R., Farokhzad, O. C. & Lippard, S. J. Targeted delivery of cisplatin to prostate cancer cells by aptamer functionalized Pt(IV) prodrug-PLGA-PEG nanoparticles. *Proc. Natl. Acad. Sci. U. S. A.* **105,** 17356–17361 (2008).

34. Dong, Y. & Feng, S. S. In vitro and in vivo evaluation of methoxy polyethylene glycol-polylactide (MPEG-PLA) nanoparticles for small-molecule drug chemotherapy. *Biomaterials* **28,** 4154–4160 (2007).

35. Esmaeili, F. *et al.* Folate-receptor-targeted delivery of docetaxel nanoparticles prepared by PLGA-PEG-folate conjugate. *J. Drug Target.* **16,** 415–423 (2008).

36. Gao, Y., Sun, Y., Ren, F. & Gao, S. PLGA-PEG-PLGA hydrogel for ocular drug delivery of dexamethasone acetate. *Drug Dev. Ind. Pharm.* **36,** 1131–1138 (2010).

37. Vega, E., Antonia Egea, M., Calpena, A. C., Espina, M. & Luisa Garcia, M. Role of hydroxypropyl-β-cyclodextrin on freeze-dried and gamma-irradiated PLGA and PLGA-PEG diblock copolymer nanospheres for ophthalmic flurbiprofen delivery. *Int. J. Nanomedicine* **7,** 1357–1371 (2012).

38. Yang, J., Yan, J., Zhou, Z. & Amsden, B. G. Dithiol-PEG-PDLLA micelles: Preparation and evaluation as potential topical ocular delivery vehicle. *Biomacromolecules* **15,** 1346–1354 (2014).

39. Peer, D. *et al.* Nanocarriers as an emerging platform for cancer therapy. *Nat. Nanotechnol.* **2,** 751–760 (2007).

40. Niu, J. *et al.* Octreotide-modified and pH-triggering polymeric micelles loaded with doxorubicin for tumor targeting delivery. *Eur. J. Pharm. Sci.* **45,** 216–226 (2012).

41. Cho, H. J. *et al.* Polyethylene glycol-conjugated hyaluronic acid-ceramide self-assembled nanoparticles for targeted delivery of doxorubicin. *Biomaterials* **33,** 1190–1200 (2012).

42. Choi, K. Y. *et al.* PEGylation of hyaluronic acid nanoparticles improves tumor targetability in vivo. *Biomaterials* **32,** 1880–1889 (2011).

43. Jamard, M., Hoare, T. & Sheardown, H. Nanogels of Methylcellulose Hydrophobized with N-tert-butylacrylamide for Ocular Drug Delivery. (2016).

44. Lai, S. K., Wang, Y. Y., Cone, R., Wirtz, D. & Hanes, J. Altering mucus rheology to 'solidify' human mucus at the nanoscale. *PLoS One* **4,** 1–6 (2009).

45. Griffith, M. *et al.* Functional Human Corneal Equivalents Constructed from Cell Lines. *Science (80-.).* **286,** 2169–2172 (1999).

46. Liu, S., Jones, L. & Gu, F. X. Development of mucoadhesive drug delivery system using phenylboronic acid functionalized poly(D,L-lactide)-b-dextran nanoparticles. *Macromol. Biosci.* **12,** 1622–6 (2012).

47. Bhatta, R. S. *et al.* Mucoadhesive nanoparticles for prolonged ocular delivery of natamycin: In vitro and pharmacokinetics studies. *Int. J. Pharm.* **432,** 105–12 (2012).

48. De Campos, A. M., Diebold, Y., Carvalho, E. L. S., Sánchez, A. & Alonso, M. J. Chitosan nanoparticles as new ocular drug delivery systems: in vitro stability, in vivo fate, and cellular toxicity. *Pharm. Res.* **21,** 803–810 (2004).

49. Calvini, P., Gorassini, A., Luciano, G. & Franceschi, E. FTIR and WAXS analysis of periodate oxycellulose: Evidence for a cluster mechanism of oxidation. *Vib. Spectrosc.* **40,** 177–183 (2006).

50. Jamard, M. & Sheardown, H. Effect of Methylcellulose Molecular Weight on the properties of Self-Assembling MC-g-PNtBAm Nanogels. (2016).

51. Yang, H. & Lopina, S. T. Penicillin V-conjugated PEG-PAMAM star polymers. *J. Biomater. Sci. Polym. Ed.* **14,** 1043–1056 (2003).

52. Chen, C., Cai, G., Zhang, H., Jiang, H. & Wang, L. Chitosan-poly(e-caprolactone)-poly(ethylene glycol) graft copolymers: Synthesis, self-assembly, and drug release behavior. *J. Biomed. Mater. Res. - Part A* **96 A,** 116–124 (2011).

53. Kang, G., Liu, M., Lin, B., Cao, Y. & Yuan, Q. A novel method of surface modification on thin-film composite reverse osmosis membrane by grafting poly(ethylene glycol). *Polymer (Guildf).* **48,** 1165–1170 (2007).

54. Gorochovceva, N. & Makuška, R. Synthesis and study of water-soluble chitosan-O-poly(ethylene glycol) graft copolymers. *Eur. Polym. J.* **40,** 685–691 (2004).

55. Jamard, M., Mangiacotte, N. & Sheardown, H. Phenylboronic Acid Functionalization of MC-g-PNtBAm Nanogels for Improved Mucoadhesion. (2016).

56. Rinaudo, M. Periodate oxidation of methylcellulose: Characterization and properties of oxidized derivatives. *Polymers (Basel).* **2,** 505–521 (2010).

57. Hornig, S., Bunjes, H. & Heinze, T. Preparation and characterization of nanoparticles based on dextran-drug conjugates. *J. Colloid Interface Sci.* **338,** 56–62 (2009).

58. Ludwig, A. The use of mucoadhesive polymers in ocular drug delivery. *Adv. Drug Deliv. Rev.* **57,** 1595–639 (2005).

59. Takeuchi, H. *et al.* Novel mucoadhesion tests for polymers and polymer-coated particles to design optimal mucoadhesive drug delivery systems. *Adv. Drug Deliv. Rev.* **57,** 1583–94 (2005).

60. Taylor, M. J., Tanna, S. & Sahota, T. The role of mucoadhesion of trimethyl chitosan and PEGylated trimethyl chitosan nanocomplexes in insulin uptake. *J. Pharm. Sci.* **99,** 4215–4227 (2010).

61. Gref, R. *et al.* 'Stealth' corona-core nanoparticles surface modified by polyethylene glycol (PEG): Influences of the corona (PEG chain length and surface density) and of the core composition on phagocytic uptake and plasma protein adsorption. *Colloids Surfaces B Biointerfaces* **18,** 301–313 (2000).

62. He, G., Ma, L. L., Pan, J. & Venkatraman, S. ABA and BAB type triblock copolymers

of PEG and PLA: A comparative study of drug release properties and 'stealth' particle characteristics. *Int. J. Pharm.* **334,** 48–55 (2007).

63. Mosqueira, V. C. *et al.* Interactions between a macrophage cell line (J774A1) and surface-modified poly (D,L-lactide) nanocapsules bearing poly(ethylene glycol). *J. Drug Target.* **7,** 65–78 (1999).

CHAPTER 6: CONCLUSIONS

In the effort to overcome the current challenges of ocular drug delivery, nanoparticle systems have aroused great interest. They have shown great potential to improve stability and permeability of the drug, prolonging its activity and therefore increasing bioavailability to the target tissue. Synthesis by self-assembly of amphiphilic polymers is a promising strategy as it avoids the use of reactive agents likely to damage the bioactive payload. Polysaccharides, biocompatible and biodegradable natural polymers, have been shown to spontaneously aggregate upon hydrophobization and have demonstrated great potential as drug delivery systems.

In this work, self-assembled nanogels were developed for use as drug carriers for ocular therapeutics. An amphiphilic copolymer was first synthesized by grafting poly(N-tert-butylacrylamide) side chains to a methylcellulose backbone. The MC-g-PNtBAm molecules spontaneously aggregated in aqueous media forming a stable suspension of spherical nano-sized hydrogel particles consisting of a hydrophilic polysaccharide-based mesh and hydrophobic PNtBAm domains. The self-aggregates of ~140 nm showed cytocompatibility with human corneal epithelial cells. Drug delivery studies demonstrated their ability to encapsulate the hydrophobic drug, dexamethasone, with efficiencies above 95% and to release it in a sustained manner over 30 days. Varying the PNtBAm content and MC chain length impacted the nanogel characteristics and drug release kinetics. Lower hydrophobization and longer polysaccharide backbones increased the swelling ability of the nanogels, and thereby their hydrodynamic diameter (up to 255 nm). An increase in the degree of PNtBAm grafting or the MC chain length was found to improve encapsulation efficiencies and slow down the release. The extent of the impact of the molecular weight of methylcellulose was found to decrease when increasing the number of PNtBAm chains grafted. The degree of hydrophobic modification and the polysaccharide length thus provide a means of tuning the properties of MC-g-PNtBAm nanogels to match the kinetic requirements of the drug to be delivered.

The newly developed particulate systems demonstrated the ability to prolong the activity of the drug by sustaining its release, thus allowing less frequent administration of the topical formulation and avoiding concentration fluctuation. In addition, tunable kinetics, achieved by changing the copolymer structure enable tailoring of the drug delivery platform.

In order to insure improved bioavailability of the therapeutics, better precorneal adsorption is essential. Since clearance from the precorneal area is a significant limitation of topical drug delivery, resulting in the removal of the drug from the eye, interaction with or penetration into the mucin layer is desirable. It is believed that this will lead to prolonged residence time at the ocular surface and intimate contact of the drug delivery system with the mucosa, thereby allowing better delivery to the corneal surface and underlying tissues. Thus, the surface of the nanogel was functionalized to further improve the performance of MC-g-PNtBAm drug carriers. Two different strategies were used to enhance drug delivery to the corneal tissue. The first one consisted in surface functionalization with phenylboronic acid to specifically target the sialic acid groups of the mucus layer covering the cornea, with the aim of prolonging their residence time on the surface of the eye. In the second one, nanogels were grafted with PEG chains in order to improve their transport in mucus by minimizing particle-mucin interaction and resulting in the entrapment of the gels within the mucin layer and hence prolonged drug release.

Cytocompatibility of the particles with human corneal epithelial cells was not impacted by PBA or PEG grafting. Both functionalization methods influenced the drug release kinetics. While loading by nanoprecipitation led to lower entrapment efficiencies than loading during synthesis, modified nanogels showed significantly higher levels of drug encapsulation compared to the unmodified ones and the extra layer hindered drug diffusion, allowing for release over longer periods of time. Dexamethasone release from PBA grafted nanogels lasted more than 12 days, with a significant decrease of the initial burst. PEGylation of the nanogels also resulted in more sustained the release of

dexamethasone phosphate, a less hydrophobic drug, with only ~45% of the payload released after 8 days. Unmodified nanogels released all of the entrapped drug within a day. Zeta-potential was used to evaluate the mucoadhesive properties of the particles. Nanogels made of short MC chains seemed to interact with mucin more than those made of longer MC chains, regardless of the PBA functionalization and coverage. As for PEG grafted nanogels, all formulations showed interaction with mucin. This interaction increased at low coverage and decreased with further PEGylation. Although zeta-potential measurements give a valuable insight into the potential of the systems to interact with the mucin layer, additional in vivo experiments are necessary to evaluate the effect of PBA and PEG functionalization on the mucoadhesive properties of the nanogels as well as the delivery of drugs and the potential increase in the bioavailability of the therapeutic cargo.

Future work should be focused in two areas. Fundamental studies of the architecture of the nanogels should be investigated. Specifically, the relationship between the copolymer structure and nanogel properties should be further investigated, looking at the distribution of the hydrophobic content in terms of PNtBAm chain number and length. This should include studies of stability and degradation. The performance of MC-g-PNtBAm nanogels in vivo should also be evaluated. Specifically it would be of interest to examine the residence time on the eye as well as tissue penetration with and without functionalization. While current topical formulations cannot maintain therapeutic concentration on the ocular surface for a prolonged time, the developed MC-g-PNtBAm nanogels as a sustained drug release system has the potential to prolong the retention time on the ocular surface, leading to the need for less frequent dosing and improving the efficacy compared to current formulations.